6 Laboratory Testing – Methodology and Apparatus

6.1 Introduction

The literature review described a number of predictive impact models. Whilst varying in complexity, none of them fully modelled a tennis impact in three dimensions. Chapter five showed that in reality, players often hit off the longitudinal axis of the racket, and generate complex racket movements. In order to re-create realistic shot conditions, a predictive model must be created that can handle impacts off the longitudinal axis, and ball and racket movements in three dimensions. This creates the need to develop a method of validating such a model through experiment.

When validating a six degree of freedom model through experimental means, the experiment must recreate the conditions found in the model. For example, any experimental impacts must include impacts off the longitudinal axis of the racket, and obliquely inclined ball trajectories. Due to a lack of such testing in previous studies, the effect of racket grip on ball velocity and trajectory for offset impacts cannot be discounted. Racket grip can be simulated by restricting the movement around the racket handle according to a restrictive torque value.

The literature review argues that a testing method in which the racket is held stationary is most appropriate; it is much easier to project a ball at a stationary racket than vice versa. Keeping the racket stationary prohibits racket movement to be included in the input parameters, but significantly simplifies the testing procedure and control over the testing inputs. Recording the inbound and outbound parameters in 3D is preferable in order to accurately monitor the effects of different impact positions, ball velocities and a restrictive torque around the racket's handle.

6.2 Aim

The aim of this chapter is to design a laboratory based impact test which measures the input and output variables of a ball impact on a stationary tennis racket.

The test must be able to vary the velocity of the ball in three dimensions, the impact position both longitudinally and transversely and a restrictive torque around the handle. The output velocity of the ball must be tracked in three dimensions so the true effect of a change in the input parameters can be monitored.

The experiment will have six input parameters; the translational input velocity in three dimensions (3), the impact position along the longitudinal and transverse axes (2), and the restrictive torque around the handle (1). The translational output velocity in three directions constitutes the output parameters (3).

6.3 Methodology Development

The development of this testing methodology consists of three stages:

- *Preliminary Testing;* Early testing was performed to assess the issues which arise when attempting to develop an overall methodology.
- *Error sourcing, methodology issues;* An investigation of the methodology issues which were uncovered during preliminary testing was performed. Experiments were executed which aimed to identify the root of experimental error.
- *Equipment design and final methodology;* Testing equipment and software were designed which attempted to solve the problems highlighted in the previous stages.

6.3.1 Preliminary Testing

A precursory investigation into offset racket impacts was performed to identify issues which might arise when performing a comprehensive impact study i.e. filming impacts in 3D, impacting the racket's offset, and equipment issues. This preliminary testing specifically aimed to identify sources of avoidable error.

Methodology

In the absence of specific testing apparatus, two impact rigs were used at The University of Sheffield and The International Tennis Federation (ITF). These had previously been used in 2D videogrammetric testing and basic speed tests using light gates. An example of such tests would be to measure the 1-dimensional inbound and outbound velocity of a tennis ball impacting a racket at different points along the longitudinal axis.

Both testing areas use pneumatically powered ball cannons to fire a tennis ball with zero spin at a tennis racket mounted on a pin (effectively freely suspended) and set perpendicular to the air cannon. The ITF's rig allows accurate movement of the racket vertically and horizontally, and was used more frequently in this series of tests.

The ball's movement was tracked using two Phantom V4.2 high speed video cameras. A volume close to the racket within the impact area was calibrated for 3D analysis so the trajectory of the ball could be tracked before and after impact. No racket markers were used in these tests; the racket's orientation and movement were not tracked directly from the recorded images. The position of impact was tracked using the racket mount apparatus, which is aligned to the air cannon used to project the ball.

The ball was fired at three speeds, 20, 30 and 40 ms^{-1} at 0, 30 and 60 mm off-set. The ball trajectories were tracked manually using proprietary image processing software and reprojected into 3D using the checkerboard calibration toolbox described in Chapter 3.

Discussion

Although only intended as a preliminary study, the results were analysed for trends and relationships between the offset impact position and post-impact speed and trajectory. Very high levels of scatter in the results and the limited variability of input parameters resulted in a failure to extract any meaningful relationships from the data, highlighting the issues and problems which arise when trying to execute work of this type. Establishing relationships between several input parameters required the minimisation of all avoidable error sources, and a refined methodology with improved equipment. Areas of error that were investigated were as follows:

- Scatter; the ball trajectories after impact showed high amounts of scatter, three possible sources of this scatter were supposed to be:
    - Air cannon; high velocity air affecting the ball's flight
    - Tennis ball; variable bounce characteristics due to non-homogenous surface
    - Ball placement; variability in impact point causing scatter in the results due to an inadequate measurement of impact position.
- *Camera/calibration error;* the impact areas used in this preliminary study were only accessible from one side. This limited camera placement options and introduced 3D point reprojection error. The impact areas, which were not designed for 3D work, have vertical struts and other visual obstructions creating blind spots in which no 3D reprojection can be carried out. A typical camera set-up and an illustrated example of the blind spots experienced in this testing are shown in figure 6.1.
- *Point tracking;* the variables in this preliminary study were kept deliberately small so that results could be obtained quickly. Six variables were to be altered independently, with a recorded impact for each, giving several hundred impacts to obtain a reasonable spread of results. The manual tracking process is slow and inefficient and an automatic tracking process was required to significantly decrease the time taken to produce 3D results.

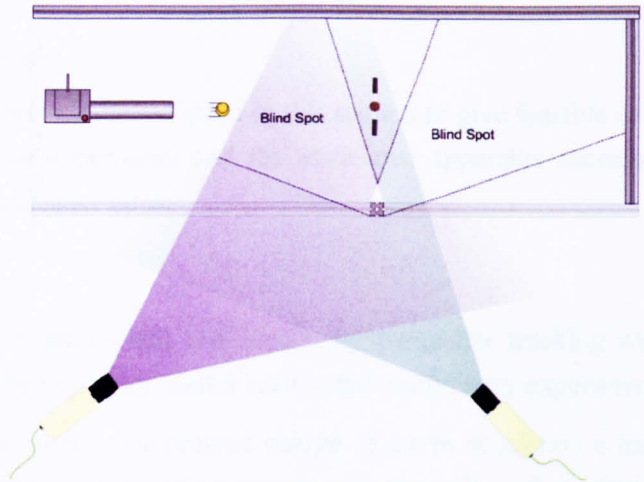

Figure 6.1. A typical camera set-up used in the preliminary testing, both cameras placed to the same side of the subject, with visual obstructions creating avoidable blind spots in the captured images.

Conclusions

The preliminary study highlighted several issues to overcome before an accurate comprehensive study could be attempted. The source of the scatter seen in the results of this experiment have been identified through further investigation into the air cannon, tennis ball bounce, and impact position measurements. It was clear that a method of identifying and utilising trends in the recorded data must be developed so that future results could be used to validate a predictive model.

The impact areas used in this study were clearly unsuitable; both allow access on one side only, making 3D videogrammetric work difficult and inaccurate. No way was possible of creating an opposing torque around the racket's handle. Improved and bespoke apparatus was necessary to maximise the efficiency and accuracy of this process. A smaller, more specific impact area, with high levels of visibility from both sides is necessary. A mount which allows restrictive torque about the racket's handle would minimise the errors present in this experiment and enable the effect of racket's grip to be monitored.

The highly repeatable images which resulted from impact testing, as highlighted in chapter 3, were ideal for an automatic tracking process. An impact area designed to minimise 'noisy' background images and allow proper illumination of the ball meant an automatic tracking program could be written. This program generates a series of 2D image points which can be reprojected into 3D, thereby reducing the time taken to analyse the results.

6.3.2 Error Sourcing

The preliminary experiment highlighted several areas of necessary improvement before a comprehensive study is entirely feasible, specifically:

- Scatter

- Calibration error
- Point Tracking

Each of these areas is investigated in this section to give feasible solutions and lead into the final design of an experiment and the associated apparatus necessary to undertake the study outlined in the chapter aims.

Scatter

The air cannon, tennis ball and inaccurate parameter tracking were all identified as possible sources of the trajectory scatter seen in the preliminary experiment.

The air cannon uses a compressed charge of air to accelerate a tennis ball toward the tennis racket. The large volume of air travels with the ball so that after the impact, the ball travels back through the moving air volume, it was hypothesised that the high resultant velocity may have noticeable aerodynamic effects on the ball's trajectory and hence be a source of scatter.

Chalk dust was added to the cannon's air volume, and a standard racket impact was recorded with a single Phantom V4.2 camera. In this way the velocity of the air volume was tracked as it reached the racket. It was found that the air volume undergoes minimal deceleration by the time it reaches the racket and is approximately equal to the launch velocity of the tennis ball. The relative air velocity moving over the ball is therefore much higher than could be expected in a realistic impact environment.

A number of alternative methods exist for ball projection in which no air volume is ejected, bowling machines use two or more rotating wheels to accelerate a ball with the added advantage of the possibility of spin. A Bola (BOLA **2007**) cricket bowling machine modified to accept tennis balls (see figure 6.2) was compared with an air cannon in order to see if scatter is reduced when no air volume is present.

Figure 6.2. The tennis BOLA ball projection device used as an alternative to the air cannon

To remove racket effects, tennis balls were fired at an angled steel plate. The plate was aligned with the air cannon in the horizontal plane and tilted at a low angle in the vertical plane. Two high speed Phantom cameras were used to track the ball's trajectory in 3D. The global axes-set were aligned to the steel plate, so that the angle of the ball's trajectory can be easily and accurately calculated. This was done by securing a rig with three reflective markers to the stand securing the steel plate. A calibration image with the relevant apparatus highlighted is shown in figure 6.3.

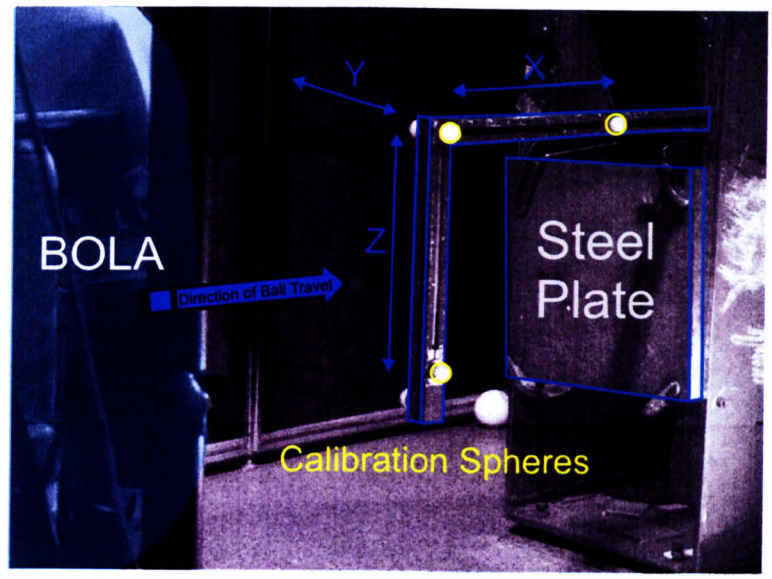

Figure 6.3. An annotated view from the left camera, showing the steel plate used as a surface and the calibration rig used to align the local axes with the plate. The BOLA is highlighted toward the left of the image.

The steel plate was set to a low angle in order to minimise skidding or rolling of the ball during impact, and ensure that the rebounding ball would be travelling through the air volume.

The tennis BOLA machine was set-up next to the air cannon as accurately as possible using the stand available. Although the angle of projection was not exactly the same as that of the air cannon it was assumed to be low enough so that their scatter values could be reliably compared.

The ball was fired 7 times from the air cannon and BOLA at the steel plate. The inbound and outbound trajectories were recorded by tracking the movement of the ball manually before and after impact. A bar plot of the inbound ball trajectories from the cannon and BOLA is shown in figure 6.4 the standard deviation of the results is shown as vertical error bars. The experimental set-up is illustrated in figure 6.5.

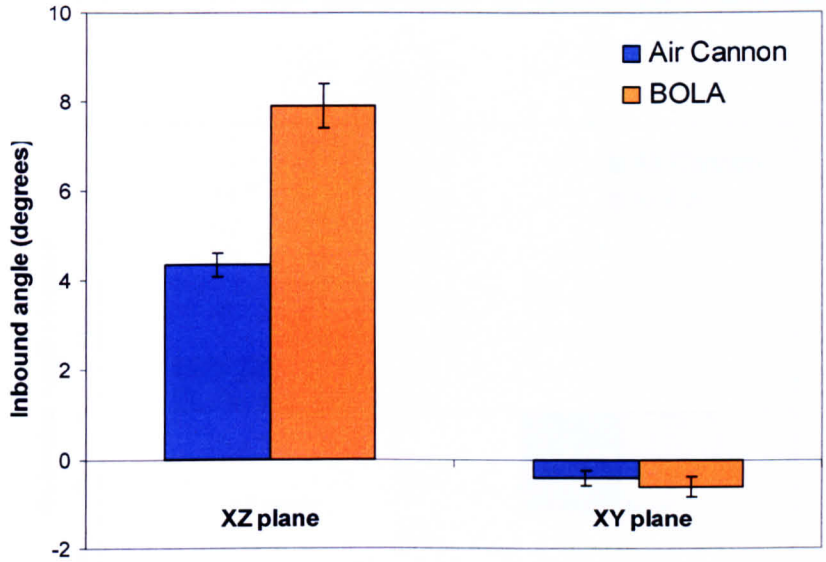

Figure 6.4. The results of a comparative experiment between a BOLA and air cannon. A bar plot of the inbound angles measured from the impact images. The standard deviation of these results is shown as vertical error bars.

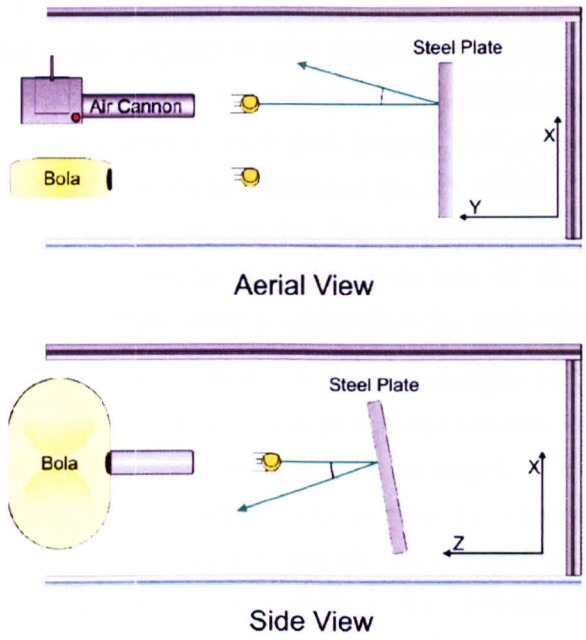

Figure 6.5. The experimental set-up of an experiment intending to compare the trajectory scatter of a tennis ball fired from an air cannon and BOLA projection device.

The inbound angle of balls projected by the BOLA has a higher standard deviation. The rotating wheels used to project the ball from the BOLA are less repeatable than the compressed air from the cannon. Before impact, balls from the BOLA have a higher mean angle in the XZ plane, this systematic difference was a result of the difficulty in manually aligning the BOLA with the steel plate.

Figure 6.6 shows the outbound angles of the air cannon and bola in the XZ and XY planes.

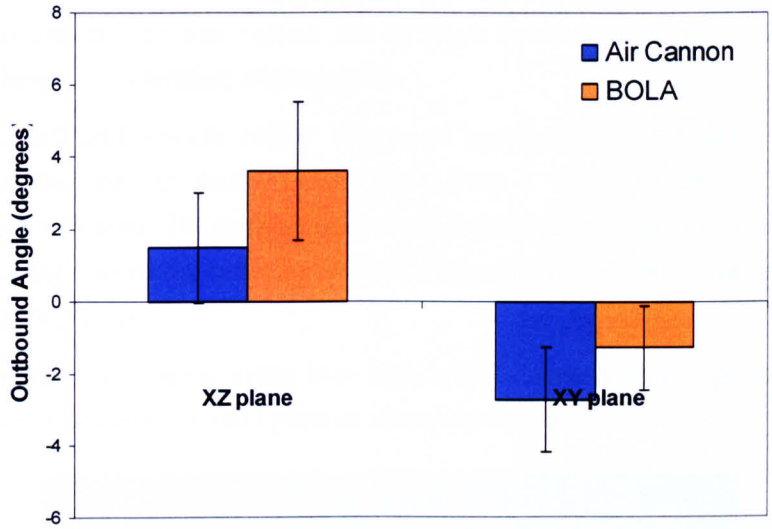

Figure 6.6. The outbound angles of ball projected by the BOLA and air cannon. The standard deviation is indicated as vertical error bars.

The outbound angle (after impact) of balls projected by the air cannon and BOLA has very similar standard deviations in the XY and XZ planes. This suggests that the air cannon does not add any significant scatter to balls post-impact. One should also note the higher mean outbound angle of balls from the air cannon in the XY plane. The mean inbound angle in the XY plane for both devices is very similar. One would therefore expect the post impact angles to be similar given the similar standard deviations of the inbound angles. This difference may be due to a systematic error resulting from the high velocity air volume.

It seems from the results, that the BOLA is the more suitable ball projection device. The variability of the launch trajectory can be improved with the addition of a barrel. This can also be used to accurately align the launch trajectory with the subject of impact. Although the air volume from the air cannon does not appreciably increase the variability of the post-impact ball trajectory, it does seem to introduce a systematic error. Regardless of this circumstantial evidence, the BOLA re-creates the most realistic impact conditions to produce the most reliable results, i.e. no high velocity air volume present at the time of impact.

The air cannon and BOLA generate very similar amounts of scatter despite the large air volume ejected from the air cannon suggesting that the main source of scatter is from the tennis ball itself.

The amount of scatter arising from the tennis ball itself was investigated by comparing its bounce repeatability with a smooth rubber sphere. The sphere was 65 mm in diameter

compared to a tennis ball's nominal 67 mm, and made from solid rubber, meaning it had a considerably higher mass than a tennis ball.

The difficulty involved in firing a rubber sphere from the available projection devices meant that this experiment was carried out at much lower speeds; the balls were simply dropped from height, accelerating under gravity.

A tennis ball and smooth rubber sphere of approximately the same diameter were dropped repeatedly onto an inclined steel plate from a height of 182cm. A mechanical 'dropper' device was used. The dropper used a pin to hold the ball at a chosen height, the pin was retracted using a solenoid, ensuring the ball dropped with zero spin and only accelerated under the effect of gravity.

A 3D system was set-up using two high speed cameras and a global axes-set was aligned to the inclination of the steel plate as shown in figure 6.7.

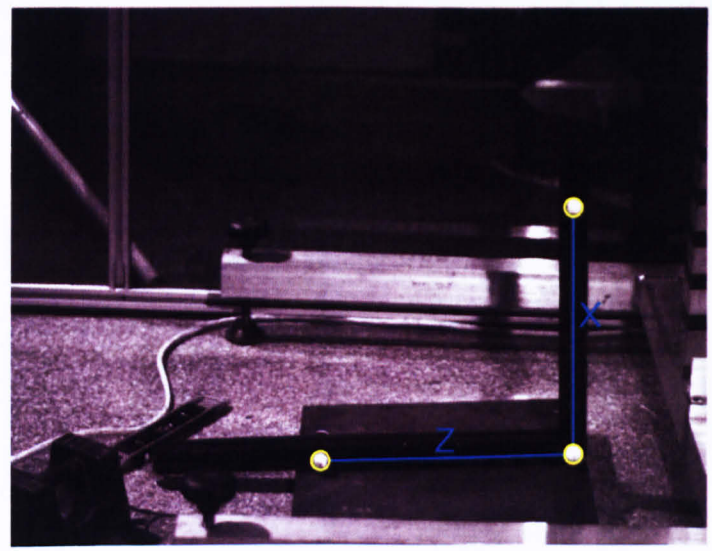

Figure 6.7. The axes-set used to compare scatter of a tennis ball with a rubber sphere, the global X-axis lies just off the vertical, aligned with the plate's perpendicular, the global *Z*-axis runs parallel with the plate's surface.

The angular inclination of the balls' velocities compared to the global X-axis was compared before and after the impact. Each impact was recorded at 200 frames per second, each ball was dropped 12 times. The angle was tracked in the XZ plane following the incline of the plate and also in the XY plane, perpendicular to the plate's incline, the results are shown in figures 6.8 and 6.9. Figure 6.8 displays the inbound angles, 6.9 displays the outbound angles. The standard deviations of the results are displayed as vertical error bars.

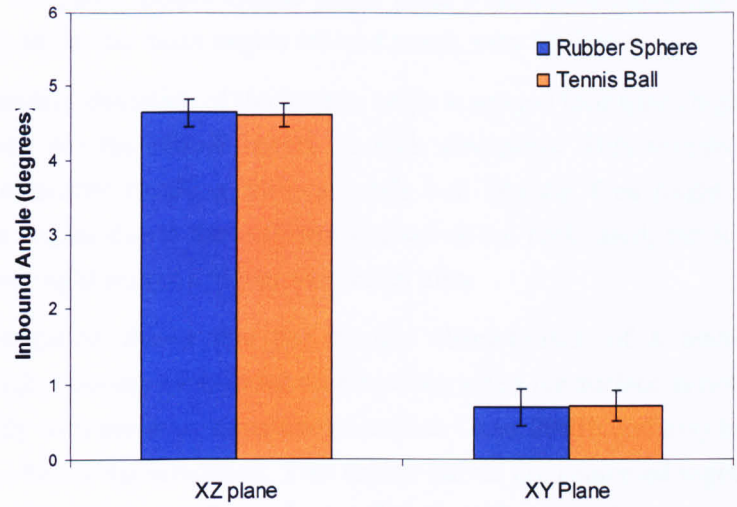

Figure 6.8. The pre-impact inbound angles of a tennis ball and rubber sphere against an inclined steel plate

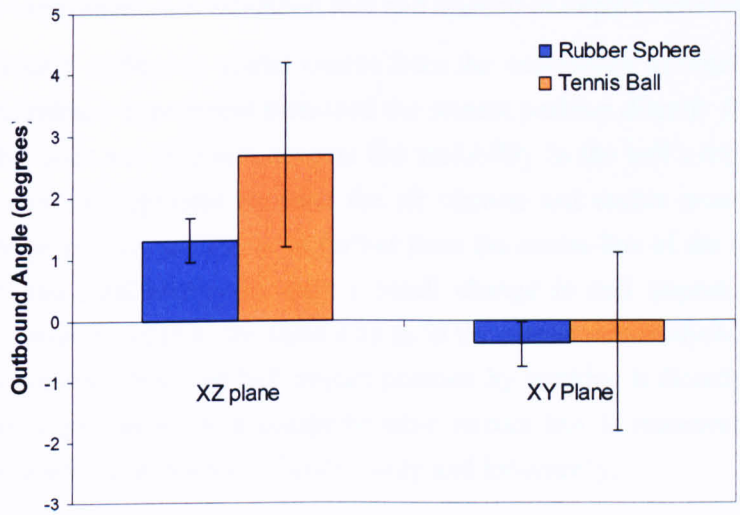

Figure 6.9. The post-impact outbound angles of a tennis ball and rubber sphere against an inclined steel plate

The inbound angle means and standard deviations are very similar for the rubber sphere and tennis ball in the XZ and XY plane. This is because both are simply dropping under gravity. Marked differences are seen after impact:

- The mean outbound angle in the XZ plane is higher for the tennis ball. The solid rubber sphere has a considerably higher moment of inertia, gaining less spin after impact than the tennis ball. The lower outbound spin of the rubber sphere causes it to bounce 'higher' and hence rebound with an angle less than half that of the tennis ball.

- In the XY plane, perpendicular to the plate's inclination, spin has no effect on the bounce angle, the mean angles are as a result, very similar.
- The standard deviation of the bounce angle is around four times higher for the tennis ball than for the rubber sphere in both directions. This reveals a much higher inherent scatter resulting from a tennis ball bounce. One might expect different bounce angles due to the different masses of the balls used, but it does not follow that one might expect a higher variability also.

This investigation shows that the bounce characteristic of a tennis ball contains comparatively high amounts of inherent scatter, even when the surface is not inclined. These scatter values tally with previous experiments such as Cross **2001b** and may be due to the way in which a tennis ball is manufactured. Two rubber halves are cemented together and covered in two felt shapes which are themselves adhered with a continuous seam. A full and comprehensive study on the effects of the seam position and variability in ball properties on bounce behaviour has never been undertaken. The observed ball scatter is something that will have to be accounted for in the design of the experiment, it is not of a level that prohibits the use of an impact experiment as a validation tool and method of impact behaviour observation.

The final source of bounce scatter comes from the uncertainty in obtaining the impact position. The preliminary experiment measured the impact position directly from the position of the racket. This does not take into account the variability in the ball's trajectory from the air cannon and any misalignment between the air cannon and racket mount. The racket's effective mass drops quickly as you move further from the centre-line of the racket, the ball's trajectory is affected significantly by only a small change in ball impact position. If the racket's position were recorded in the same way as in the player shot analysis, a large amount of uncertainty is removed from the ball impact position by tracking it directly. It is therefore essential that every parameter of a comprehensive impact test is measured as directly as possible, removing avoidable sources of uncertainty and inaccuracy.

Calibration Error

The camera positioning used in the preliminary testing was done through necessity rather than to minimise reprojection error. The impact areas used in the study allowed the impact to be observed from one side only, therefore limiting the possibilities in terms of camera positioning. An essential aspect to minimising calibration error is to ensure that principal movement is roughly aligned with the image plane. For example, a camera viewing a ball moving directly towards it will not be able to measure any movement, because the movement lies completely out of the image plane. The less well aligned the camera is with the principal movement, the smaller the associated movements in the image plane and the larger the relative error (see figure 6.10).

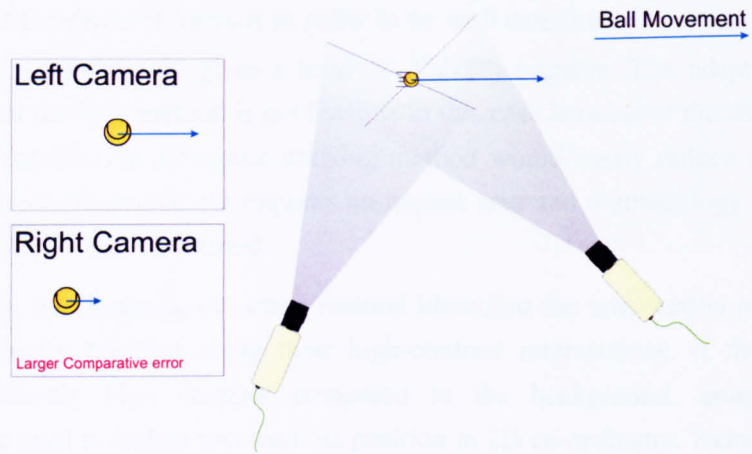

Figure 6.10. A diagrammatic representation of error caused by camera positioning, the camera on the right is poorly positioned.

In order to be able to measure the ball's deviation after impact it is preferable to align the camera roughly 45° with the ball's principal movement before impact, each camera should also be mutually perpendicular (chapter 3 contains a more in-depth investigation into calibration error). Figure 6.11 shows a more suitable way to position the cameras, although this would require an impact area in which both sides are visually accessible, such an impact area would also have to have no obvious visual obstructions like those seen in figure 6.1.

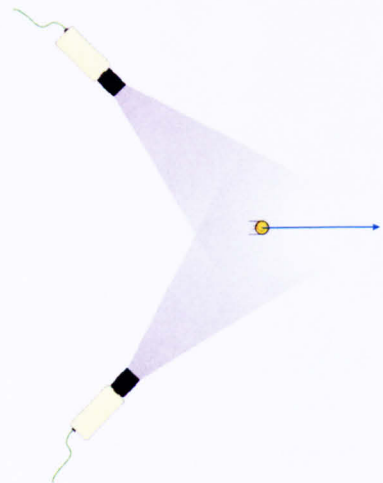

Figure 6.11. A diagram showing how two cameras might be positioned to offer a more accurate view of a racket impact.

Point Tracking

Before any analysis of ball movement can take place, the 2D position of the ball must be tracked in each impact and reprojected into 3D. With the player shot analysis, this was

done manually for a total of 106 shots. A comprehensive impact test, with six variables will have to consist of hundreds of impacts in order to be well determined. Varying each variable only three times independently gives a total of 3^6 (729) impacts. The adaptable but time consuming manual tracking method is not feasible in this case because of the sheer amount of time this would require. An automatic tracking method would vastly reduce the amount of time taken to extract 2D points, but requires an impact area and methodology customised to give images suitable for such a method.

In chapter 3, an automatic detection method identified the intersection points of black and white squares by tracking along their high-contrast intersections. If the ball creates images of sufficiently high contrast compared to the background, image processing techniques can be used to isolate and track its position in 2D co-ordinates. Extraneous aspects of the original image which may cause interference with the processing techniques such as the image of the racket, reflections and light regions are cut out by trimming the image so that it only contains the image of the ball. The cameras do not move between each impact, so this trimmed region need only be specified once per experiment. The rest of the image processing can be done automatically using a Matlab routine; these stages are displayed graphically in figure 6.12.

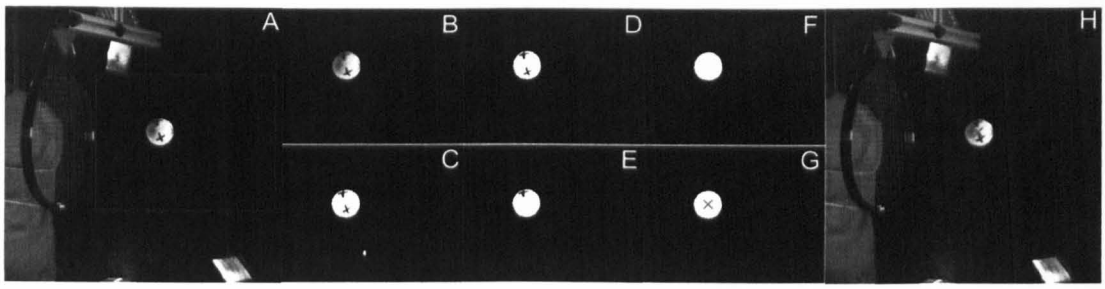

A. Original image trimmed to remove background noise and isolate ball, giving B

B. Trimmed image transformed to black and white according to a grey threshold, giving C

C. White regions smaller than the area of the ball are removed, giving D

D. Black 'orphan' regions within the ball are removed, giving E

E. The ball region related to a disk shape, removing remaining black regions, giving F

F. The centroid of the white 'ball' region is calculated as U V co-ordinates highlighted in G

G. The U V co-ordinates are related back to the original image to give a 2D position used in 3D reprojection.

H. The original image with the detected co-ordinates of the ball's centre marked.

Figure 6.12. The image processing stages used to extract the U V co-ordinates of the ball from high contrast experimental images

When applied to every image in the impact, the pre and post impact co-ordinates can be quickly extracted from each impact in the experiment. Racket markers used to give the position of the racket for each impact cannot be automatically tracked using this process, but they need only be tracked once in each impact to give the impact position.

Section summary

This section showed that the ball scatter is mostly a combination of the tennis ball itself and the inaccuracy of tracking the impact position. The impact position can be more accurately tracked by directly calculating the impact position using racket markers and the bisection method used in player shot analysis. The ball scatter is largely unavoidable but can be accounted for in the experimental results by introducing an appropriate confidence value.

A new impact area is required to improve the accuracy of the calibrated system. Viewing the impact from either side improves the resolution of the recorded images as the ball movement is better aligned with the image plane of each camera. The careful design of a new impact area will also enable automatic ball tracking, considerably speeding up the analysis of recorded impacts.

The next section goes through the design of a new impact area incorporating the improvements highlighted in the last two sections. It also outlines the analytical processes and software used to track the experimental input and output parameters.

6.3.3 Equipment Design and Final Methodology

It has been shown in the previous section that in order to perform a comprehensive impact test, specific equipment must be designed and manufactured to perform the test accurately and efficiently. Furthermore, analysis software must be written so that the results can be obtained quickly and accurately.

This section describes the elements of an impact area designed specifically for such an impact test, outlining its main features and how they relate to the experiment. Software written to analyse the images obtained from using such an impact area will also be discussed, and the design of the final experiment will finish off this section.

Impact Rig

The necessary requirements of an experimental impact area are as follows,

- Size

  An impact area smaller than those used in the preliminary study will be much more effective. It will be quicker to reset the racket into position and retrieve fired tennis balls and the lighting will be more effective and fewer materials are needed in its construction.

- Visibility

  The racket and ball must be visible over the entire impact, not obscured, and visible from both sides to maximise the effectiveness of a 3D analysis method.

- Ball Projection

  The ball must be projected repeatedly and accurately onto the racket face. It must be possible to reliably set the ball's trajectory to hit a specific area on the racket face.

- Lighting

  A large amount of lighting is required to fully illuminate the ball and enable automatic tracking. High levels of lighting also allow smaller camera apertures, and faster shutter speeds, which improves recorded image quality

- Racket Mount

  A racket mount must be used which can change the impact position of the ball on the racket, and also restrict movement around the handle according to a limiting torque.

BoschRexroth **2007** aluminium extrusions were used to manufacture an impact area which incorporates the necessary features listed above. Figure 6.13 shows the completed impact area with major dimensions shown and separate areas highlighted in different colours. The specific features of the impact area are discussed below.

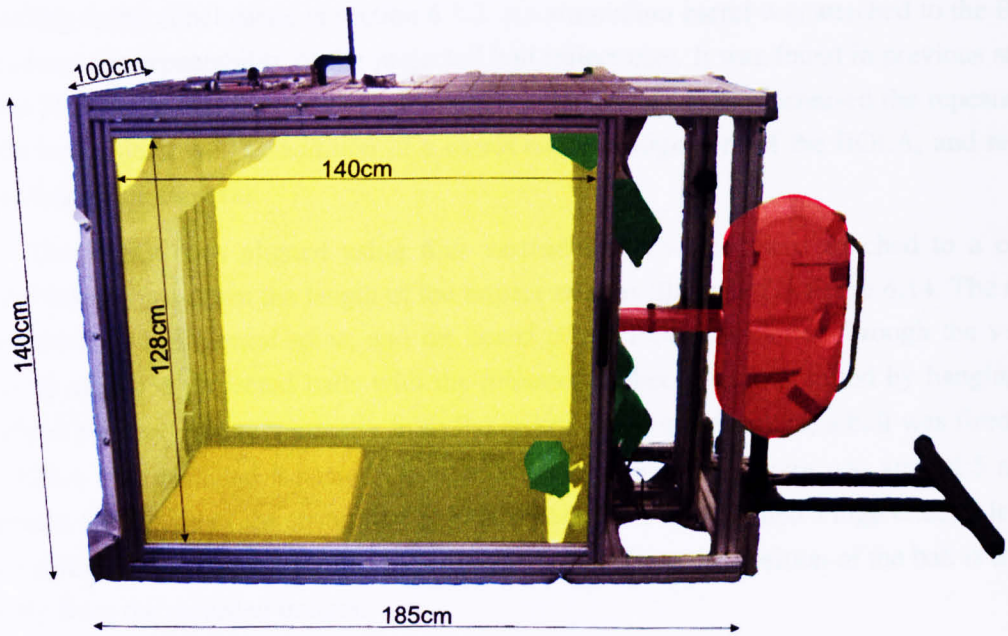

Figure 6.13. The impact area designed for a repeatable, comprehensive tennis impact test intended to validate a 6 degree of freedom predictive model

Size

The impact area is 185 cm long, 100 cm wide and 140 cm high. These dimensions were chosen to minimise the space required for the impact area, leaving sufficient space to capture the required images of the ball before and after impact. The space must also be large enough to accommodate a person and checkerboard in order to calibrate the volume for 3D analysis. A volume of approximately 140 × 140 × 100 cm is fully enclosed by wire mesh and archery netting so that the ball cannot leave the impact area during testing. The archery netting is placed at the rear of the impact area to absorb energy from the racket or ball. The front of the impact area is used to accommodate lighting and the ball projection device.

Visibility

The impact area is fully enclosed from each side by polycarbonate windows 140 × 128 cm in size, highlighted in yellow in figure 6.13. Each polycarbonate pane is part of a sliding door which allows physical access to the testing area and grants visual access to the entire impact area without obstruction. This allows the cameras to be positioned ideally, minimising the errors in 3D reprojection.

Ball Projection

A BOLA ball projector (highlighted in red in figure 6.13) was chosen to project the ball according to the conclusions in section 6.3.2. An aluminium barrel was attached to the BOLA to increase the repeatability of the projected ball trajectories. It was found in previous studies by the ITF **2007a** that the addition of an aluminium barrel greatly increased the repeatability of the ball trajectory. The addition of a barrel enabled alignment of the BOLA, and reliable triggering of the cameras.

The BOLA was aligned using four vertical struts which were attached to a central 'spine' which runs down the length of the impact area, as illustrated in figure 6.14. The racket is mounted on this central spine, and the barrel of the BOLA is slotted through the vertical struts to align the projected balls with the mounted racket. This was tested by hanging two weighted pieces of string vertically from the central spine arrangement; a ball was fired from the BOLA ten times and it passed through the strings each time, there was around 5 mm of clearance either side of the string for the ball to pass. This was deemed a high enough level of repeatability and alignment for this experiment, especially as the position of the ball is tracked directly from the recorded images.

The balls are fired from the BOLA by manually feeding them into two spinning wheels; this causes problems with triggering the cameras used to record the impact. Manual triggering is subject to large human error and large amounts of data must be recorded for each impact. An automatic triggering device was manufactured from a photodiode emitter and receiver; this was mounted half way up the barrel so lighting used in testing does not interfere with its operation. Each time a ball blocks the path of the photodiodes a 5 Volt pulse is generated which triggers the cameras. The time-frame which is then captured is very repeatable, allowing a very small time frame to be captured. This means that fewer images need to be saved to ensure capturing the impact with the camera. Fewer images means a shorter download time, meaning impacts can be recorded more frequently and with greater accuracy. The resulting images are easier to process, and take up a smaller amount of hard disk space; all of these advantages make the testing process very efficient.

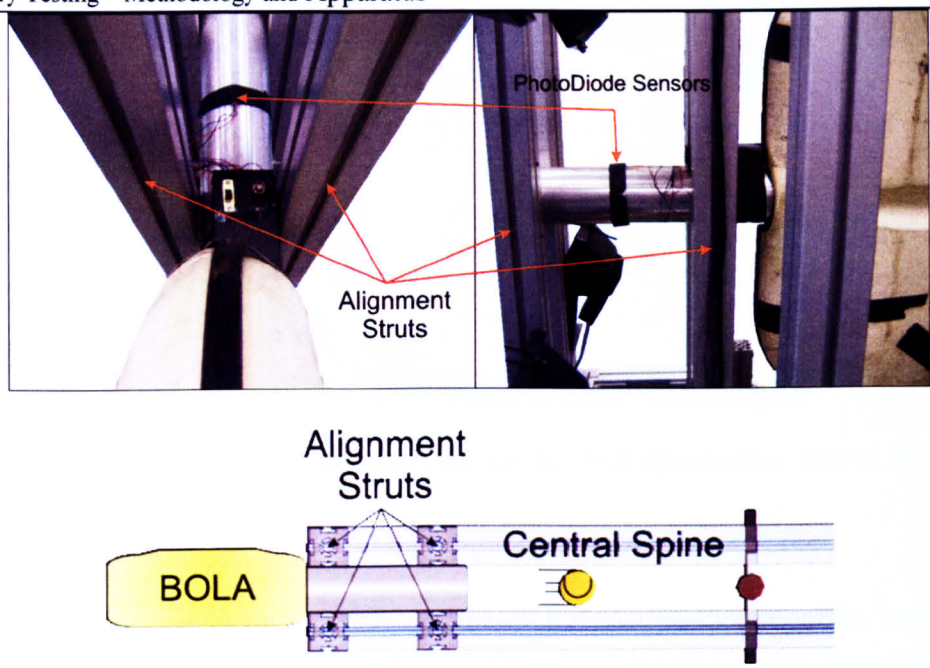

Figure 6.14. The trigger sensors and alignment struts used to increase efficiency and accuracy when using the BOLA

The central spine of the impact apparatus is also used to mount a global axes set which is accurately orientated to the BOLA cannon. A set of 3 reflective markers mounted on a movable mount is used to define two of the global axes.

Lighting

Large amounts of filament lighting were used in the impact area to fully illuminate the ball for automatic tracking and enable smaller camera apertures and faster shutter speeds (shown in green in figure 6.11). Nine 500 Watt lights were used, with a total of 4500 Watts of heat and light output the testing must be completed in batches so the racket and balls used in the testing do not become too warm, invalidating the testing. Wire grilling used at the top and front of the impact area means that convective heat can easily escape.

Figure 6.15 shows the arrangement of the high output filament lamps with regards to the impact area, lighting above and below the ball was necessary so that the ball appears as a circle in every image.

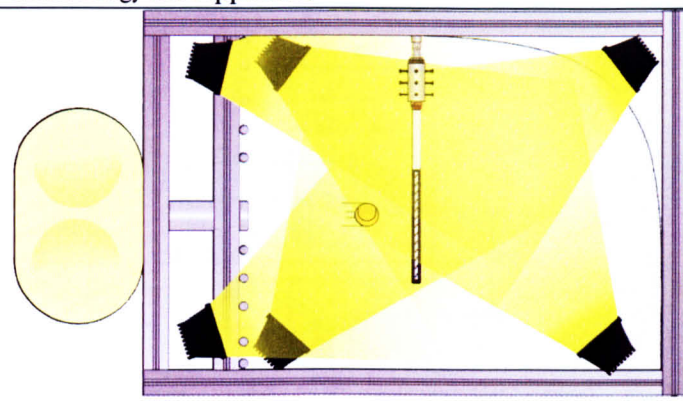

Figure 6.15. The lighting arrangement used for full ball illumination shown from a side view.

Racket Mount

The racket mount serves two purposes, firstly it allows positioning of the racket so the impact point can be varied and secondly, it generates a restrictive torque around the racket handle to simulate grip for offset impacts.

The torque is generated using a small torque limiting clutch manufactured by Cross+Morse **2007**. The clutch restricts rotational movement using a leather pad kept under pressure by two conical springs. The force exerted by the springs is altered by tightening or loosening a restraining nut. The clutch is locked in position until a torque is exceeded, causing the clutch to slip. A schematic of the clutch used is shown in figure 6.16. The capacity of the clutch is 3 - 15 Nm, DTI **1998** has recorded that the mean 'grip' torque that can be applied by a male, whilst holding an object of diameter 66mm is 9.67 Nm with a standard deviation of 2.2 Nm. Although 66mm is larger than a standard tennis grip size, this guideline value was used as an absolute maximum in selecting the appropriate clutch device.

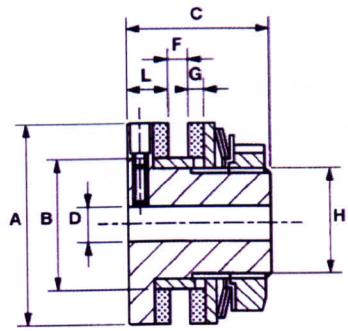

A	B	C	D	F		G	L	H	Weight
				Min	Max				
40mm	26mm	28mm	7mm	3.5mm	5mm	2.8mm	8mm	22mm	0.16kg

Figure 6.16. The design and dimensions of the torque limited clutch used in the racket mount

The clutch device was attached to a cylindrical racket mount and universal joint, the racket, once secured into the mount is free to move in every direction except around the longitudinal axis. This is equivalent to a pin jointed structure, which has been theoretically shown by Cross **1999b** to be equivalent to a freely supported racket. Freely supported rackets are used by consensus to be most equivalent to a hand-held condition (See Chapter 2 for more details).

The off-set impact position is altered by clamping the racket mount into different positions across the impact area. The longitudinal impact position is altered by changing the height of the BOLA ball projection device. A diagram of the finished racket mount is shown in figure 6.17.

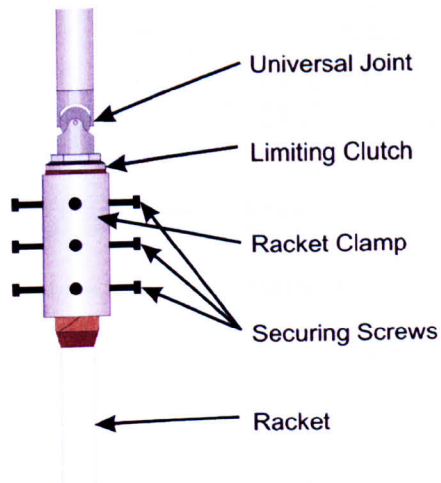

Figure 6.17. The racket mount used to restrict rotation

The torque level of the clutch is set by tightening the restricting bolt and measuring the torque using a torque wrench.

The impact area solves a number of problems that were found to exist with existing apparatus when recording off-set impacts in 3D, the accuracy of the results, and time taken to perform the tests should be greatly improved when using this equipment with an appropriate methodology.

Analysis Software

The recorded impact images required an accurate point extraction program to describe the location of specific points within the images. Without this no useful results could be obtained.

Bespoke analysis software was written to process the image files obtained from testing. An automatic image processing sequence as described earlier in the chapter automatically detects the co-ordinates of the ball's centre and outputs them as a single Excel data-sheet, listed by frame number.

The program is able to process more than one test in succession, the manual stages of the processing, such as image cropping, grey threshold and ball size definition, need only be done once prior to processing. In this way, a full days testing can be analysed with minimal manual interaction. A graphical user interface was designed to increase the usability of the program, a screenshot is shown in figure 6.18.

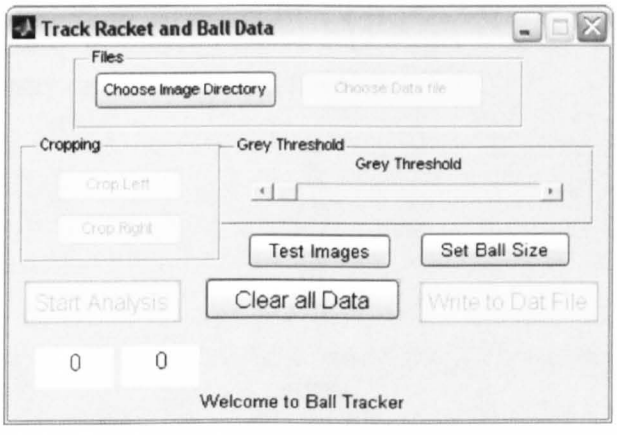

Figure 6.18. A screenshot of the ball-tracking Matlab GUI. Each button executes a separate routine, most of the processing is automatic. The two numbers in the bottom left hand corner correspond to the image number and test number being processed.

Methodology Routine

A total of six input parameters and three output parameters were chosen to be included in this impact study. The input parameters consist of the inbound translational ball velocity in three directions, the impact position in two directions and the restrictive torque around the

racket handle. The output parameters are the ball's velocity in three directions. In order for the experiment to be well determined, each of the input parameters must be varied independently. Due to the high dimensionality of the experiment, the results cannot be monitored visually. To obtain meaningful relationships from the data, a multi-variate regression fit must be used to generate an algebraic relationship which describes how the outputs vary relative to the inputs. The 'curse of dimensionality' Bishop **1995** states that as the number of variables or dimensions *'d'* increases, the size of the input domain increases exponentially according to M^d, where M is the number of variations in each dimension. It follows that the amount of data needed to accurately map the input variables to the output also increases exponentially. Varying six variables only five times each gives 15,625 separate input points, performing a test of this scale is not feasible in the scope of this overall study. The number of parameters and the number of times they are varied will have to be limited to make this experiment feasible. The input domain must still remain large enough to cover a realistic range of input parameters. When fitting data, a sufficient spread of inputs must be obtained. A multi-variate fit cannot be used to 'model' or predict experimental outcomes outside of the included input domain.

Velocity Variation

In a testing scenario where the racket is kept stationary, it is useful to state ball movements with reference to an axes set aligned to the racket prior to impact. This is equivalent to the local axes set as defined in chapter 4. Figure 5.20 in chapter 5 shows that racket velocity in the local y direction is much more significant than movement in the local x direction for the majority of players. Figure 6.19 shows how the local x and y axes set correspond to a stationary racket in a testing situation.

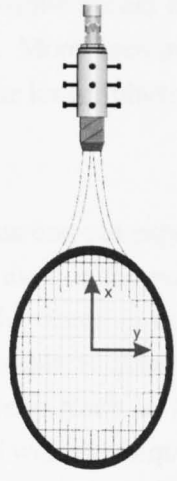

Figure 6.19. A racket held stationary vertically, and how the local x and y directions correspond to its face

By varying the inbound velocity in the local z (perpendicular to the racket) and local y directions only, the number of data input points is reduced considerably whilst maintaining

realistic input conditions. The velocity of the ball is varied by changing the settings of the BOLA ball projector. By rotating the racket so that it is oblique to the incoming ball, the ball is moving in both the local z and y directions, the magnitude of these velocities depends on the amount of racket rotation and the BOLA settings. The results in chapter 5 suggest that the local z movement of the ball should be between 20 and 40 ms^{-1}, and the local y direction between 0 and 20 ms^{-1} (taken from resultant racket and ball velocities).

Impact Position Variation

Assuming that impact effects are symmetrical around the racket's longitudinal axis, the impact position in the local y-direction need only be varied on one side of the racket. This restricts the physical distance over which the impact position needs to be varied in this direction. This is further restricted toward the throat and tip of the racket, where the racket body is less wide. If the experimental parameters were restricted to the realistic shot conditions obtained in the player shot analysis, the area of impact would be further restricted. Player's hit a relatively small region centred on the rackets node point very repeatedly, at least in practice conditions. However, in terms of creating a well conditioned set of experimental inputs, it is wise in this case to utilise as much of the racket's face as is possible. This will also enable use to validate the model at all possible impact positions. Preliminary testing revealed the inherent scatter involved with offset racket testing. A possible source of this was the impact position of the ball on the racket's face and it's variability. By widening the input domain beyond the range one might expect a player to use, any fit to the experimental outputs that can be established is much more likely to be due to a change in the input parameters than to inherent and largely unavoidable noise.

The impact position should be varied in both directions to the extent of the racket frame without making contact. The off-set position should be restricted to one side of the racket to further restrict the data input points. More increments should be tested in the local x (longitudinal) direction to account for the longer physical length being tested.

Torque Variation

It was found that the highest torque one can expect from a human grip is around 10 Nm as sourced from DTI **1998**. The clutch used on the racket mount has a capacity of around 15 Nm. Unfortunately, the simplicity of the clutch (a necessity to keep weight to a minimum) means that the torque applied at the handle is quite variable. The high speeds, shocks and impulse forces present in the impact may result in the effective torque around the handle being different from the value measured with the torque wrench.

It was decided to use zero torque, an intermediate torque of 7.5 Nm, and a maximum torque of 15 Nm, a value greater than one might expect to be seen in reality. In this way, approximate effects can be established within realistic limits of torque applied around the racket handle.

Value variation and measurement

By varying every input at specified increments, a uniform mesh of inputs is achieved; it is possible to look in singular dimensions of this mesh to visually observe the effect of one or two variables by keeping every other constant. A visual example of this would be to take a single 'slice' of a 3D surface plot in order to dismiss the effects of a single variable (as shown in figure 6.20), only in this case, six dimensions are involved rather than three.

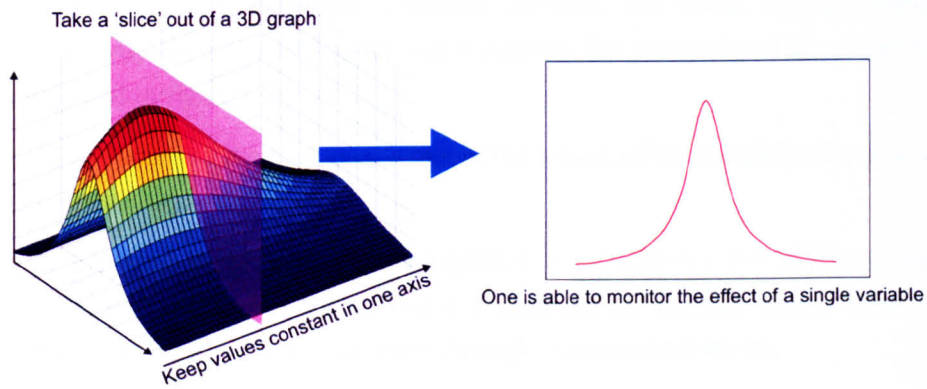

Figure 6.20. A diagrammatic explanation of how the effect of a single variable can be monitored by keeping all others constant, in this case using a 3D surface plot as an example.

In reality the situation is not as simple. It is inherently difficult to control an input variable to the required degree of accuracy, especially when the equipment dictating the input parameters are subject to inherent scatter; the rotating wheels of the BOLA controlling ball speed, its aluminium barrel controlling impact position, and a simple leather pad controlling the handle's restrictive torque. Even if specific intervals were imposed on the input parameters and each value was quoted with a confidence value of several ms^{-1}, mm and Nm for the velocity, impact position and torque respectively. The variance in the output parameters within these relatively unrealistic confidence parameters would be too large, rendering the advantage of being able to visualise a change in the input parameters worthless.

Altering the parameters within more approximate intervals and measuring them directly from the images where possible is a more accurate approach. It eliminates any possibility of visualising a relationship between the inputs and outputs directly; but means the values are stated with a higher level of accuracy. For example, if the velocity of the ball is varied four times, set at 10, 20, 30 and 40 ms^{-1} using the BOLA apparatus, a good spread of input parameters is obtained and a more accurate value of velocity can be obtained from the images using the technique discussed in chapter 4. The actual recorded values may be 12, 21.2, 31.5 and 38 ms^{-1}, eliminating any uniform variation, but increasing the confidence in the actual values.

The variables were altered as follows:

- *Velocity:* There were four ball velocity increments between 20 and 40ms^{-1}. The local y and z velocities were altered by varying the racket's orientation relative to the BOLA. When the racket was set perpendicular to the BOLA, the local y velocity is at zero, and when the racket angle was approximately 30 degrees, the y velocity was 20 ms^{-1}.
- *Impact Position:* The longitudinal position was altered 10 times at approximately equal intervals from the top of the racket to the throat (this distance depends on the racket's offset). Constituting a smaller distance, the offset impact position was altered only six times, and again was limited by the proximity of the racket frame as illustrated in figure 6.21.
- *Handle Torque:* Using a torque wrench, the torque of the clutch limiter was set to 0, 7.5 and 15 Nm.

Altering the input variables in this way gives $4 \times 4 \times 10 \times 6 \times 3 = 2880$ separate input points approximately distributed throughout a 6 dimensional domain space. This is still a considerable amount of data points to acquire through experimental means.

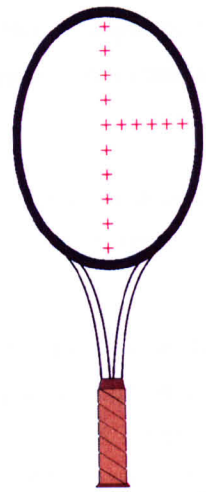

Figure 6.21. A depiction of 10 impact positions along the longitudinal axis, and six impacts along the transverse impact.

6.4 Summary

This section discussed what equipment, software and specific methodology would produce the most accurate results in a comprehensive impact test.

An impact area was designed to be small, with large polycarbonate windows on each side increasing camera visibility. Nine 500 watt lights illuminated the racket and ball evenly to allow automatic tracking. A racket mount which used a simple clutch to create a torque around the racket's handle was used to mimic hand grip. The restrictive torque was part of an

investigation on the effects of handle grip on ball rebound characteristics. A BOLA ball projection device was modified with an aluminium barrel, allowing accurate projection and reliable camera triggering.

A custom Matlab routine employs the automatic ball tracking process outlined in section 6.3.2. Impact images recorded using high speed cameras were analysed to automatically obtain a series of 2D co-ordinate points. These were used to give the ball's 3D co-ordinates, associated velocity and impact point.

When conducting an experiment, it is important to carefully control the variation in input parameters. The relatively large amount of separate parameters means that an experiment quickly becomes infeasible if each parameter is varied unnecessarily.

The ball velocity was altered in the local y and z directions from 0 to 20 and 20 to 40 ms^{-1} respectively, four times in each direction.

The impact position was altered 10 times along the longitudinal direction, and 6 times in the offset direction.

The torque at the handle was altered three times at 0, 7.5 and 15 Nm.

This methodology gave 2880 different input points and hence 2880 recorded impacts. With around 50 recorded images per impact, this translates as 144,000 images.

6.5 Chapter Summary

This chapter describes a methodology for a comprehensive impact test. This test can record impacts in three dimensions with six different input parameters; ball velocity, impact position and racket torque.

A series of preliminary tests were executed in order to uncover methodological issues and avoidable sources of error associated with such a test. These revealed considerable experimental scatter, apparatus limitations and a need to quickly and accurately extract ball co-ordinates. Further investigation into these areas enabled the design of specific experimental equipment, automatic tracking software, and a more specific methodology.

The impact apparatus, manufactured from Bosch Rexroth aluminium extrusions is smaller than that used in the preliminary investigations, has increased visibility and is designed specifically for an automatic tracking method.

Careful consideration of the experimental parameters and how they should best be varied resulting in an experimental procedure giving 2880 tests.

The apparatus, software and methodology designed in this chapter can be used to give a series of experimental data points. These points can be analysed with appropriate fitting techniques to reveal relationships between the experimental input and output parameters. This is a powerful tool when trying to experimentally validate a six degree of freedom predictive model.

7 Laboratory Testing – Testing and Results

7.1 Introduction

An impact area was designed in order to conduct a series of impact tests intended to validate a six degree of freedom predictive model. Using the methodology described in chapter 6, a series of impacts were recorded using high speed video and the 3D methodology used throughout this study. Six input parameters and three output parameters were obtained from the recorded images to a high degree of accuracy using calculations outlined in chapter 4. These parameters included the inbound and outbound ball velocity, the ball impact position and a restrictive torque around the racket handle. Multi variate regressive fitting techniques (Seber and Wild **2003**) such as polynomial regression and neural networks were used to find algebraic relationships between each variable. An accurate regressive fit is a powerful tool for visualising and investigating trends between individual input and output parameters. This chapter includes such an investigation. The physical relationships uncovered during this investigation provide invaluable information with regards to the design of a predictive model. The results obtained from a multi variate fit can also be used to validate such a predictive model. This fit would allow accurate and limitless comparison between the model outputs and those obtained through experiment.

7.2 Aim

Using a multi-variate fit, this chapter aims to obtain comprehensive results from the methodology and apparatus designed in chapter 6. The multi-variate fit will allow accurate comparison of the output velocities in the y and z direction with each of the six input parameters.

7.3 Methodology

7.3.1 Experimental Procedure

An impact test as described in chapter 6 was carried out using 3D videogrammetric methods to track the ball. Two Phantom V4.2 cameras were used to record 900 ball racket impacts. Slazenger Wimbledon 2004 tennis balls were used in the test. Each was marked using a textile marker to track their orientation and spin.

It was thought that any offset effects resulting from handle grip would be most apparent when using a very stiff racket and hence Head™ Ti S6 rackets were used. The racket stiffness was obtained from a large database of racket data located at USRSA **2007**. The Ti S6's frame stiffness of 76 puts it much higher than the typical value of 60 for graphite framed rackets. The racket stiffness is quoted in Babolat RDC units, a propriety unit used by the Babolat Racket Diagnostics Centre (figure 7.1). The Babolat RDC is a device which measures the weight, frame stiffness, stringbed stiffness, balance point and swingweight of a tennis racket.

The RDC unit is primarily used for comparison and is given as a value between 0 and 100. The racket was strung at 272 N tension using a Prince™ 3000 stringing machine.

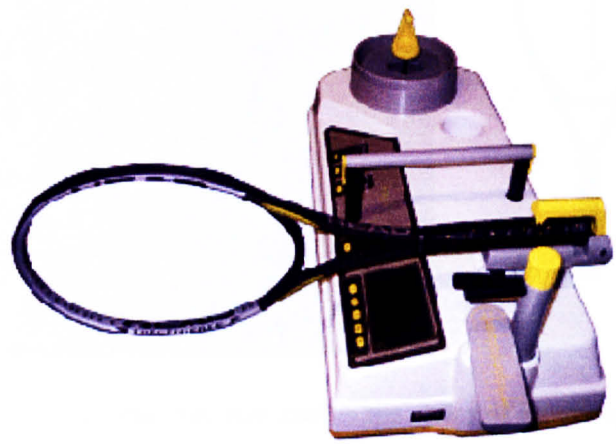

Figure 7.1.The Babolat Racket Diagnostics Centre

The racket was equipped with reflective markers in order to track its orientation prior to impact and calculate a local axes set aligned to the racket face. Using this information the ball's velocity was transformed into local co-ordinates. The racket markers also enabled the impact position to be calculated accurately using the bisection method outlined in chapter 4.

A total of 900 impacts were recorded as opposed to the proposed 2,880 because of the following methodological constraints:

- The number of impact positions in the transverse axis was limited when performing impacts with an angled racket. This was due to the risk of hitting the frame.
- High speed, high torque offset impacts also tended to fracture the racket frame. After two rackets had failed in this way, it was decided to limit the testing further to avoid exhausting the supply of Ti S6 rackets which could be used for testing.

The 2D ball positions were extracted from the impact images using the automatic tracking software discussed in chapter 6. The initial orientation of the racket was necessary in order to calculate the impact position. The initial orientation was calculated from the positions of the racket markers. The racket markers were tracked manually for each impact. It was only necessary to extract the marker positions from a single image, therefore the manual extraction of the racket markers' co-ordinates was not prohibitively time consuming.

The 2D co-ordinates were re-projected into 3D space according to a global axes set defined at calibration as in figure 7.2.

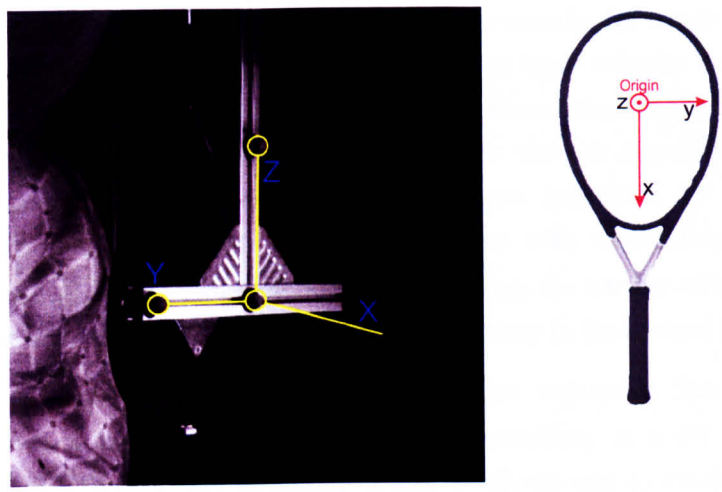

Figure 7.2. The global and local axes sets used in the series of impact tests.

The ball velocities and impact positions were calculated from the reprojected 3D points according to the methodology outlined in chapter 4.

In total 878 successful impacts were obtained from the testing. Of these, 22 tests were unusable due to poor images or methodological mistakes. The ball velocities were transformed into local co-ordinates using the racket marker co-ordinates extracted from the impact images.

7.3.2 Data Fitting

Figure 7.3 shows the outbound velocity in the local z direction according to the longitudinal impact position for every recorded impact.

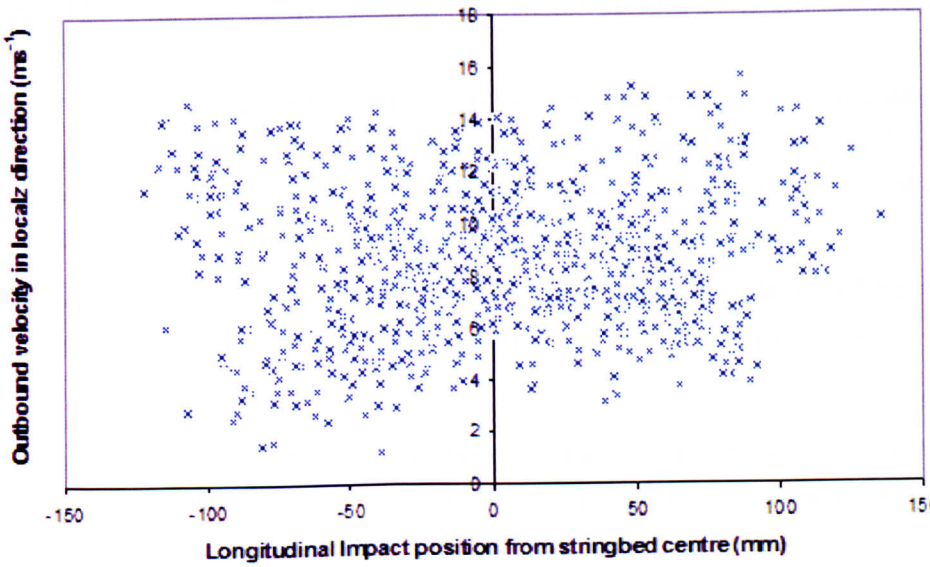

Figure 7.3. A plot of the outbound ball velocities in the local z direction against the longitudinal impact position. Every recorded data point is included.

Figure 7.3 shows clearly the difficulty in obtaining meaningful trends from the results. The experiment contained 6 input parameters in total; the input velocity in 3 directions, the impact position in 2 directions and a restrictive torque around the handle. In a 2D plot it is impossible to view more than one parameter at any one time. It is possible to filter these results by artificially restricting the input parameters not accounted for in the plot. For example, it might be useful to only include data points with inbound velocities in the z direction of 30 ms^{-1} ±2.5 ms^{-1}. This method severely reduces the number of usable data points and introduces an unavoidable noise related to the uncertainty in the omitted parameters.

Appendix B describes and evaluates multi-variate regressive fits. A multi-variate regressive fit gives a predicted experimental value according to a set of chosen input parameters. An advantage of this technique is that it allows one to choose a set of input parameters which were not present in the experiment. The multi-variate fit accounts for every included data point at the given values. This is in contrast to filtering the results, which reduces the included data points and introduces scatter.

A multi-variate fit uses an equation, including a set of weighted terms to predict experimental values. With respect to this experiment, the multi-variate fit predicts outbound velocity in the local y or z direction according to a set of six input parameters. The input parameters are the same as those used in the experiment. These are; the inbound velocity in three directions v_{ix}, v_{iy} and v_{iz}, the impact position in two directions i_{px} and i_{py} and a restrictive torque around the handle T. It was found that a polynomial fit of the second order was the most appropriate and accurate. This resulted in an equation of the form:

$$v_{po} = \left(A + B \cdot v_{ix} + C \cdot v_{iy} + D \cdot v_{iz} + E \cdot i_{px} + F \cdot i_{py} + G \cdot T\right)^2 \qquad [7.1]$$

where the capital letters A, B, C, D, E, F and G are a set of weights and v_{po} is the predicted output velocity.

A MATLAB command specifically created to generate multi-variate fits calculated the relative weighting of all 28 terms which result from an expansion of equation 7.1. The full text and operation of the MATLAB command *polyfitn* which was used in this case is shown in appendix C.

The accuracy of the results given by a multi-variate fit is dependent on the accuracy of the experimental inputs and how well they are distributed within the input domain.

7.3.3 Input distributions

This sub-section investigates the distribution of the input parameters over each separate input domain. An even distribution is associated with a well-determined and accurate multi-variate fit.

Impact Position

Five concentric elliptical bands, centred on the geometric stringbed centre are used to measure the frequency of impact on the stringbed face. Figure 7.4 shows the density of impact along the racket face sorted by separate elliptical area.

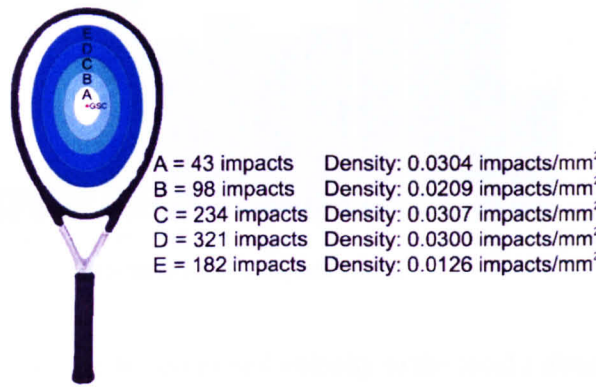

Figure 7.4. The distribution of impact density upon the racket face, as measured from the geometric stringbed centre.

As the area of the ellipse consecutively increases, so does the frequency of impact. The density of impact stays relatively constant suggesting a good spread. The impact density decreases in the outermost ellipse, due to the increased likelihood of frame impact.

The accuracy of the impact position is high because it is independent of the repeatability of the projection device. The ball is well defined within the impact images with a pixel/mm ratio of around 1:1. Given that the ball position is tracked automatically, the manually tracked racket marker position will be subject to the most error. This is due to the human interaction and difficulty in tracking the square markers' centres. Repeatedly tracking racket markers and reprojecting the distance between them shows a maximum error of ± 2 mm.

Ball velocity

Figure 7.5 shows the local *z* direction ball velocity (perpendicular to the racket face) frequency distribution. The frequency of impacts between -34 and -18 m/s is high (over 50) being suitable for a multi-variate fit. A slight decrease in the frequency of the velocities between -36 and -42 m/s reflects the caution that was exercised toward the end of testing after several racket failures.

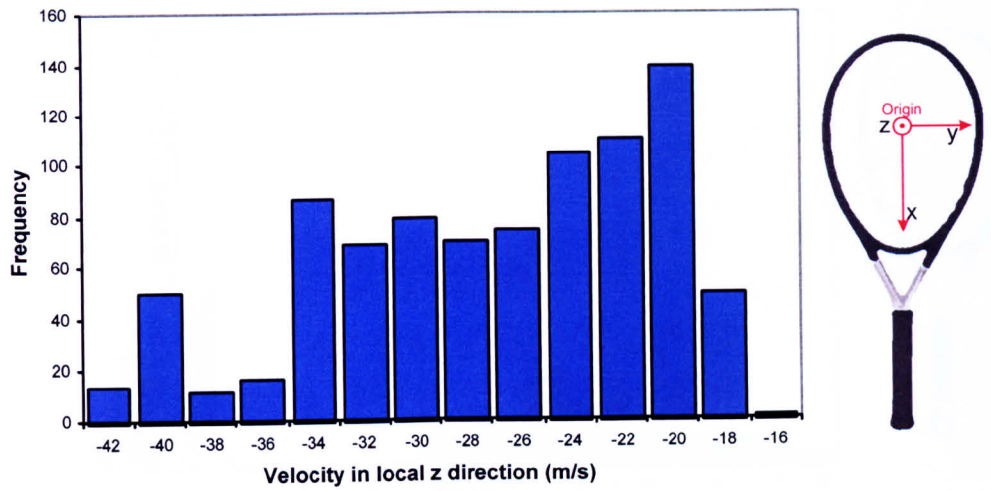

Figure 7.5. A frequency distribution of ball velocity in the local *z* direction

Figure 7.6 shows the frequency histogram of the inbound velocity in the local *y* direction. Two separate distributions can clearly by seen. The first, which constitutes the larger proportion, is centred on 0 ms^{-1}. The second is centred on 11 ms^{-1}. These two distributions represent the following separate sections of testing:

1. The first involved setting the racket perpendicular to the inbound ball and controlling the ball speed via the BOLA. This varied the local velocity in the *z* direction without significantly affecting the velocity in the local *y*. The variation in inbound ball velocities in this distribution comes from slight variations in the racket's orientation. Small rotations away from the perpendicular at impact result in the small deviation away from the mean seen in this distribution.

2. The second distribution results from purposefully setting the racket at an oblique angle to impact. Varying the inbound ball speed changes both the local *y* and *z* velocities. A wider distribution is seen in this case because it was necessary to get a good distribution of local *y* velocities. The upper velocity is limited in this case by the angle of the racket. If the racket was set too obliquely the moving ball was obstructed from the camera's field of view.

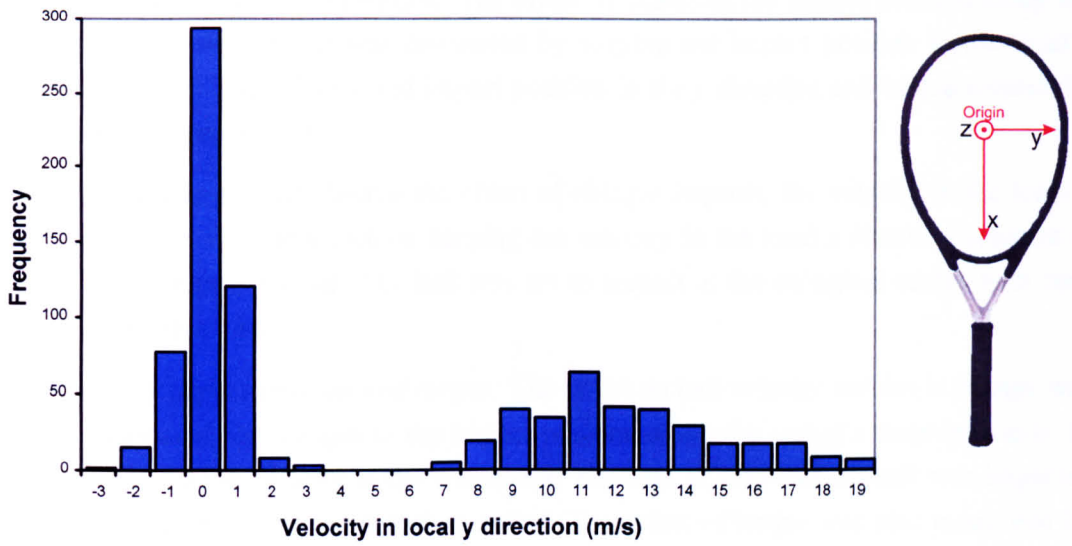

Figure 7.6. A frequency distribution of ball velocity in the local *y* direction

A good distribution of *y* velocities is seen from 7 to 19 ms^{-1} regardless of the high concentration of impacts at low values of *y* velocity (-3 to 3 ms^{-1}).

The positions and velocities are calculated automatically from the recorded images. The position of the ball was generally accurate to within a millimetre; it is therefore a very conservative estimate to state the velocity values to within ± 0.1 ms^{-1}. This accounts for further possible errors in the calibration software, automatic tracking algorithm and any defects in the recorded images.

Torques

Three levels of torque were used in the experiment, they were assumed to be at 0, 7.5 and 15 Nm. The value was measured before impact at low dynamic loading and it is unknown whether this value differs from the actual value during impact. The high impulse during impact may affect the effectiveness of the clutch. This potential error will be visible in the recorded results.

7.4 Results:

The response of the multi-variate fit is used to generate appropriate results. The multi-variate fit is able to provide a predicted experimental output when given a series of experimental input parameters. By keeping every parameter but one constant, the experimental response of the variation in a single parameter can be observed.

The experimental response of changes in the following parameters will be shown:

- *Impact velocity:* To observe the response of the experiment at different impact velocities, the local *z* velocity was varied whilst impacting the stringbed centre, at zero restrictive torque.

- *Longitudinal impact location:* The effect of changing the impact position along the racket's central axis was monitored by varying the impact position in the local x direction. The velocity and impact position in the y direction and torque around the handle was set to zero.
- *Impact angle:* To observe the effect of oblique impacts, the velocity in the local y direction was varied whilst keeping the velocity in the local z direction constant at an appropriate value. The ball was set to impact at the stringbed centre with zero restrictive torque.
- *Offset impact position and torque:* The effect on ball velocity and angle change was monitored for changes in the impact position along the racket's transverse axis. In this case the velocity in the y direction was kept at zero and the ball was impacted transversely from the stringbed centre. The effect of torque was also monitored by changing the transverse impact position at torque levels of 0, 7.5 and 15 Nm.

In each case, the values of every parameter v_{ix}, v_{iy}, v_{iz}, i_{px}, i_{py} and T will be given as according to equation 7.1.

7.4.1 Impact Velocity

Figure 7.7 shows the experimental response for a change in the inbound z velocity. The uncertainties in the predictions from the multi-variate fit are shown as solid lines. They represent two standard deviations from the mean. These were generated using the MATLAB function used to calculate the multi-variate fit. The function calculated the weighting of 28 separate functions. Each of these weights were given uncertainty values which were then used to generate the solid lines seen in figure 7.7.

Inbound velocity x (ms^{-1})	Inbound velocity y (ms^{-1})	Inbound velocity z (ms^{-1})	Impact position x direction (mm)	Impact position y direction (mm)	Torque (Nm)
0	0	-15 to -40	0	0	0

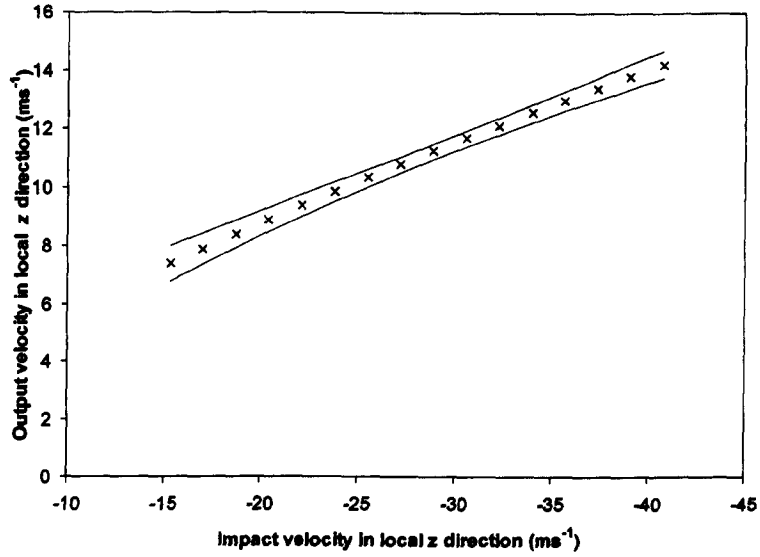

Figure 7.7. The experimental response for a change in the inbound local z velocity as predicted by a multi-variate fit. The uncertainty in the results is shown as two solid lines.

Figure 7.7 shows a roughly linear increase in the outbound z velocity for an increase in the inbound z velocity.

7.4.2 Longitudinal Impact Location

Figure 7.8 shows the experimental results as the longitudinal impact position changes. An impact position of 0 corresponds to an impact on the stringbed centre. Negative values denote impacts toward the tip. Positive values denote impacts toward the racket throat.

Inbound x velocity (ms^{-1})	Inbound y velocity (ms^{-1})	Inbound z velocity (ms^{-1})	Impact position x direction (mm)	Impact position y direction (mm)	Torque (Nm)
0	0	-30	-110 to 115	0	0

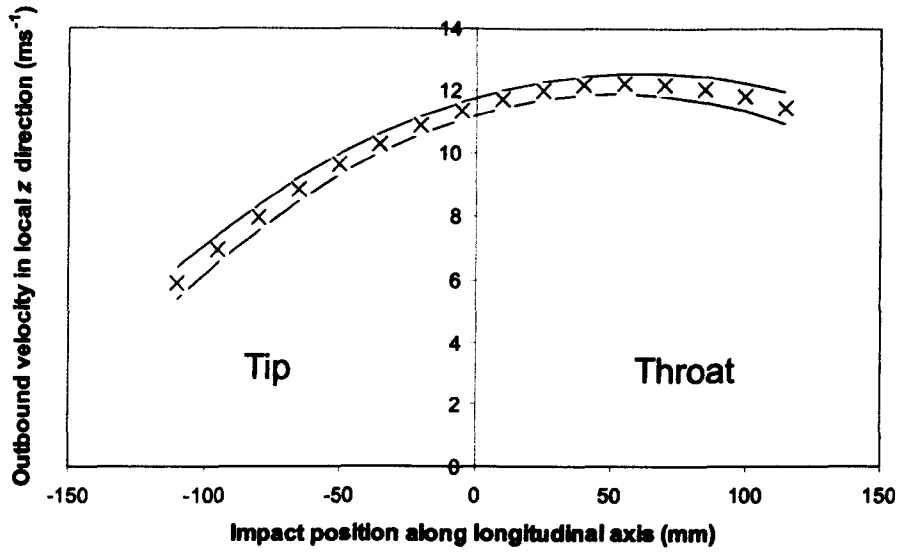

Figure 7.8. Predictions of the experimental outbound z velocity according to the longitudinal impact position.

Figure 7.8 shows a continual increase in outbound velocity for impacts from the racket tip towards the stringbed centre. This behaviour is as expected. The experiment involved hitting a stationary racket with a moving ball. In this situation, the post-impact ball velocity is maximised by maximising the effective mass of the impact point. The centre of mass of a racket is typically situated around the throat. As the impact point moves from the tip towards the throat, the outbound ball velocity correspondingly increases.

The increase in rebound velocity from the tip to the stringbed centre seen in figure 7.8 does not continue toward the throat. This is despite a continual increase in effective mass. The impact causes vibration in the tennis ball and racket frame. The vibration in the tennis ball is relatively independent of impact position, whilst the vibration in the racket frame is strongly dependent. Impacts towards the racket throat cause large amounts of frame vibration. This frame vibration constitutes a larger proportion of the impact energy as its magnitude increases. As such, the rebound velocity in the throat region of the racket is not as great as one might expect. Examples and further explanation of this behaviour is included in chapter 2.

7.4.3 Impact Angle

Table 7.9 shows the input parameters used when validating the inbound and outbound impact angle. This corresponds to an inbound angle of -30 to 15 degrees.

Inbound x velocity (ms^{-1})	Inbound y velocity (ms^{-1})	Inbound z velocity (ms^{-1})	Impact position x direction (mm)	Impact position y direction (mm)	Torque (Nm)
0	-8 – 17	-30	0	0	0

Table 7.9. The range of input parameters used when validating the inbound and outbound impact angle.

Figure 7.10 shows the results for the experiment with regards to the outbound velocity in the local z direction. As the velocity in the local y direction increases (increasing the inbound angle) the rebound velocity in the local z direction stays relatively constant. This is as one might expect, the inbound velocity in the z direction is constant over the input range. This shows that for a stationary racket, the y and z velocities are relatively unrelated. An increase in the inbound y velocity does not result in any significant change in the outbound z velocity. An increase in y velocity would be associated with an increase in ball spin and outbound angle. When forming a predictive model it seems that the rebound and spin models can be kept relatively separate.

The uncertainty in these results is largest towards the edge of the predictive range. This is most probably due to a relative scarcity of results for these inputs.

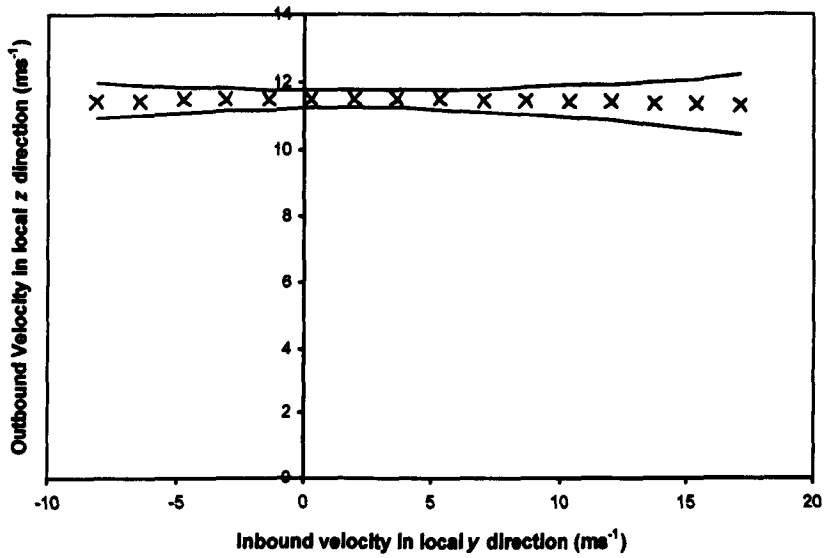

Figure 7.10. A plot of the outbound velocity in the z direction for a range of inbound y velocities.

Figure 7.11 shows the results with respect to the outbound velocity in the local y direction. As the inbound velocity in the y direction increases, a linear increase in outbound y velocity is observed. Goodwill et al. **2006** showed that at inbound angles of around 60° the ball slips along the racket stringbed. For inbound angles of around 40° the ball rolls along the racket stringbed. This suggests that the transition between slipping and rolling exists somewhere between these two inbound angles. The inbound angles seen in the experiment are

below both of these values and reflect the inbound angle values obtained during the player testing in chapters 6 and 7. The linear increase seen in the results suggests that no transition between slipping and rolling occurs over the range of angles seen in the results.

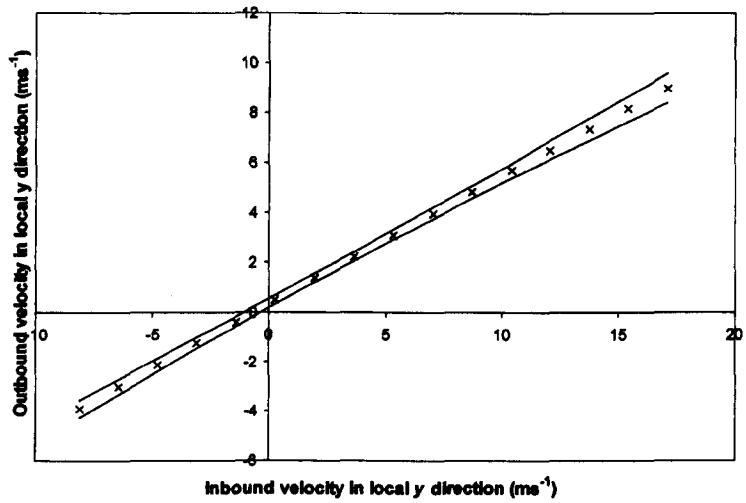

Figure 7.11. A plot of the experimental data with regards to inbound and outbound velocity in the y direction.

If instead of velocity in the y direction, the inbound and outbound impact angle is plotted, a similar relationship is revealed. A plot of the inbound and outbound angle, as in figure 7.12a reveals that the outbound angle is consistently larger than the inbound angle. This is the opposite of what one might expect in a standard impact. Figure 7.12b reveals why this might be the case. The local axes remains fixed during impact yet the racket rotates, meaning that the outbound angle is consistently larger.

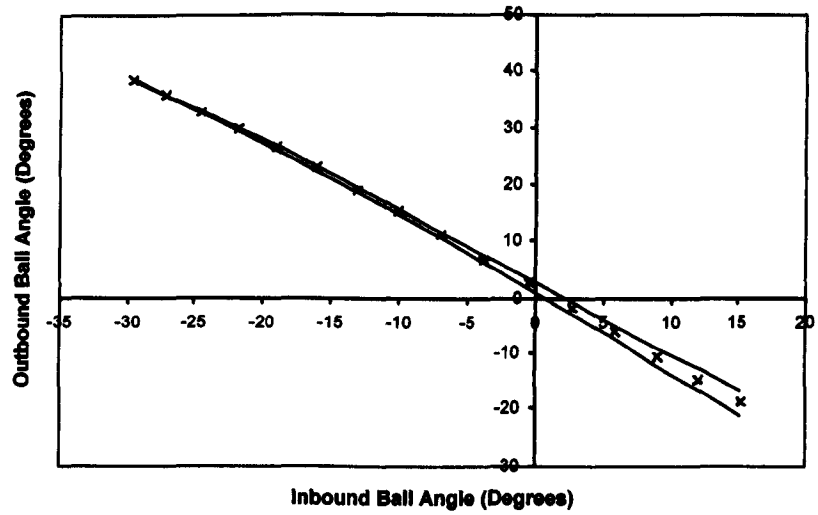

Figure 7.12a. A plot of the inbound and outbound ball angle in degrees.

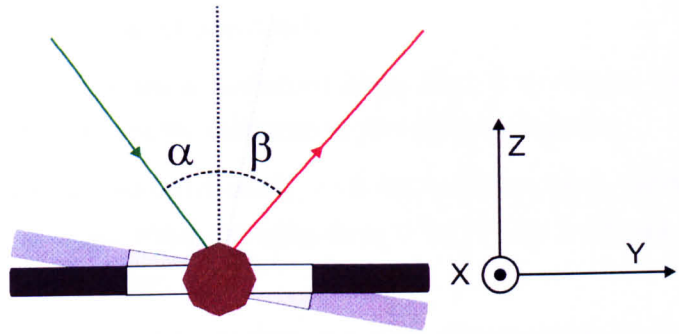

Figure 7.12b. The outbound angle in figure 7.12a is consistently larger than the inbound. The racket rotates during impact, but the local axes remains fixed. This means that relative to the fixed axes the angle β is consistently larger than α.

7.4.4 Transverse Impact Position and Torque

To explore the effect of off-set impacts, the impact position in the transverse direction was altered whilst monitoring the effect on the outbound angle. The effect that torque around the racket handle has on outbound angle was also included.

Figure 7.13 shows the experimental input parameters and experimental results for a series of impact positions and three torque values.

Inbound x velocity (ms^{-1})	Inbound y velocity (ms^{-1})	Inbound z velocity (ms^{-1})	Impact position x direction (mm)	Impact position y direction (mm)	Torque (Nm)
0	0	-30	0	0 to 64	0 to 15

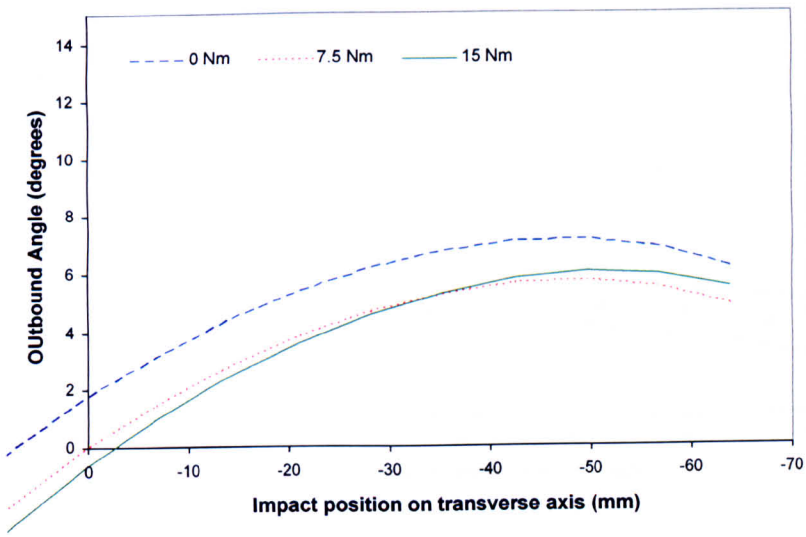

Figure 7.13. A comparison of the experimental response at three levels of torque.

From figure 7.13 we can see two trends:

1. A continuous increase in outbound angle from 0 to 50 mm off the central axis. Above 50 mm off set, the outbound angle begins to decrease.
2. A reduction in outbound angle with the addition of a restrictive torque. The reduction in angle when changing from 0 to 15 Nm is around 2° at all positions along the tennis racket.

The systematic difference exists even at a value of 0 mm from the transverse axis. This result does not follow reasoned thinking. One would not expect angular deviation for impacts along the racket's central axis. It is possible that a restrictive torque stabilises the rotation of the racket. In reality a number of outbound angles will result from an impact at the stringbed centre with zero restrictive torque. The multi-variate fit gives the most representative value due to this scatter. This can result in the apparent result seen in figure 7.13.

As the impact moves away from the central axis, the force resulting from impact acts to rotate the racket. This rotation results in a deviation of the ball's trajectory away from the normal, resulting in the trend seen above. The outbound angle is a maximum at around 50 mm from the central axis and begins to decrease above this value. The reason for this is revealed by observing the separate trends in the outbound y and z directions.

Figures 7.14 and 7.15 show the outbound ball velocities in the y and z directions respectively for zero restrictive torque around the handle. This is with the experimental input parameters seen in figure 7.13.

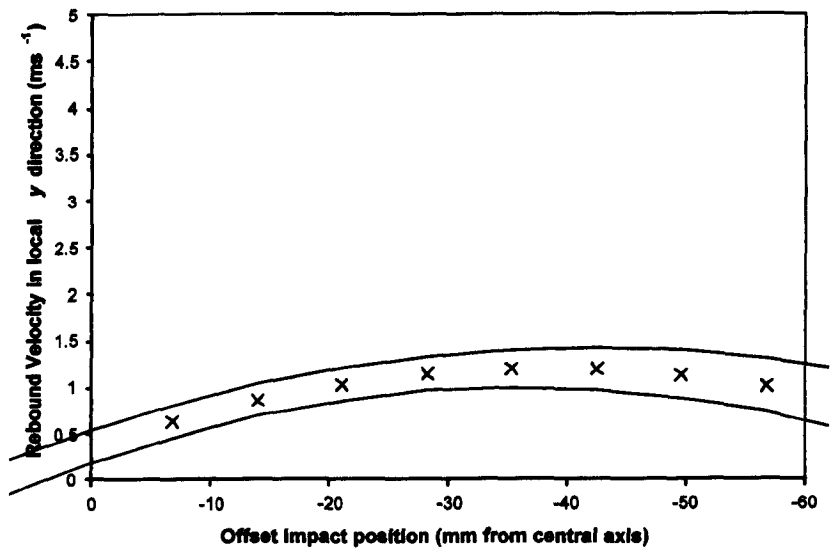

Figure 7.14. The outbound velocity in the y direction according to the offset impact position away from the central axis.

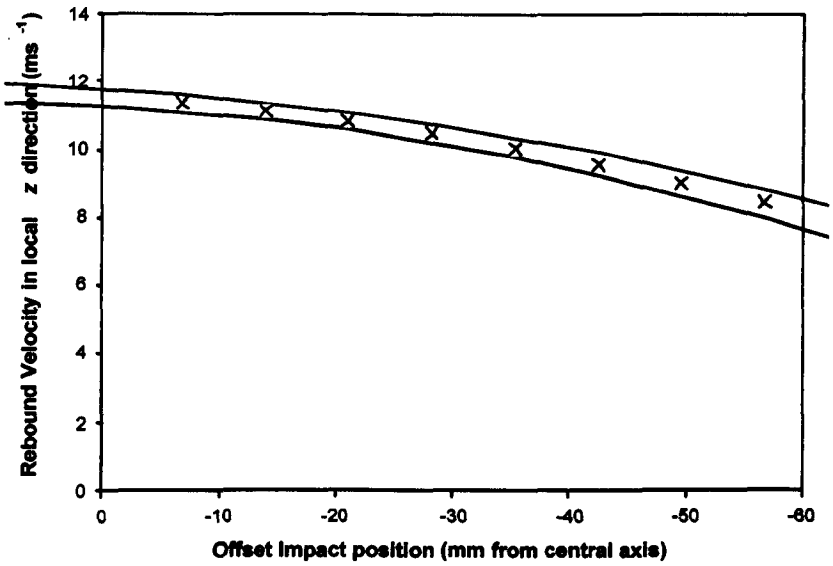

Figure 7.15. The outbound velocity in the z direction according to the offset impact position away from the central axis.

The effective mass of the impact point decreases rapidly as the impact moves away from the central axis. Figure 7.15 shows that the velocity continually decreases as the impact position moves away from the central axis. The force involved in the impact lowers as the impact moves away from the central axis. The ball and stringbed deform less and the change in velocity is reduced. This reduced force results in a lower resultant ball velocity. Towards the very edge of the racket frame the resultant ball velocity is greatly reduced. This is clearly shown in the *z* direction and also in the *y* direction which begins to reduce beyond 50 mm offset from the central axis. There is another possible factor which might be responsible for the lowered velocities. An internal study by Whyld **2004** has shown that the stringbed has a correcting action away from the central axis. This is explained in further detail in chapters 2 and 9. If isolated, the stringbed has been shown to alter the trajectory of ball hit along the transverse axis. This results in the ball leaving the stringbed travelling back to wards the stringbed centre. This effect could be a contributory factor in the reduction of the *y* velocity towards the edge of the racket. This subject will be discussed in more detail in chapters 8 and 9.

Figure 7.13 shows very little difference between 7.5 and 15 Nm of torque. A value of 15 Nm is higher than the maximum level of grip one might expect from a player. The results seen in figure 7.13 suggest that no discernible advantage is gained from gripping higher than 7.5.

7.5 Discussion of Results

A multi-variate fitting technique is clearly an effective way to observe the results obtained in the laboratory testing described in chapter 6. It allows individual input and output

parameters to be compared visually with a high degree of accuracy. This chapter has also shown that the range of input parameters is sufficient to provide a high degree of prediction accuracy.

The response of the experiment has been observed for a change in several input parameters:

- Impact velocity
- Longitudinal impact location
- Impact angle
- Offset impact position
- Torque

The physical response of a typical ball/racket impact is illustrated by the plots given in this chapter. It has been observed that frame vibration dissipates the energy of an impact towards the racket throat. The velocity is lower than one might expect closer to the racket's centre of mass. For the angles tested, the ball does not change the mode of rolling between slipping or rolling. As the velocity in the y direction increases, the outbound velocity in they y direction increases linearly. It was also shown that the z velocity is relatively independent of increase in the y velocity.

This information is invaluable when creating a predictive model. Physical relationships will dictate how force and spin are generated on the racket stringbed. Knowing that the generation of perpendicular force and spin is relatively independent means that two sub-models can be used to determine the individual outputs.

It is clear from these results that frame vibrations affect the outbound ball velocity significantly. Modelling frame vibrations negates the possibility of a rigid body model. The added complexity this would introduce in a model would have to be weighed up against the extra accuracy which would result.

It has been shown in this chapter that a torque around the racket handle does act to stabilise the outbound ball. That is, to reduce the outbound angle away from the perpendicular. Very high levels of restrictive torque are not seen to have a significant effect over more moderate amounts of restrictive torque. This result is inconclusive; the torque level is not measured directly but prior to impact at very low dynamic loading compared to the high level of dynamic loading at impact. A more accurate method of measuring the impact torque is necessary to prove this result conclusive.

This section has displayed the effectiveness and clarity a multi-variate fit can provide. The trends observed have revealed a variety of physical relationships for a number of different input parameters. These relationships can be used as guidelines when creating a

predictive model based on such physicality. The multi-variate fit can also be used to validate the results given by such a model.

7.6 Summary

This chapter displayed the experimental results obtained in chapter 6. A multi-variate fit was applied to the 878 well distributed data points which had six independent input parameters and two output parameters. It was found that:

- An increase in the impact velocity resulted in a linear increase in the outbound ball velocity.
- As the ball impact position moved towards the racket throat, racket frame vibration increased resulting in lower than expected rebound ball velocities.
- A change in the inbound ball angle resulted in a linear change in the outbound ball angle. It was concluded that this was due to a single phase of spin (rolling or slip) occurring throughout the range of inbound angles.
- The levels of torque and the effect this has on the ball rebound angle are not yet conclusive. A more accurate method of measuring the torque levels during impact is required to fully ascertain a relationship between grip and stability.

The physical relationships which have been displayed in this chapter provide useful guidelines on how to construct a physically based predictive model.

8 Modelling Reality - The Development of a Predictive Model

8.1 Introduction

Predictive models are used primarily to monitor the effect of changing a system's parameters. A predictive model can be created from a series of experiments, or from using known physical principles to model different aspects of the system.

In the experimental method, multi-variate techniques are used to generate a predicted value by tracking the effect of a change to the input parameters.

A physical model assumes aspects of a system's behaviour so it can be represented with Newtonian equations of varying complexity.

An experimental approach will always contain experimental errors and soon becomes impractical in size as the number of input parameters increase (see chapters 6 and 7). A physical model will always contain assumptions that distance the model's results from reality; the fewer assumptions made, the more complex the model becomes. A physically based model requires experiments to form the basis of the model's assumptions and to validate its results.

The advantage of a model based on physical systems is the understanding that it grants of the system it is attempting to model. Levels of complexity can be added to better represent aspects of the system, and with better understanding comes the ability to modify or augment aspects of a system to improve performance. A prediction based solely on experimental results gives no insight into physical relationships and how individual modifications might affect performance.

In this study both methods are explored. Predictions based on a series of experiments (chapters 6 and 7) will be used to form the validation of a six degree of freedom, physically grounded tennis impact model.

In the past, individual aspects of a tennis impact have been modelled in various ways (see literature review). A comprehensive six degree of freedom model should include every aspect of a tennis impact to some extent, effective in 3 dimensions, including:

- Ball forces, deformations and rotations
- Stringbed forces and deformations
- Racket frame forces, accelerations and rotations
- Ball, stringbed and racket characteristics

Once all of these aspects are modelled according to robust Newtonian mechanics, the results can be validated using the experimental fit described in the previous chapter.

8.2 Aims

This chapter shows the development of a predictive model based on Newtonian mechanics;

The model should have:

- Six degrees of freedom and include aspects of the ball, stringbed and racket frame
- The ability to alter the characteristics of the racket, ball and stringbed which will dictate the response of the model and allow the effects of different equipment to be monitored.

Each of these model aspects should be assessed and compared to the experimental results obtained in the previous chapter.

8.3 Model Overview

Before any singular aspect of the model is described in detail it is necessary to outline how the overall model will function, how each aspect will interact and how the calculations governing its behaviour will be executed.

8.3.1 Model Orientation

A global and local axes set are essential in the formulation of a six degree of freedom model. Global axes keep a constant frame of reference from which to observe subject translations and rotations. A local axis fixed to a subject facilitates the calculation of locally based effects such as spin and force generation.

Like the 3D methodology used throughout this testing, the local axes set is fixed to the racket face and initially aligned to the global axes set, which in the absence of any larger frame of reference is arbitrarily orientated.

8.3.2 Sub model interaction

The model will consist of three constituent segments or sub-models which will incorporate all of the essential aspects listed in the aims:

- Ball/stringbed deformation
- Ball/stringbed spin
- Racket frame

Dividing up the model in this way allows each segment to be discussed in turn. From a logistical standpoint it allows modifications to be made to an individual segment without affecting another.

If each sub-model is considered as an element of a flowchart, the output of one element becomes the input of another. More generally, the interaction between the ball and stringbed generates a force which creates ball and racket accelerations and rotations. The relative ball

and racket velocities, deformations and displacements dictate the magnitude of these governing forces which, in turn affect the behaviour of the ball and racket. Figure 8.1 illustrates this using a flowchart.

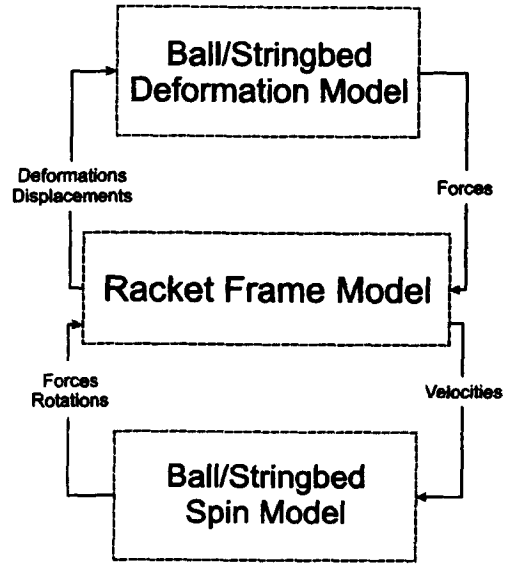

Figure 8.1. A flowchart illustrating how each of the three sub-models interacts with a series of individual inputs and outputs

A cyclical process is created and an iterative time-step approach means that the outputs from one instant are inputted to the next, allowing the state of the model and its behaviour to be monitored at any instant.

A time-step approach assumes that the model forces and accelerations are constant over a small time period. Given a small enough time-step, very complex relationships and behaviours can be modelled.

The ball deformation and spin sub-models interact with the racket frame model via their outputted forces. These forces act locally on the racket frame to produce racket movements and rotations within the global framework.

Ball Spin Model

If we assume that the forces generated during ball spin act entirely in the plane of the stringbed we can limit the forces generated from spin effects to the local x- and y-directions (as illustrated in figure 8.2.). This is not an unreasonable assumption. Cross **2002a** noted a small off-set tangential force during a ball bounce, but this is small enough to be discounted. The over-spinning effect this tangential force accounts for can be re-created in other ways (see the specific section on the ball spin model later in the chapter).

Ball Deformation Model

By assuming the stringbed deforms uniformly over the entire racket face, we can assume that the force generated by the deformation model acts perpendicularly to the racket face, or in the local z direction, as illustrated in figure 8.2.

As the racket frame translates and rotates, these forces will continue to act in the same respective local directions. The ball spin and deformation models determine the magnitude of these forces. The racket frame model determines the orientation of the racket frame and the direction in which these forces act globally. In this way, the post-impact ball velocity and trajectory in three dimensions can be determined using a time-step method based on Newtonian mechanics.

The following sections discuss the characteristics of each sub-model and how they interact to form a complete six degree of freedom model.

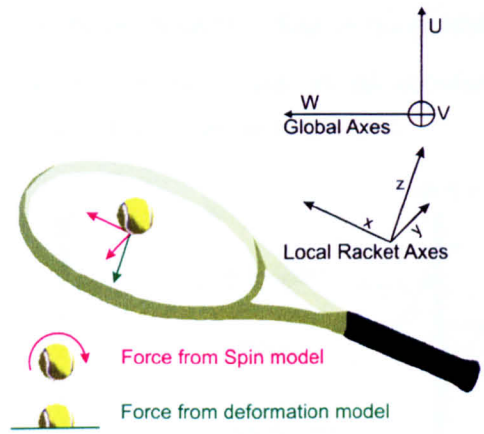

Figure 8.2. A depiction of the ball spin and deformation models acting locally on the racket frame model. The forces from each model acting in separate local directions.

8.3.3 Model Construction

Microsoft Excel was used to construct the model, as the program lends itself to an iterative approach. Different variables were represented in separate columns whilst the rows of the spreadsheet corresponded to separate time-steps. The equations governing the separate variables could be quickly altered and copied automatically; values from any instant of the iteration could be easily referenced and used in a calculation. Individual worksheets were used for each sub-model. This means that changes could be made to one sub-model without interfering with the operation of another, but allowing values to be easily referenced between sub-models when required.

Displacements, Velocities and Accelerations

The overall model, being grounded in Newtonian mechanics, is primarily concerned with displacements, velocities and accelerations. These may be pure translations, rotations, or

a combination of the two. Forces generated within the model result in accelerations, which in turn dictate the velocities and displacements over a single time-step. In assuming that the forces (and hence accelerations) are constant over a time step, it enables relatively simple constant acceleration equations to be used in most cases.

Over each time step, the model has constant accelerations, linearly changing velocities and parabolic displacement changes, as illustrated in figure 8.3a. The forces change from one time step to the next which enables very complex relationships to be modelled with relatively simple governing equations.

Due to the nature of the time step method, the velocities and displacements are continuous over the modelling period, whilst the forces and accelerations undergo discontinuous step changes from one time step to the next. It is important to account for this when calculating values at each time step. For example, the velocity and displacement values are given at the beginning of each time step, meaning that the acceleration value used in their calculation must be taken from the previous time step, as illustrated in figure 8.3b.

The following sections describe how each of the sub-models utilise this time-step construction to reproduce the behaviour of physical systems

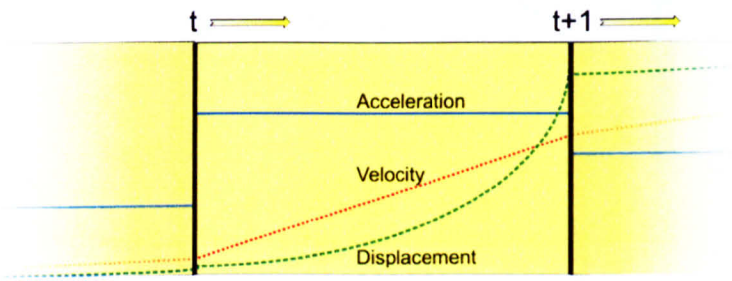

Figure 8.3a. An illustration of the acceleration, velocity and displacement values over a single time-step. Even if accelerations are assumed to be constant, relatively complex relationships can be modelled if small enough time steps are used.

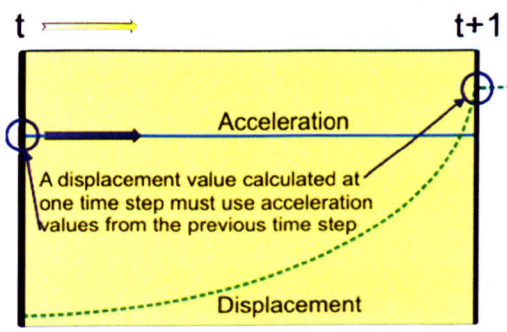

Figure 8.3b. A diagram illustrating how a displacement value (as way of an example) must be calculated from acceleration values taken from the previous time-step.

8.4 Ball and Stringbed Deformation Model

The literature review gives details of the stringbed/damper model developed by Goodwill **2002**. The robust development and validation that went into its development means that it forms the basis of the deformation sub-model.

Although the spring damper model in itself is relatively complex, it can be broken down into three essential elements: a point mass representing the ball, a massless stringbed, and a stationary surface, each connected by a series of springs and dampers. The spring and damper coefficients vary according to inherent characteristics and factors such as ball momentum flux (see literature review). This is shown diagrammatically in figure 8.4.

The model outputs a force value according to an inputted ball velocity and displacement. All of the other factors are internal to the model.

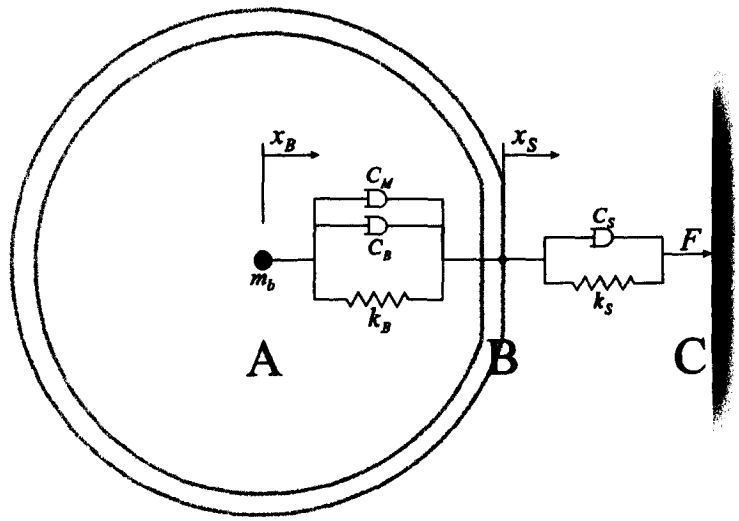

Figure 8.4. A schematic of the ball and stringbed spring damper model. This consists of a ball of point mass (A), massless stringbed (B) and stationary surface (C).

Due to the large amount of validation of this spring damper model performed by Goodwill it was not deemed necessary to validate the spring damper model in isolation. The only modification necessary to incorporate it into the overall model is how it interacts with the rigid body racket frame model.

The Spring damper model was re-created in an Excel spreadsheet using the equations in Goodwill **2002**.

Separate columns were created for the displacements, velocities and accelerations of the ball $(x_B, \dot{x}_B, \text{and } \ddot{x}_B)$ and stringbed, $(x_S, \dot{x}_S, \text{and } \ddot{x}_S)$, several other columns were created to calculate the variables associated with the spring and damper coefficients. The spring damper variables are discussed in the literature review and won't be considered here.

A small section of the iterative time-step model is shown in figure 8.5. It shows the ball's displacement, velocity and acceleration over several time steps and illustrates how each variable is ordered in columns and each row corresponds to a common time instant.

Iteration	Time Step	x_B	x'_B	x''_B
-1	-0.00005	0.00025	-5.000	0.000
0	0.00000	0.0000	-5.000	0.000
1	0.00005	-0.00025	-5.000	54.202
2	0.00010	-0.00050	-4.997	98.201
3	0.00015	-0.00075	-4.992	151.04
4	0.00020	-0.00100	-4.985	203.19

Figure 8.5. A small section of the spring-damper model as written in a spreadsheet. Each variable is ordered in a separate column with the time-steps of the model ordered in separate rows.

The effective radius of the ball can be easily calculated as the difference between the respective ball and stringbed displacements:

$$\text{Radius} = r_0 - (x_S - x_B) \qquad [8.1]$$

where r_0 is the non-deformed radius of a tennis ball (a value of 33.5 mm was used in the model). This is the middle value between the upper (2.700 inches) and lower (2.575 inches) limits of ball size given by the ITF **2007a**.

The radius of the ball is an important characteristic to track over the duration of the impact. It quickly tells the user whether the model is behaving as expected (no negative radius values etc.), and tells the model when the ball leaves the racket stringbed. The time instant when the ball radius returns to r_0 is the instant when the ball has left the racket stringbed. Another indicator of the end of impact is the instant at which the deformation force drops to zero. This was implemented into the model and found to make very little difference to its operation.

Figure 8.5 shows how the modelled radius of the ball changes through impact for various initial ball velocities. In this case the model is uncoupled from the racket frame model, effectively representing an impact against a head-clamped racket. It can be seen from the figure how the deformation is greater for a ball at a higher initial velocity, as one would expect. The dwell time on the strings (duration of impact) is also reduced for higher velocity balls, a characteristic noted often by Brody **1987b** but not physically observed by Goodwill **2002** to the extent seen in figure 8.6. To test the physical validity of the results in figure 8.6, the damping was reduced to zero and an energy balance was performed. The energy balance showed a conservation of energy. These results illustrate the effectiveness of the model at simulating different ball velocities. They also highlight the need to be able to track the instant at which the ball leaves the stringbed; it varies considerably for different ball velocities.

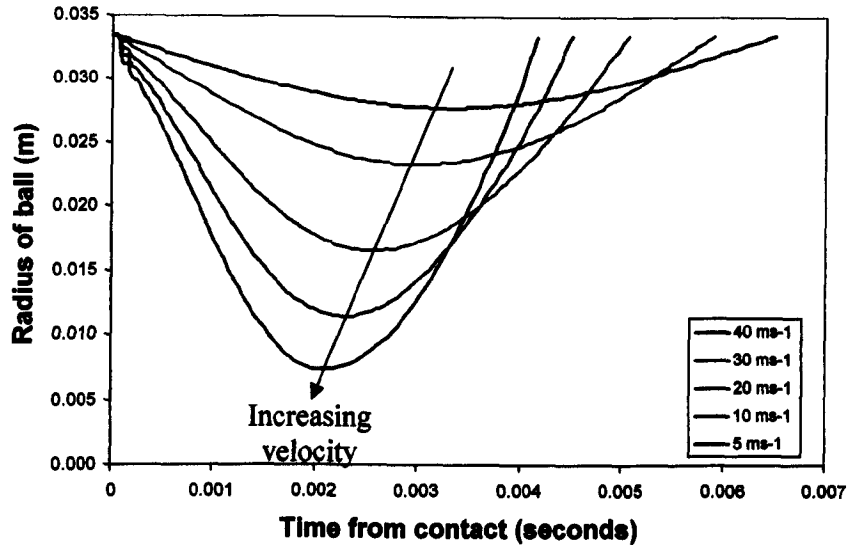

Figure 8.6. The model output of ball radius over the duration of an impact for five different inbound ball velocities.

This deformation sub-model can easily be incorporated into a complete six-degree of freedom model with minor changes. The spring damper model illustrated in figure 8.3 states that *C* is a stationary surface; because *C* represents the racket frame, this is clearly not the case. This can be accounted for by ensuring that the velocity of *A* is the relative velocity between the ball and racket frame. The velocity of the impact point on the racket frame is subtracted from the velocity of the ball to give the appropriate relative velocity.

8.5 Ball Spin Model

Several different models of ball spin have been developed. The simplest, by Daish **1972** uses a rigid ball and a simple slip/rolling condition to dictate behaviour. Cross **2002a** modified this model by altering the conditions of rolling and introducing a tangential off set force. Haake **1996** modified the impact conditions to include a deformable ball and surface.

The overall model already includes a ball deformation model and it can be seen that at impact speeds as low as 5 ms^{-1} ball deformation is around 5 mm. Clearly a non-deformable spin model is not appropriate in this case.

Both Haake and Cross mention a phenomenon known as overspin where the ball spin decreases toward the end of the impact, after a period of high spin in the middle of the impact. Cross accounts for this with the offset force, Haake with the rolling condition as the radius of the ball decreases.

Overspin and ball deformation will be accounted for in this ball spin model by including ball deformation and a slip/rolling condition.

8.5.1 Slip and Rolling

The slip and rolling conditions dictate how the ball and stringbed interact in the plane of the stringbed.

- *Slip:* The ball and stringbed move relative to each other. The force acting on the ball is given by $F=\mu R$.
- *Rolling:* The ball rolls along the surface of the stringbed; there is no relative movement between the two. Daish reasoned that in a non-deformable system, the force will drop to zero. In the absence of an external force the spin will also remain constant. This is not the case in a deformable system, and will be discussed below.

The conditions which dictate whether the ball is slipping or rolling affect the accuracy of the model and how well it reflects the experimental results. Two triggering conditions were considered for this model, and are described later in this section.

8.5.2 Deformation and Rotation

When using a spin model that includes deformation, several issues arise.

When the ball is slipping the frictional force acts to increase the ball's spin about its centre. As the ball deforms, and its effective radius decreases, the torque alters also, changing the spin characteristics.

If the ball is rolling, the relative velocity of the contact point between the ball and stringbed must be zero. As the radius of the ball decreases, the spin of the ball must increase to maintain the rolling condition.

In reality, as a hollow elastic sphere (like a tennis ball) deforms, it will distort outwards and a section of the ball will come to rest on the stringbed. This is illustrated well in a finite element impact model by Goodwill et al. **2005**.

For the purposes of this model, it is convenient to think of the deforming tennis ball as a shrinking sphere. This simplifies the rotation model used to calculate spin, and always assumes a point contact between the ball and stringbed. This is illustrated in figure 8.7.

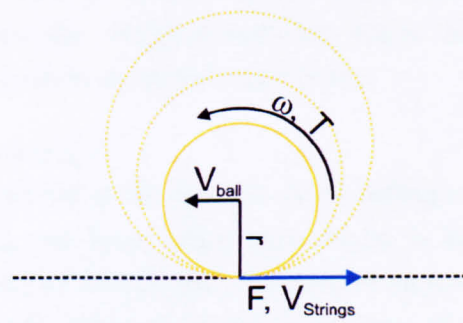

Figure 8.7. A depiction of the deformation assumption used to simplify spin calculations. By assuming the ball is a sphere of decreasing radius the contact between the ball and stringbed remains as a point.

If we assume that the ball maintains its mass throughout deformation, the above assumption suggests a corresponding decrease in the moment of inertia. It is assumed that the ball is a hollow sphere with a constant wall thickness of 3 mm, and mass of 57 g. It is possible to calculate the change in the moment of inertia according to the radius decrease shown in figure 8.6 for a ball travelling at 40 ms^{-1}. This is shown in figure 8.8. This assumption results in an approximately 28 fold decrease in the moment of inertia during impact. The finite element model by Goodwill et al. **2005** showed that in fact the moment of inertia of a tennis ball decreases by less than 10% during an impact. This is due to the increase of the size of the tennis ball in the plane of the stringbed as it deforms. The finite element model calculates the value of the moment of inertia (MOI) by calculating the individual MOI of thousands of small cells within the tennis ball model. Taking this result into account, and considering the unnecessary complexity of calculating the ball's moment of inertia accurately, the moment of inertia will be assumed to remain constant throughout the impact in this model.

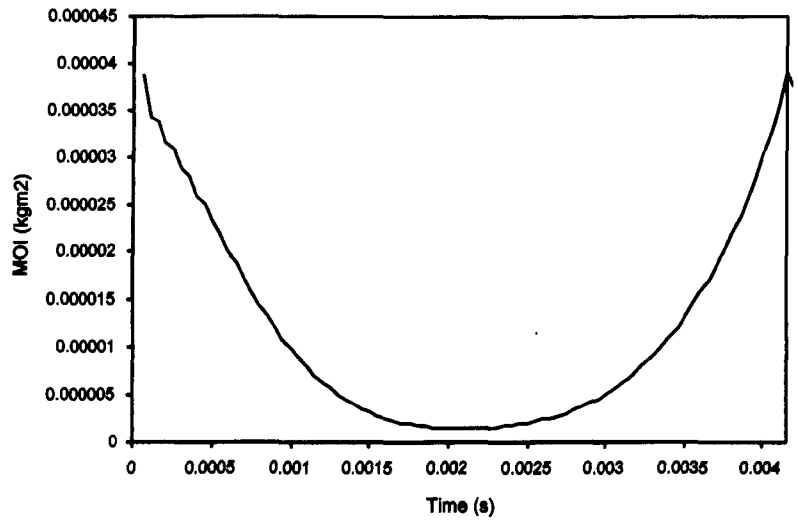

Figure 8.8. A plot showing the change in moment of inertia of a hollow sphere of decreasing radius, constant mass and constant thickness.

The stringbed deformation is not accounted for in this version of the model. The point contact assumption between the stringbed and ball means that the stringbed essentially remains as a flat surface perpendicular to the racket frame.

8.5.3 Force and Spin Generation

The force generated by the model depends on the rolling condition. It has already been stated that during slipping, the force acting tangentially is equal to the frictional force occurring between the surface of the ball and stringbed. From now on, this will be referred to as the *threshold* of the system. The force acting in the plane of the stringbed cannot exceed this threshold value. For example, if the coefficient of friction is 0.3, and the normal force is 1000N the system has a threshold of 300N. The threshold value will be used in forming one

of the trigger conditions which dictate whether the ball is slipping or rolling. This is discussed later in this section.

Daish reasoned that during rolling, the force drops to zero as the relative velocity between the surface and balls drops to zero. In a deformable model the spin must increase as the radius of the ball decreases for the rolling condition to remain valid. If we assume that the inertia of the ball remains constant throughout compression, the zero force assumption breaks down.

During rolling, the ball spin is analogous to the relative motion between the ball and stringbed. From the simple diagram in figure 8.7:

$$\omega = \frac{V_{Ball} - V_{Strings}}{r} \qquad [8.2]$$

In assuming that the ball radius decreases uniformly through compression, very high spins occur at large deformations. The time-step model assumes constant forces and accelerations between each time step. The force necessary to increase the ball spin from one step to the next is calculated from Newton's laws:

$$F = \frac{\omega_t - \omega_{t-1}}{\Delta t \cdot r} \cdot I \qquad [8.3]$$

Using the deformation values in figure 8.6, the spin and force values were calculated assuming that the ball's tangential velocity was 5 ms^{-1} (the perpendicular velocity was 40 ms^{-1}). These are shown in figure 8.9 for the duration of an impact. The impact was assumed to be against a stationary surface and rolling throughout the impact. The force from equation 8.3, would usually cause the ball to decelerate throughout the impact according to $F = ma$. In this case the velocity has been kept constant at 5 ms^{-1}. When the model was constrained to be constantly rolling, the high forces seen in figure 8.9 cause the model to become unstable. In reality the ball would begin to slip against the surface. This and the unstable effects will be discussed later in this section along with the necessary trigger conditions to start rolling or slipping.

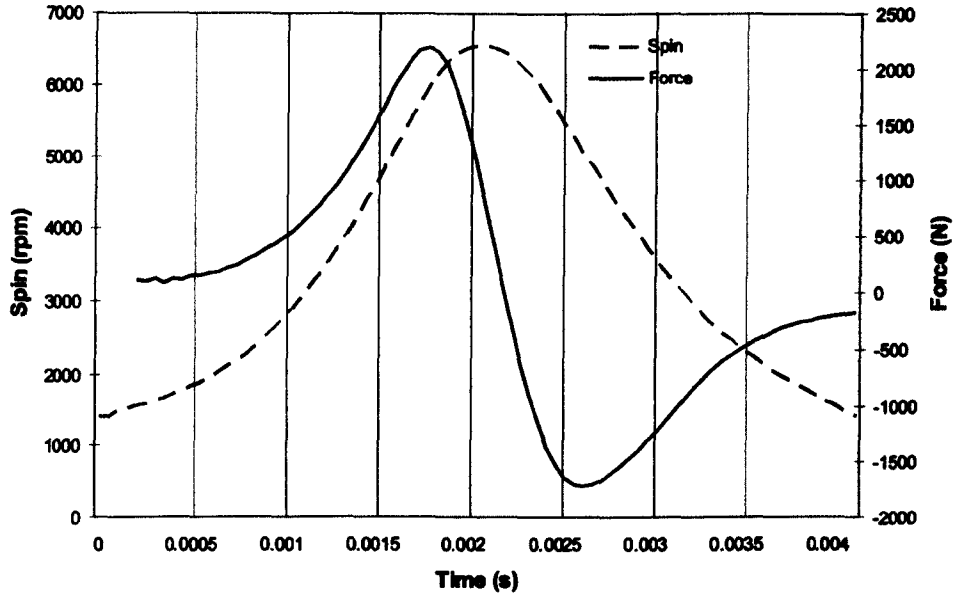

Figure 8.9. The force and spin values for a ball travelling at an angle of 7.1° and speed of 40.3 ms^{-1} to a stationary surface.

Figure 8.9 shows that at high deformation values, the instantaneous spin value is much higher than the spin value after impact. This effect is the 'overspin' effect cited by Haake et al. **2005** and Cross **2002a.**

The force value reverses during the second half of the impact, this is as the ball expands and the spin values start to decrease.

During slipping, the ball's rotational velocity and acceleration are dictated by the force acting on its surface. This frictional force is a product of normal force due to impact, and the coefficient of friction on the stringbed.

$$F = \mu \cdot R \qquad [8.4]$$

In this case R is the force acting perpendicular to the stringbed. Ashcroft and Stronge **2002** found the coefficient of friction between a ball and stringbed to be around 0.45, and is the coefficient of friction value initially used in this model.

The rotational acceleration from one time step to the next is according to the torque acting around the ball's centre. According to figure 8.7, this can be described as:

$$T = F \cdot r \qquad [8.5]$$

$$\dot{\omega} = \frac{T}{I} \qquad [8.6]$$

The force and deformation values for a 40 ms^{-1} impact were used to model the spin of a ball which slips during impact. In this case the tangential velocity of the ball was increased to 30 ms^{-1}. Slipping generally occurs at higher tangential ball velocities. When the system was

modelled with the ball velocity at 5 ms^{-1} as used above, it quickly slowed to 0 ms^{-1} under the frictional force occurring during slipping.

It is important to note the direction of the frictional force occurring during impact. In this case it is assumed that the ball is slipping for the duration of the impact. As the frictional force acts, it increases the ball spin but decreases its tangential velocity. In the case of a static surface, as in this simplistic representation, the relative velocity between the ball and surface drops to zero. After this point the frictional force reverses direction as the relative velocity becomes negative.

Figure 8.10 shows the tangential velocity of the ball's COM, the velocity due to spin (ωr), and the relative velocity between the ball and stationary surface.

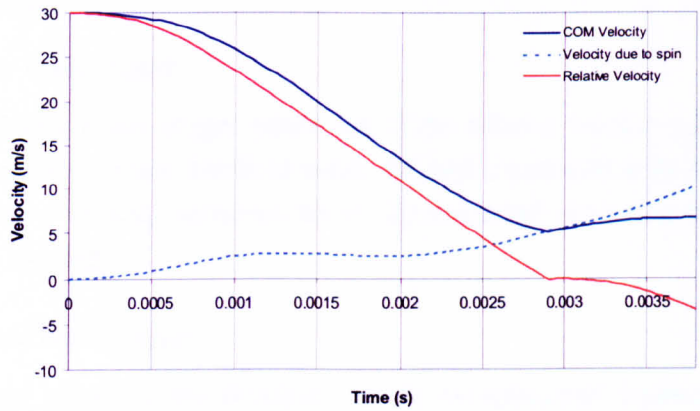

Figure 8.10. A plot showing the ball's tangential velocity, velocity due to spin and relative velocity over the duration of an impact.

Figure 8.11 shows how the force and spin change over the duration of the impact.

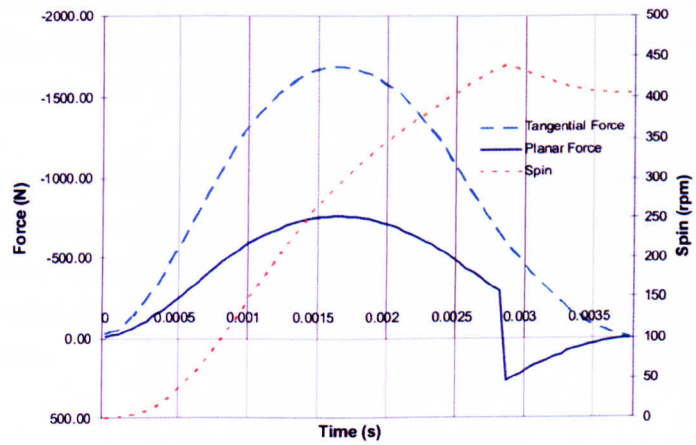

Figure 8.11. The force tangential to the stringbed, the force in the plane of the stringbed, and ball spin generated during a ball impact. In this case the ball was assumed to be slipping throughout the impact.

The sudden force change shown in figure 8.11 is also analogous to the overspin effect cited earlier, but it is physically unrealistic that such significant forces would act at such low relative velocities and switch so suddenly.

In reality, if the ball is slipping at the start of the impact, it would begin to roll as the relative velocity between the ball and surface drops.

It is the trigger determining whether the ball is rolling or slipping which dictates much of the model's behaviour. Two possible triggering conditions are considered below.

8.5.4 Triggering conditions

The triggers to switch between slipping and rolling which have been considered are based on the relative velocity between the contacting surfaces and the threshold of the stringbed/ball interaction.

- Velocity based trigger

  The velocity based trigger states that if the relative velocity of the two surfaces drops below a certain threshold value, the ball is assumed to be rolling. As soon as the relative velocity increases above the threshold value, the ball is assumed to resume slipping.

- Threshold based trigger

  A trigger based on the *threshold* of the stringbed/ball interaction. If the force required to cause the ball to begin rolling from one instant to the next is within the threshold of the system, then the ball begins rolling. If from one instant to the next the force required to maintain rolling exceeds the threshold of the system, the ball begins to slip.

  This is best described through an example. Table 8.12 contains typical values from a spin model, from consecutive time instants. The incident velocity, initial spin and ball radius are arbitrarily selected. The rolling spin at the next instant is calculated using equation 8.3. The force is calculated from a rearrangement of equations 8.4 and 8.5.

  If the threshold of the system between the two instants is 500 N, then the ball begins to roll because the force does not exceed the frictional force available. If the threshold is lower than 434.7 N, then the ball slips. It is irrelevant whether the ball was slipping or rolling prior to this time-step as the triggering conditions apply without bias.

Incident Velocity (ms^{-1})	Initial Spin($rads^{-1}$)	Radius (m)	Spin at next instant if rolling ($rads^{-1}$)	Force required to execute change (N)
5	150	0.03	166.7	434.7

Table 8.12. An example set of ball characteristics to illustrate the threshold based trigger system.

The two triggering conditions were incorporated into simple spin models in which the contact surface is kept stationary.

Figure 8.13 shows the model results when the velocity based trigger is used. Figure 8.14 shows the results using a threshold based trigger. A ball with an incident velocity of 15 ms^{-1} was used in both models.

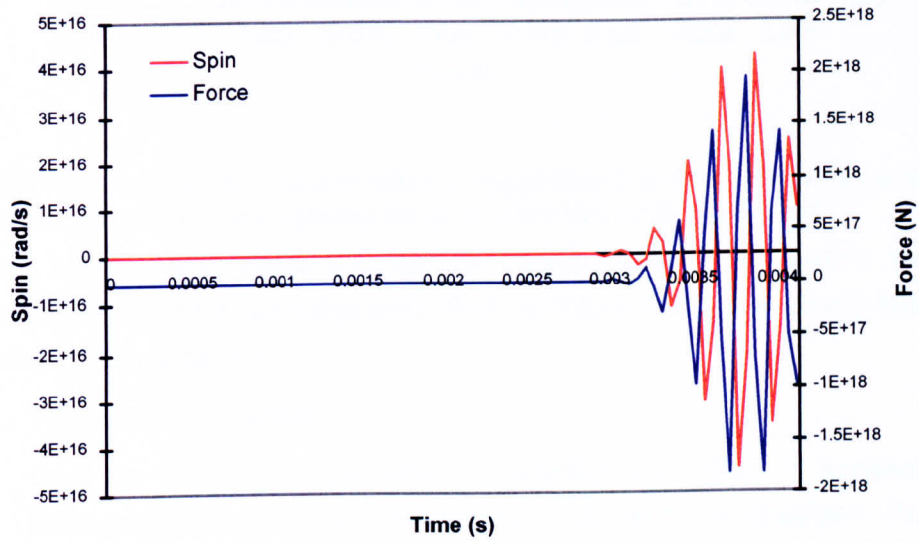

Figure 8.13. A spin model response when a velocity based trigger is used. This shows the spin and force response for a ball of an incident velocity of 15 ms^{-1}.

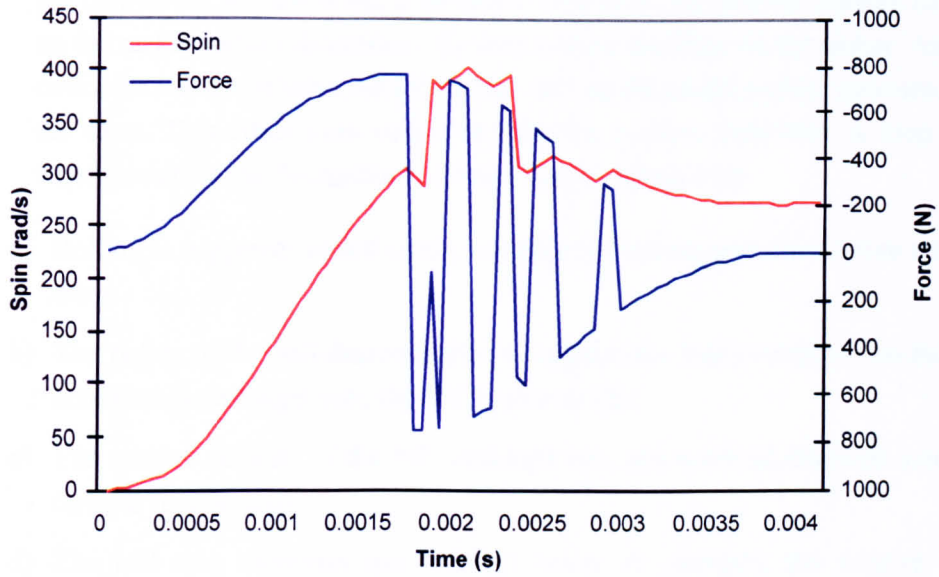

Figure 8.14. A spin model response when a trigger based on the system's threshold is used. The spin and force response are shown for an incident ball velocity of 15 ms^{-1}.

It is apparent from figure 8.13 that the velocity based trigger system immediately becomes unstable with the conditions used. There are two factors of the velocity based trigger which result in this instability:

1. Triggering is permanent

   Once the relative velocity drops sufficiently, and rolling is triggered, this is permanent. This causes any instabilities in the model to propagate. This will be remedied in the overall model because the contact surface (the stringbed) is not stationary.

2. System threshold is not considered

   The time steps used in the model are at intervals of 0.00005 seconds. Once rolling, the spin changes dictated by the rolling condition can cause extremely high forces, as seen in figure 8.9. If these forces exceed the threshold of the system, slipping is not triggered, causing the instability to propagate uncontrollably. Because of the nature of the trigger, slipping can not be re-established once rolling has commenced.

In contrast, the model using the threshold trigger is more stable but still shows large fluctuations in the force value, and a sudden spike in the spin value shortly after 0.0015 seconds. The reasons for these responses are as follows:

1. Direction of slipping force.

   When the ball slips on the racket surface, the force is dependent only on the coefficient of friction and the normal force on the system. The relative velocity of

the ball on the surface is not considered. However, the relative velocity of the ball on the racket surface determines the direction of the force on the racket. As the ball overspins and the relative velocity of the ball on the racket surface reverses, so does the force. This effect even occurs at very low relative velocities. A loop is setup which results in the fluctuations of force seen in figure 8.14:

a) Rolling is triggered; which causes the spin to increase and the relative velocity to drop;

b) The radius of the ball decreases due to impact, the ball overspins and the rolling condition is no longer met, the ball begins to slip;

c) The relative velocity of the ball, although low, has reversed direction causing the force to reverse also;

d) The ball spin decreases and the ball ceases to overspin, the relative velocity remains low, but reverses direction, causing the force to reverse direction once more;

e) The loop continues.

This effect can be best observed by replacing the spin from figure 8.14 with the relative velocity, as seen in figure 8.15.

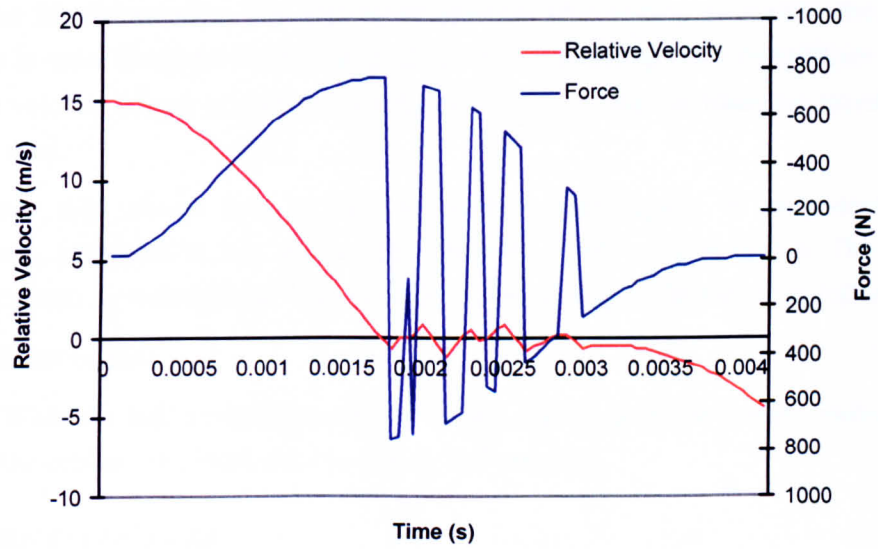

Figure 8.15. A plot of the force and relative velocity for a spin model using the threshold based trigger. The ball's incident velocity is 15 ms^{-1}.

2. Velocity based spin values

The velocity based trigger assumes rolling begins once it has reached the appropriate spin value. The threshold based trigger assumes rolling begins once it is possible within the constraints of the frictional force available on the stringbed. In a

physical sense, this results in the ball catching on the racket stringbed and suddenly increasing spin. The spin when rolling is strongly dependent on the ball radius, which changes throughout the impact. This sudden increase in spin also quickly changes the relative ball velocity, resulting in the instability discussed in the first point.

It would seem obvious from the above analysis that the threshold based triggering system is most suitable as the velocity based trigger is inherently unstable in this form.

Several attempts were made at solving the oscillation problem. In reality, the force oscillation represents a rapid vibration of the ball's surface even though a tennis ball is not sufficiently stiff to allow this to happen. Damping, moving point averages and a 'second shell' were all used as potential solutions to the problem. Although the effect was reduced, it was not possible to eliminate it entirely. This led to a different appraisal of the problem altogether.

8.5.5 The rolling condition, a reappraisal

The unstable responses observed above suggest that the initial assumptions are unsuitable in some way. The rolling condition stated by Daish **1972** applies to a non-deformable ball. The assumption that as the ball deforms, it uniformly decreases in diameter is unreasonable. It is equally unreasonable to continue to apply the rolling condition throughout this deformation. The high spins resulting from rolling necessitate the generation of a force in order to adhere to physical principles. The resulting force destabilises the system when the velocity trigger is used and produces a force oscillation when the threshold based trigger is used.

Figure 8.16 shows how a ball in reality might appear in cross-section under compression, compared to how the model represents a ball in compression. The disparities between the two representations when considering the rolling condition are as follows:

- Point contact

  When the ball compresses, the model ball maintains point contact whilst in reality the contact area increases throughout deformation.

- Rolling deformation

  Whilst the model ball simply rolls along the contact surface, in reality the rolling condition requires constant deformation of the ball's surface. The rubber of the ball must change and deform in order to maintain the condition of zero relative velocity between the two surfaces. It is hard to define exactly what 'rolling' is at high deformations. In reality the ball is no longer spherical and the angular velocity is difficult to accurately define.

- Rolling force

  The model generates a force during rolling based on the increase in spin. This force has no physical source in reality. As a result it destabilises the model, probably due to the unreasonable assumptions on which it is based.

It is unlikely, given the considerations above, that the rolling condition – as defined – would result in the high instantaneous spins that the model produces. At higher deformations, rolling causes the ball to deform rotationally. The viscosity of the ball's rubber would require a significant amount of energy to reach the spins predicted by this model. Any spin increase resulting from the decrease in effective radius is likely to be cancelled out by the increase in contact area and requisite viscous energy to maintain a higher spin rate. Goodwill et al. **2005** showed that the felt of a tennis ball grants significant pliability during rolling. The core of the ball is able to overspin without immediately interacting with the contact surface. This model assumed the ball is rigid horizontally and rotationally, giving rise to an instantaneous destabilising force.

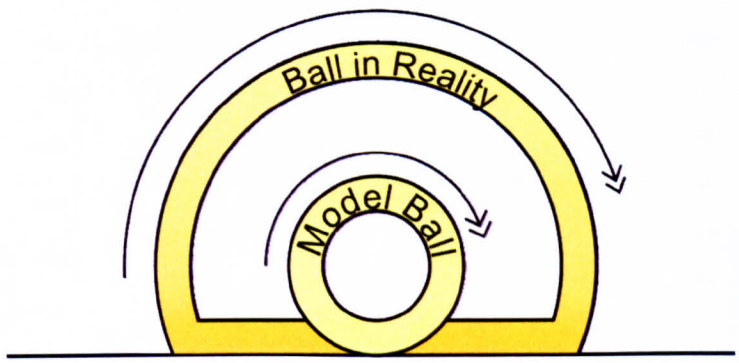

Figure 8.16. A stylised representation of a compressed ball in reality compared to the model's representation of a ball in compression.

It is therefore better to assume that the force which destabilises the model is invalid. We also assume that the MOI of the ball throughout compression is constant; in the absence of an external force, the spin must remain constant when rolling. This was implemented into the velocity triggered model. The threshold based trigger is no longer valid when the rotational force due to rolling is disregarded.

The ball deformation model was incorporated into the rolling model. The radius and force output were used to govern the friction and rotation of the ball. The response of the model was observed by plotting the force and spin output over the duration of an impact.

Figures 8.17 – 8.19 show the model responses during constant slip, overspin, and when the ball leaves the stringbed whilst rolling.

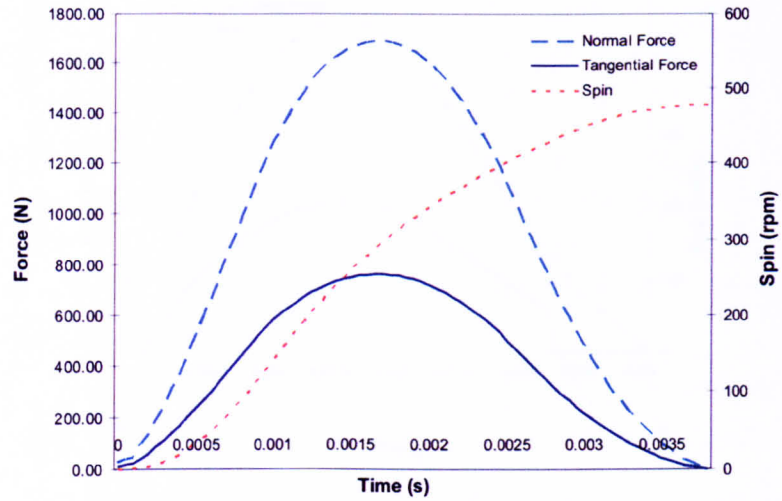

Figure 8.17. The model force and spin response in which the ball slips throughout the duration of impact.

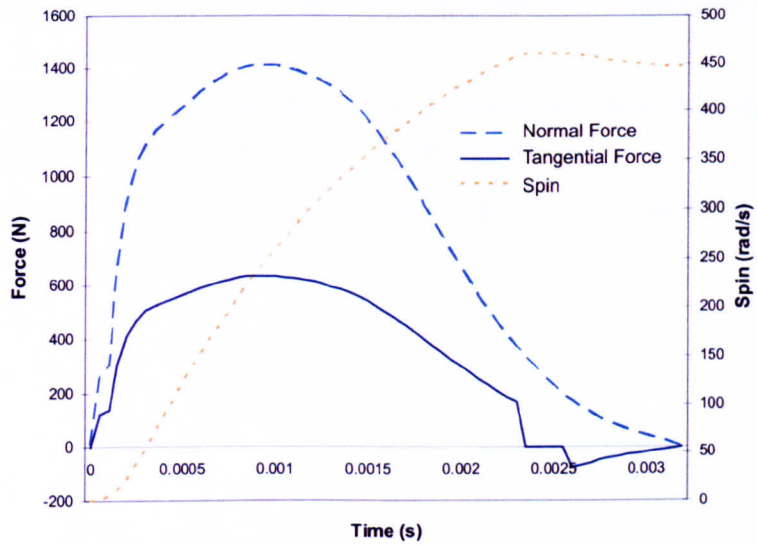

Figure 8.18. The force and spin response of the model in which overspin can be observed. The asymmetrical force curve is due to the high inbound velocity used to generate the curve. A short period of rolling can be seen, in which the force is zero, before the planar force reverses direction.

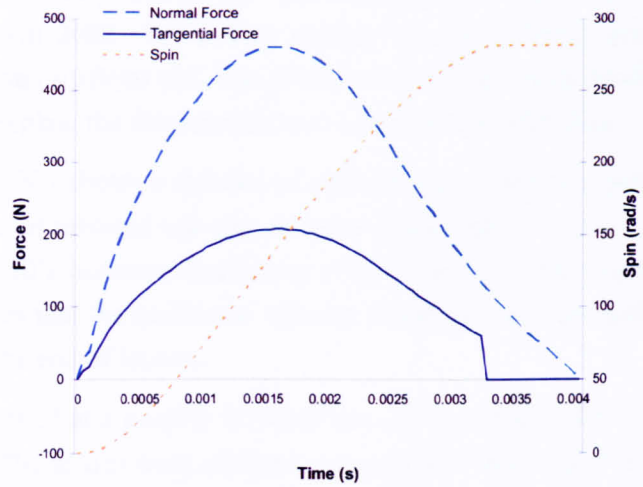

Figure 8.19. The force and spin response where the ball leaves the stringbed whilst rolling.

The outbound velocities of the spin/deformation model were compared with experimental results from an internal report Kirk **2003**. The experiment involved firing tennis balls at stationary surfaces, measuring the angle of incidence, velocity and spin before and after impact.

The recorded inbound velocities from the experiment were input to the spin/deformation model and the results compared with those from the experiment.

Figure 8.20 shows the results from repeated firing of a ball at around 20 ms^{-1} at an inbound angle of around 10 degrees.

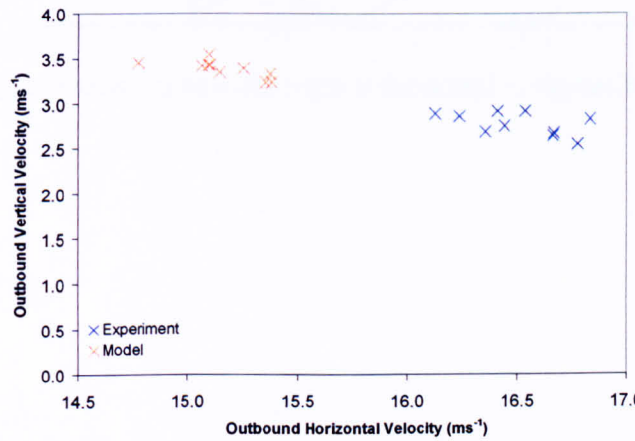

Figure 8.20. A comparison of the spin/deformation model and an impact experiment by Kirk **2003**

The model predictions are relatively accurate, although it under-predicts the horizontal velocity, whilst over-predicting the vertical velocity. Although the coefficient of friction was used as denoted in the report, this could be a source of the horizontal discrepancy. The

vertical velocity is entirely due to the ball deformation model which has been robustly validated in Goodwill **2002**. The impact surface was modelled as entirely rigid whilst in reality the surface was artificial turf. The pliability of the turf could result in a damping of the ball's energy, and explain the discrepancy seen in the vertical direction.

Haake et al. **2005** shows a number of comparisons between experiment and a specific spin model in terms of rebound velocity, rebound angle and 'spin ratio'. The spin ratio is the ratio between the ball's outbound horizontal velocity and the ball's surface velocity. A spin ratio of one indicates that the horizontal velocity is equivalent to the surface velocity and the ball was rolling at the end of impact.

The ball was fired at a number of velocities onto a surface with a measured coefficient of friction of 0.51. The results were obtained using a single high speed video camera.

The experiments in this case show that for a ball inbound at 30° the rebound spin ratio lies between around 0.9 and 1.4 in no particular correlation. For a ball inbound at 12°, the spin ratio lies between 0.3 and 0.7. A plot of the spin/deformation model results is shown in figure 8.22 along with regions depicting what one might expect from the experiment. Figure 8.23 shows a comparison between the impact speed and rebound angle. The range of experimental results

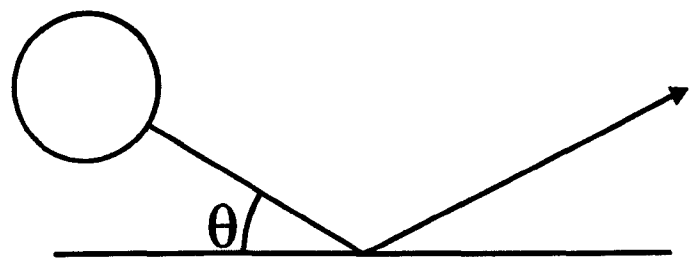

Figure 8.21. A diagram showing how the angle is measured in figures 8.22 and 8.23.

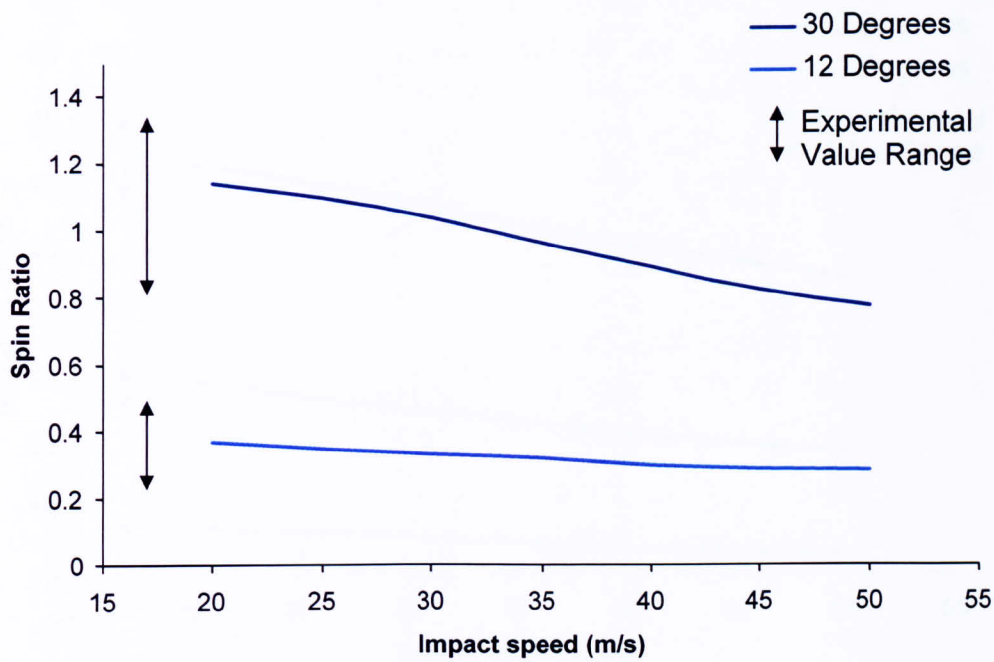

Figure 8.22. Results from the spin/deformation model showing how the outbound spin ratio varies with impact speed. The ball is incident at two angles. The arrows depict the range of values obtained from experiment according to the values from Haake et al. **2005**.

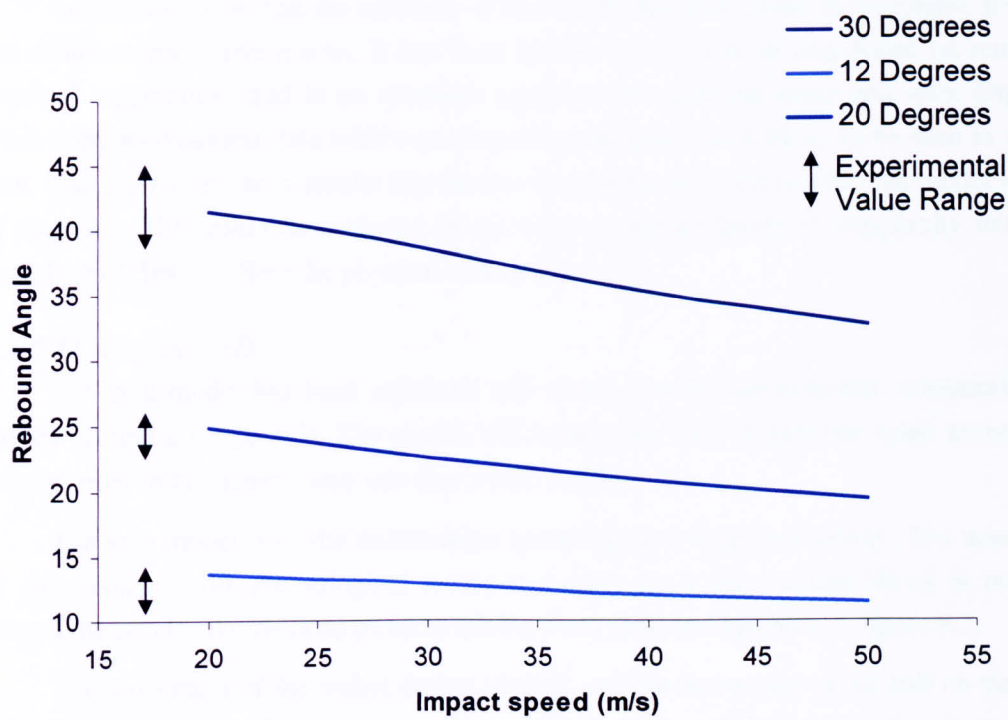

Figure 8.23. Results from the spin/deformation model showing how the rebound angle varies with impact speed. The ball is incident at three angles. The yellow regions depict what might be expected from experiment according to the values from Haake et al. **2005**.

The model predicts the spin ratio and rebound angle reasonably well. The discrepancy between the experimental results could be due to the coefficient of friction value used, or the impact surface, which was modelled as rigid. The model becomes less accurate at higher impact speeds, especially for the rebound angle. It should be noted that the angles of incidence used in these experiments are much steeper than those observed in the player shot analysis.

A more promising but perhaps more limited comparison comes when using values from Goodwill et al. **2006**. A head clamped tennis racket had balls fired at it at 30 and 50 degrees (according to the above convention) at 25 ms^{-1} and with 100 $rads^{-1}$ of backspin. The racket was strung with nylon string at 60 lbs, the standard configuration used in the deformation model.

At 50° the outbound ball spin was between 190 - 230 $rads^{-1}$, the model predicts 217 $rads^{-1}$, at 30° the outbound spin was between 320 - 380 $rads^{-1}$, the model predicts 313 $rads^{-1}$. The 50° angle is at the uppermost bound of the playing angles observed in the player shot analysis. It is therefore very reasonable to assume that players are capable of this shot behaviour, especially in competition play. Therefore when compared against spin results from a tennis racket, at angles that have been observed in normal play conditions, the model shows much more satisfactory results.

In conclusion, within the confines of this study, the spin model is acceptable for use in the complete predictive model. It has been shown to be stable in use, based on reasonable physical assumptions and is an adequate predictor of outbound angle and spin. Especially when compared against data with experimental parameters more likely to be seen in a tennis shot. It is clear from these results that further development would benefit this model in terms of accuracy. This could be achieved by introducing further levels of complexity within the model which better reflect the physical reality of spin.

8.5.6 Moving into 3D

The spin model has been validated and tested in a 2D environment, considering spin strictly around a single axis. The model will have to be able to generate spins around three axes in order to be incorporated into the overall model.

The spin model, like the deformation model, operates entirely locally. The assumption of point contact with the stringbed means that spins need only be considered in two axes, around the two local directions of force arising from spin, as illustrated in figure 8.2.

The movement of the racket during impact, and the movement of the ball on the racket stringbed mean that the ball may have spin in three global axes after impact. The transformation of local co-ordinates into a global framework will be considered later in this chapter.

The spin is resolved into a single direction on the racket stringbed. The relative velocities of the ball surface and racket stringbed are calculated in the local x and y direction and resolved into a single direction. This resolved direction is assumed to be the direction in which any forces arising from spin act. If the ball is assumed to be slipping, the frictional force acting in each local direction is calculated according to the magnitude of the relative velocities in each local direction, as illustrated in figure 8.24.

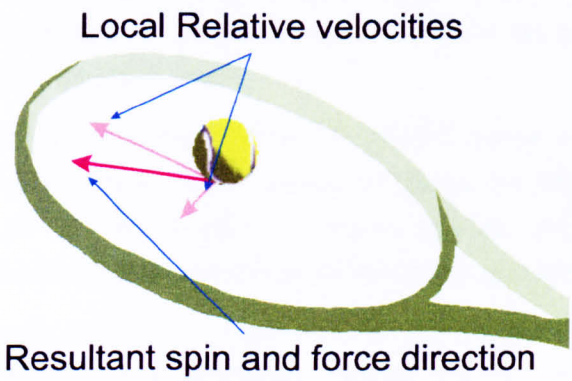

Figure 8.24. An illustration of the local velocities being resolved to determine the direction of the resultant force and spin.

In this way, the torques can be determined around the local x and y axes at the beginning of each time step according to the ball's velocity at that instant in the same way that forces

determine a linear acceleration. The torques result in angular accelerations which are said to be constant over the time step used. This results in appropriate angular velocities and displacements which are used to determine the resultant ball spin, and the distance travelled by the ball over the duration of the impact.

When incorporated into the racket frame model, the relative displacements between the ball and stringbed are important to consider. They will be described in the next section.

With a usable and validated deformation and spin model, a suitable racket frame model is necessary. This will knit each aspect of the model together, simulate the movement and physical properties of the racket, and create a reference from which to transform the locally defined results of the deformation and spin models into a usable global framework.

8.6 Racket Frame Model

The racket frame deformations and movements have been represented in various ways in previous studies, the most accurate of which is the 2D, multi-sectioned finite element model developed by Goodwill **2002**.

The level of complexity involved in expanding a finite element model into 3D was deemed too high for a first attempt at a six degree of freedom model. For this reason the racket frame is assumed to be a rigid body. Goodwill showed that due to an inability to model vibration, a rigid body becomes increasingly poor at modelling as the impact point moves away from the node point of the racket. Chapter 5 showed that most players aim to strike the node point of the racket. For this reason it was deemed that using a rigid body to model the racket frame is a worthwhile compromise between accuracy and complexity.

The racket frame model serves a number of purposes:

- *Accurately predict racket frame translations and rotations:* Although the movement of the racket after impact is not as useful as post-impact ball speed, the relative velocities and rotations of the frame are essential for the correct operation of the spin and deformation sub-models.
- *Track the position of the impact point:* The relative motion of the ball on the racket stringbed means the impact point changes throughout the impact. The racket model keeps track of the impact point to ensure that the physical reaction of the deformation model remains appropriate to the changing conditions.
- *Generate a model response:* A local axes-set fixed to the racket body serves as a reference for the spin and deformation sub-models. The orientation of the racket frame within global space enables the local results from the sub-models to be translated into the more relevant global reference space.

The racket frame is represented as a single plane, with associated mass and moments of inertia. These properties govern the racket's translational and rotational accelerations and

displacements. A point on the plane, represented as the racket's centre of mass (COM) gives a reference as the centre of rotations and a means by which to calculate torques arising from impact. This concept is represented diagrammatically in figure 8.25.

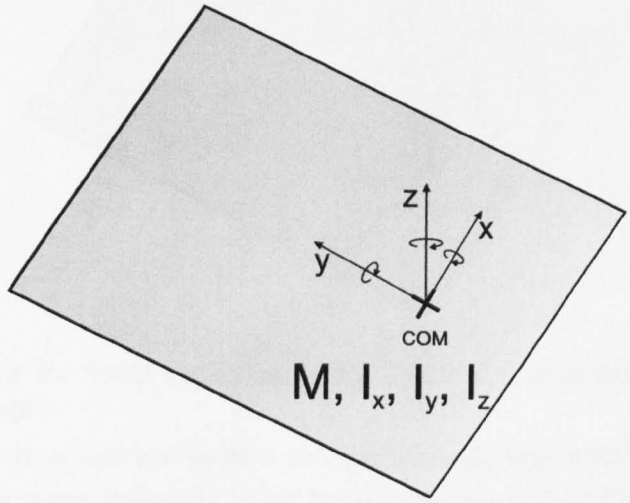

Figure 8.25. A planar representation of the racket frame with an associated mass and moments of inertia and a point with which to represent the COM.

If the linear and angular accelerations, velocities and displacements of the COM are known at each instant, the instantaneous velocities of any point on the racket plane can be calculated.

The model generates no physical constraint on the racket movement other than a restrictive torque around the local *y* axis. This is intended to model racket grip, and reflect the restricted racket mount used in the series of experiments described in chapter 6.

The relative accelerations, velocities and displacement of the impact point are necessary to generate accurate values from the spin and deformation sub-models. The impact point is a vital element of the racket frame model. Whilst the linear and angular accelerations are calculated as acting about the COM, all of the forces generated within the model act at the impact point. These forces create accelerations and torques about the COM, as displayed in figure 8.26.

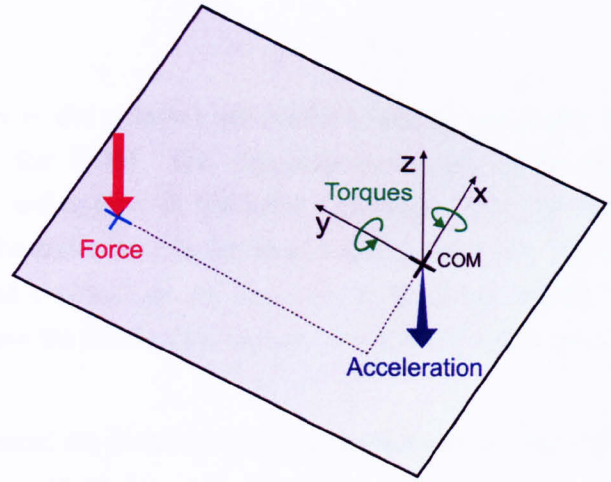

Figure 8.26. All of the forces generated in the model act about the COM, resulting in accelerations and torques.

The forces, accelerations and torques create a feedback loop which operates within the time-step model. The forces generated at the impact point cause the racket frame to translate and rotate. This affects the relative velocities between the impact point and ball, which in turn determine the forces generated by the deformation and spin sub-models. The location of the impact point on the racket face affects how the racket rotates and the forces generated by the sub-models. The calculations and processes involved in determining the racket frame rotations and translations are outlined below.

8.6.1 Racket Frame Translations and Rotations

Every translational and rotational movement is calculated in each of the local axes according to the forces acting in each direction. Each calculation refers to movement of, or about the COM.

The translational acceleration of the COM during a particular time step is easily determined using Newton's second law.

$$\bar{a}_i = \frac{F_i}{M_{COM}} \qquad \textbf{[8.7]}$$

where i refers to any of the three local axes.

The displacement of the COM during a time-step in a particular axes is defined using simple constant acceleration mechanics (finite difference method):

$$S_t = 2S_{t-1} - S_{t-2} + \bar{a}_{t-1} \cdot \Delta t^2 \qquad \textbf{[8.8]}$$

where S is the displacement at the denoted time step, and Δt denotes the duration of each time step.

Similarly, velocity is calculated from these displacement values:

$$v = \frac{S_t - S_{t-1}}{\Delta t} \quad [8.9]$$

The magnitudes of the rotations around the COM are dependent on the distances of the impact point from the COM. The deformation model produces a force completely perpendicular to the racket face, in the local z direction. The spin model produces a force directly in plane to the racket face in the local x and y directions. The rotations of the racket about the local x and y directions are due only to the force arising from the deformation model. Rotations about the local z direction are due to the friction force arising from the spin model.

If a and b represent the distances from the impact point to the COM in the x and y axes respectively, the torques about the x and y axes are:

$$T_x = F \cdot a \quad [8.10]$$

$$T_y = F \cdot b - T_r \quad [8.11]$$

where T_r represents the restrictive torque around the grip. This torque is such that it *always* opposes the direction of the torque acting. This was achieved using an appropriate *if* statement within the Excel spreadsheet.

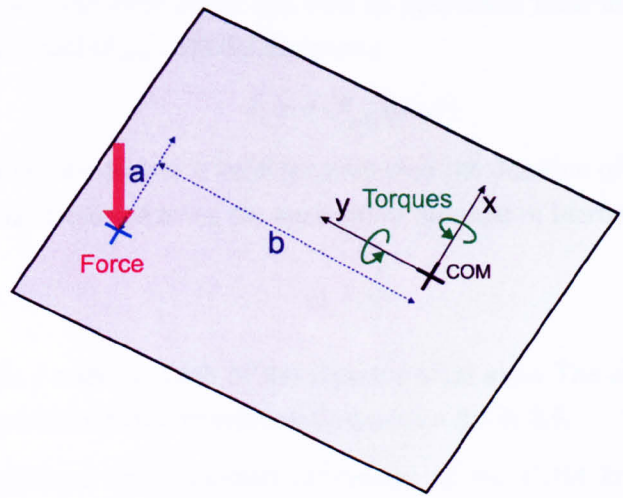

Figure 8.27. Distances a and b on a planar representation of the racket face.

The torque acting about the local z axis is more complex. The force arising from the spin sub-model acts in both the local x and y directions in variable magnitudes. Figure 8.28 shows a diagram illustrating how the torque about the local z axis is calculated. The distance c is the straight line distance between the COM and impact point. The force acting directly perpendicular to this distance determines the magnitude of the torque. In order to do this, it is necessary to calculate the angle between the distance c and the resultant force from the spin model.

$$\theta = \cos^{-1}\left(F_{spin} \cdot |c|\right) \quad [8.12]$$

$$|F_{spin}| = \sqrt{F_x^{\,2} + F_y^{\,2}} \qquad [8.13]$$

$$|c| = \sqrt{a^2 + b^2} \qquad [8.14]$$

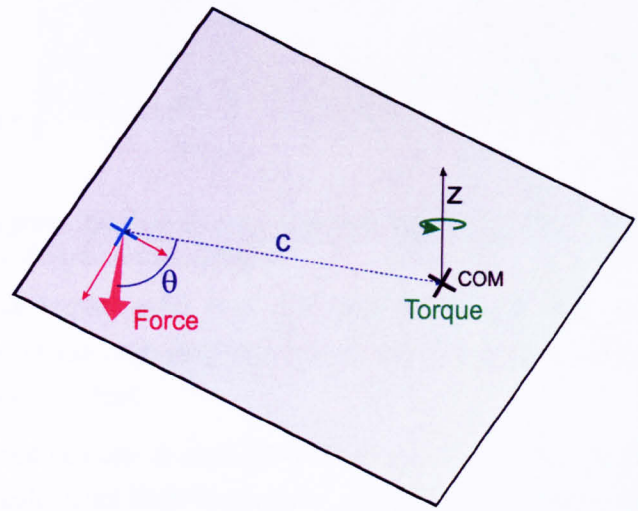

Figure 8.28. A diagram showing the distance between the impact point and COM necessary to calculate the torque around the local *z* axis.

The torque around the local *z* axis can then be calculated from the magnitude of force arising from the spin model (F_{spin}) and the distance *c*.

$$T_z = c \cdot F_{spin}(\sin\theta) \qquad [8.15]$$

Like accelerations, the torque is held constant over the duration of the time period. The angular acceleration is calculated using the appropriate moment of inertia:

$$\dot{\omega}_i = \frac{T_i}{I_i} \qquad [8.16]$$

where the suffix *i* refers to each of the separate local axes. The angular velocities and displacements are equivalent to the translational equations 8.8 & 8.9.

With the translational and rotational movement of the COM known, the associated movement of the impact point can be calculated.

It is important to consider the translation and rotation of the racket frame over the duration of the time period.

The acceleration of the racket frame acts in the same global direction over the entire period, whilst the racket frame rotates under the angular acceleration. For example, an acceleration aligned to the local *z* direction at the beginning of the time period, is no longer aligned to the *z* axis at the end of the period due to frame rotation. This will be explained in more depth in a later section dedicated to axes transformation and is displayed in figure 8.29.

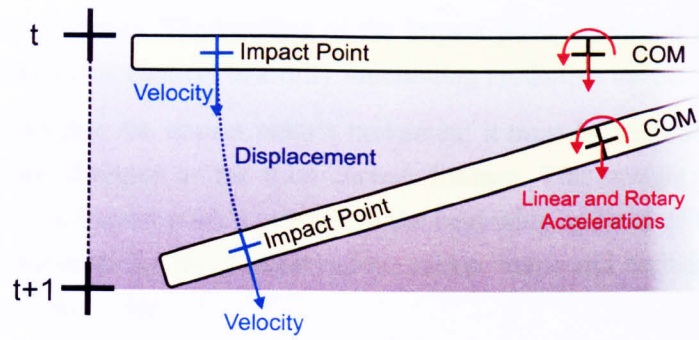

Figure 8.29. A diagram showing that the accelerations acting about the COM continue to act in the same direction despite frame rotation.

In terms of the impact point it is important to consider that not only will the local velocity be different at the beginning and end of the time period, but the orientation of the local axes will also be different.

The impact point velocity is calculated at the end of each time period. The velocity due to frame rotation is calculated from the angular velocity. In the x and y directions the velocity is a component of the angular velocity around the z axes, according to the value θ calculated in equation 8.13.

$$v_{angx} = (\omega_z \cdot c)\cos\theta \qquad [8.17]$$

$$v_{angy} = (\omega_z \cdot c)\sin\theta \qquad [8.18]$$

The local velocity in the z direction is a summation of the angular velocity in the x and y directions.

$$v_{angz} = (\omega_x \cdot a) + (\omega_y \cdot b) \qquad [8.19]$$

A local velocity vector v_{ang} is formed from these three elements:

$$v_{ang} = (v_{angx}, v_{angy}, v_{angz}) \qquad [8.20]$$

v_{ang} is transformed into a global velocity vector V_{ang} and summed to the global velocity vector of the COM to give the global velocity vector of the impact point V_{IP}:

$$V_{IP} = V_{ang} + V_{COM} \qquad [8.21]$$

The velocity vectors are transformed into global co-ordinates so that the velocity of the impact point and COM are equivalent. The process of transformation is described later in this chapter.

The velocity of the impact point is used to give relative ball velocities when calculating the output from both the spin and deformation sub-models.

As can be seen in figure 8.29, the displacement of the impact point over a time period is described by an arc; as such it is not possible to use the impact point velocity to calculate

straight line displacements. The tracking of the impact point's position in space, and on the racket stringbed is a vital element in a fully functioning predictive model

When considering the impact point's movement it must be decided whether this refers to the straight line distance or the total curved distance. The straight line distance is the distance between the impact point's position at the beginning and end of the time period. The curved distance accounts for the rotations of the racket frame and includes the total distance travelled by the impact point.

It is much simpler to calculate the position of the impact point at the end of each time-step and disregard the distance travelled in the intervening period.

Impact Point Position and local co-ordinate transformation

In order to describe the calculation of the impact position, it is necessary to introduce the concept of co-ordinate transformation.

Two co-ordinate transformation techniques are used in the racket frame model:

1. Axes transformation;
2. Rotational transformation.

Both are utilised in calculating the impact point's position from instant to instant.

Initialising local axes

In order to perform transformations and define a local reference frame, a set of local axes must be defined. They are used to define the spatial relationship between the local and arbitrary global reference frames. The local x, y and z axes are defined as unit vectors in global space.

Initially, the local and global axes are aligned as in figure 8.30 such that:

$$\mathbf{x} = (0 \quad 1 \quad 0) \qquad [8.22]$$

$$\mathbf{y} = (0 \quad 0 \quad 1) \qquad [8.23]$$

$$\mathbf{z} = (1 \quad 0 \quad 0) \qquad [8.24]$$

at $t = 0$.

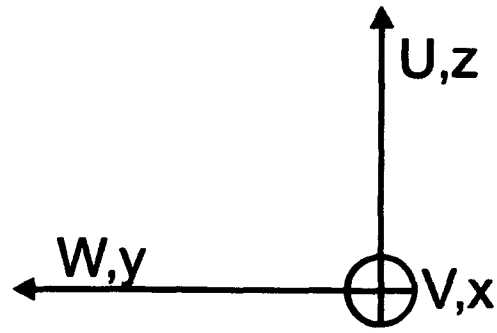

Figure 8.30. The local and global axes are initially aligned within the racket frame model. The global *U* axis is aligned with the local *z*, the global *V* with the local *x* and the global *W* with the local *y*.

These local axes are modified at each time step according to the rotations of the racket frame. Any position on the racket can be defined using the local axes, and the position of the COM.

COM Position

The position of the centre of mass is tracked using the linear displacements over each time step. Initially the COM is at the global origin:

$$\mathbf{p}_{COM} = (0 \quad 0 \quad 0) \qquad [8.25]$$

The displacement of the COM in the local reference frame is calculated using equation 8.8. In order to use the COM displacement to modify the impact point's position vector, it is first transformed into global co-ordinates.

Local to global axes transformation

A local vector can be transformed in the global reference frame by using the local axes set.

$$\mathbf{V}=\mathbf{v}\cdot\mathbf{T} \qquad [8.26]$$

The transformation matrix **T** is formed from the three unit vectors which form the local axes set.

$$\mathbf{T}=\begin{bmatrix} x_i & x_j & x_k \\ y_i & y_j & y_k \\ z_i & z_j & z_k \end{bmatrix} \qquad [8.27]$$

This technique was used frequently throughout the rigid body model to switch a value between the two reference frames.

A separate worksheet was created within the model which contained the transformation matrix. A simple referencing system was used to enable the appropriate transformation at each time step.

The local axes vectors were kept aligned to the racket frame by subjecting them to a rotation transformation at each time step, according to the racket frame rotations occurring about the COM.

Rotation transformations

There are several methods for defining and executing rigid body rotations. The most commonly utilised is the Euler convention, which is described in detail in Goldstein **1980**. It is possible to rotate a body according to an axis of rotation and angle of rotation about that axis.

The axis of rotation is defined globally by the relative magnitudes of angular velocity in each of the global axes. The angular velocity is transformed into the global reference frame using the calculations in equations 8.26 and 8.27.

$$\hat{\mathbf{e}}_{(X,Y,Z)} = \left(\omega_X / \overline{\omega}, \omega_Y / \overline{\omega}, \omega_Z / \overline{\omega} \right) \qquad [8.28]$$

where $\overline{\omega}$ is the resultant angular velocity.

A rotational transformation matrix is formed from the axes of rotation and the magnitude of angular rotation. The rotational transformation matrix is specific for each time step.

$$\mathbf{R} = \begin{bmatrix} \cos\theta + (1-\cos\theta)\cdot \hat{e}_X^{\,2} & (1-\cos\theta)\cdot \hat{e}_X \cdot \hat{e}_Y - \hat{e}_Z \sin\theta & (1-\cos\theta)\cdot \hat{e}_X \cdot \hat{e}_Z + \hat{e}_Y \sin\theta \\ (1-\cos\theta)\cdot \hat{e}_X \cdot \hat{e}_Y + \hat{e}_Z \sin\theta & \cos\theta + (1-\cos\theta)\cdot \hat{e}_Y^{\,2} & (1-\cos\theta)\cdot \hat{e}_Y \cdot \hat{e}_Z + \hat{e}_X \sin\theta \\ (1-\cos\theta)\cdot \hat{e}_X \cdot \hat{e}_Z - \hat{e}_Y \sin\theta & (1-\cos\theta)\cdot \hat{e}_Y \cdot \hat{e}_Z + \hat{e}_X \sin\theta & \cos\theta + (1-\cos\theta)\cdot \hat{e}_Z^{\,2} \end{bmatrix} \qquad [8.29]$$

The rotational transformation matrix is used to transform the local axes set from one time step to the next such that:

$$\begin{pmatrix} \mathbf{x} \\ \mathbf{y} \\ \mathbf{z} \end{pmatrix}_{t+1} = \mathbf{R}_t \cdot \begin{pmatrix} \mathbf{x} \\ \mathbf{y} \\ \mathbf{z} \end{pmatrix}_t \qquad [8.30]$$

Using the distances a and b as defined in figure 8.27 the position of the impact point can be calculated in the global reference frame as:

$$\mathbf{p}_{IP} = \mathbf{p}_{COM} + a \cdot \mathbf{x} + b \cdot \mathbf{y} \qquad [8.31]$$

The values of a and b change according to the ball's position on the stringbed.

Ball Position

The impact position of the ball on the stringbed changes throughout the impact, this is especially relevant during relatively oblique impacts. The values a and b are modified throughout the impact depending on the relative movement of the ball and racket frame.

The ball's COM accelerates according to the force acting on the stringbed. A local force vector is formed from the forces resulting from the spring and deformation models. This local force vector is transformed into global co-ordinates. The ball's global acceleration, velocity and displacement over each time step is calculated according to the procedure outlined in equations 8.7 – 8.9.

According to the global/local relationship outlined in equations 8.22 – 8.24, the ball's position at t = 0 can be described as:

$$\mathbf{p}_{ball} = (a \quad b \quad r_0) \qquad [8.32]$$

locally and:

$$\mathbf{p}_{BALL} = (r_0 \quad a \quad b) \qquad [8.33]$$

globally, where r_0 is the initial radius of the tennis ball.

The ball displacements modify the effective radius of the ball and its position on the stringbed from one instant to the next, changing the values of r, a and b which are used in the model.

The calculations outlined above enable the model to accurately calculate the position of the impact point according to the:

- Displacement of the COM;
- Rotation of the racket frame;
- Relative movement of the ball on the stringbed.

8.6.2 Generating the model response

In order for the model to give an accurate series of outputs, it must be able to determine the instant at which the impact ends. The model values from this instant are then output as the final model conditions.

The ball radius is the most reliable way to track the stage of impact. When the ball radius returns to its initial value, the impact is over and the ball has effectively left the racket stringbed.

The ball radius was tracked from instant to instant within the model. The model output values were taken from the time-step at which the radius returns to its original value.

An input/output front end data sheet was generated to control the model. This contains the model's initial conditions and the physical characteristics of the ball, racket and stringbed. A screenshot of the model's front end data sheet is shown in figure 8.31.

The data sheet was split into several sections according to the conditions of the ball, stringbed, racket and impact position.

- *Ball:* The ball section contains the initial velocity of the ball in the global reference frame, and its initial spin. One can also control the spring and damping values used in the deformation model and the physical dimensions of the ball. These include the radius, wall thickness and coefficient of friction. The moment of inertia is calculated automatically.

  A separate section shows the output conditions of the ball and its linear and angular velocity.

- *Stringbed:* The stringbed section includes the physical aspects governing its response within the ball/stringbed deformation model, such as the spring and damping coefficients.

- *Racket:* The initial linear and angular velocity of the racket are included, as well as the racket's mass and moments of inertia. There is also the possibility of adding a restrictive 'grip' torque about the racket's handle.

- *Impact position:* The impact position is input according to the local x and y axes, as metres from the COM. This modifies the initial values of a and b as described above.

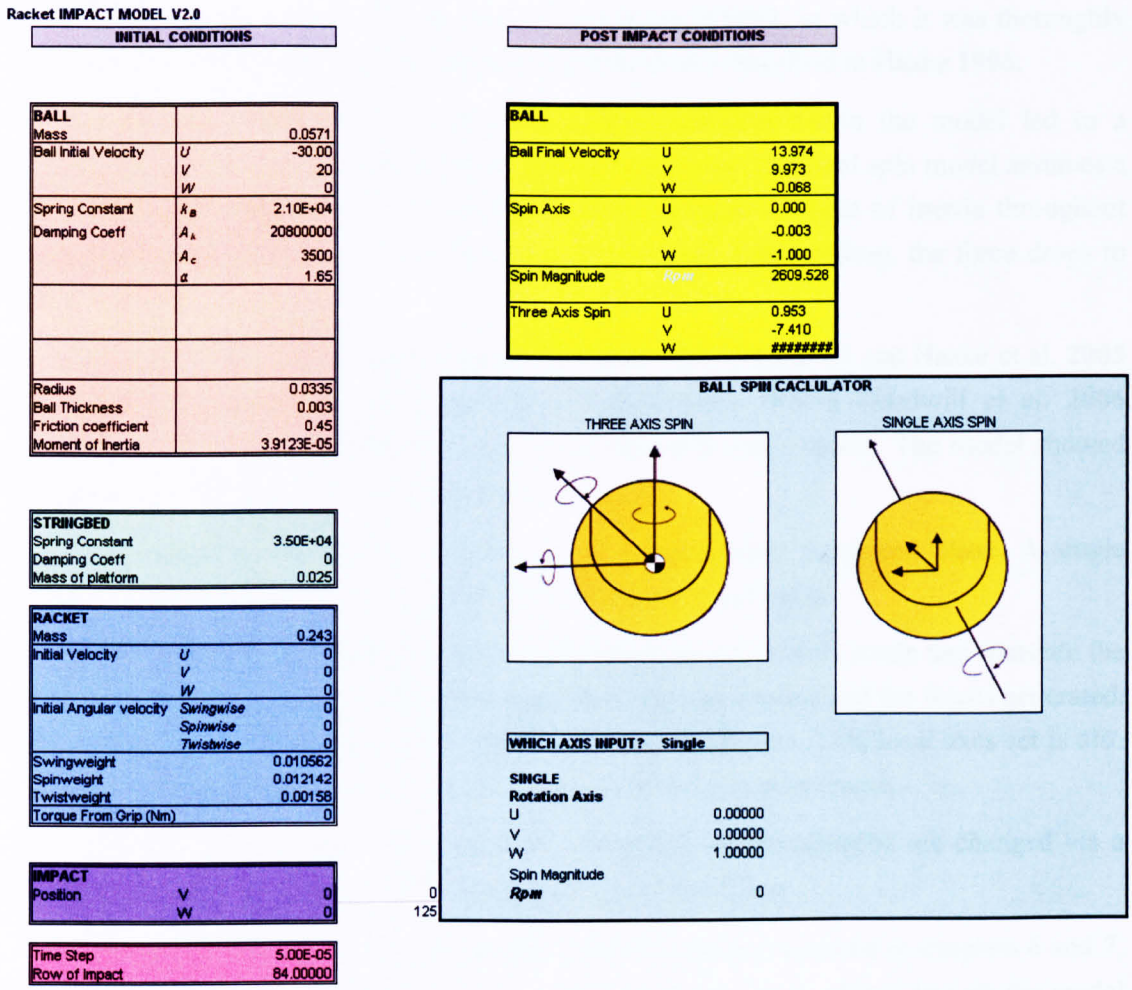

Figure 8.31. The input/output section of the predictive model. Separate sections are used to input the model initial conditions and physical characteristics.

Using the front end, the initial conditions, and physical characteristics of the model can be altered and the response of the ball after impact can be monitored.

The validation of this model is described in the next chapter. The experimental data obtained in the laboratory testing is used to provide a basis against which the model outputs can be compared.

8.7 Chapter Summary

This chapter described the details of a six degree of freedom predictive model. The model used a time-step method to predict the ball's linear and angular velocity after impact.

The racket frame was modelled as a rigid body with a point centre of mass and associated angular momentum. The ball/stringbed interaction was modelled as a spring damper in the perpendicular direction. A deformable spin model with two phases of operation was used to model ball/stringbed interaction in-plane.

The spring damper model was taken from Goodwill **2002**, in which it was thoroughly validated. The spin model was adapted from the spin model described in Haake **1996**.

Issues with force generation and the rolling condition within the model led to a modification of the model's rolling and triggering conditions. The final spin model assumes a point contact between the ball and stringbed and a constant moment of inertia throughout compression. During slip, frictional force acts on the ball. When rolling, the force drops to zero.

The spin model was validated against previous work. Kirk **2003** and Haake et al. **2005** investigated the impact of tennis balls on court surfaces. Whilst Goodwill et al. **2006** investigated the impact of tennis balls on a head-clamped tennis racket. The model showed the best correlation against Goodwill's work.

The racket frame model is represented as a quasi-freely supported plane. A single restrictive torque acts around a local axis to represent the handle grip.

The forces resulting from the spin and deformation sub-models rotate and translate the racket frame. This movement affects the response of the sub-models and the forces generated. The orientation of the racket frame is tracked via a local axes set. This local axes set is also used to transform the ball's output velocity into the global reference frame.

The physical characteristics of the ball, racket and racket stringbed are changed via a data sheet which is also used to alter the model's initial conditions.

Using the results from the experimental laboratory testing outlined in chapters 6 and 7, the predictive model can be validated. Individual parameters can be altered in both the model and experiment, and the relative responses can be compared.

9 Modelling Reality – Predictive Model Validation

9.1 Introduction

Any predictive model must be validated in order to verify its results. In most cases this involves comparing predicted results with verified experimental outcomes.

If the model generates sufficiently accurate predictions over a range of input parameters, its results can be used with a measured amount of confidence.

This section describes the validation of the predictive model outlined in chapter 8 against the experimental results in chapter 7. Individual parameters can be altered by changing the initial conditions and physical conditions of the predictive model. The experimental results are represented using a multi-variate polynomial fit.

If validated with sufficient accuracy, the response of the model will be compared to a number of real-life tennis shots obtained in the player shot analysis.

9.2 Aim

This chapter aims to validate the response of the six degree of freedom predictive model against experimental results.

9.3 Methodology

The predictive model was validated against a series of laboratory tests. Instead of comparing the experimental results with the model directly, a multi-variate fit was applied to the experimental results in order to compare individual parameters. This multi-variate fit is described in more detail in chapter 7.

9.3.1 Validation of parameters

The advantage of using a multi variate fit is that individual parameters can be altered whilst keeping every other constant. Six individual input parameters were originally included in the experiment: The ball inbound velocity in three directions, the ball's impact position in two dimensions and the restrictive torque around the racket handle. Chapter 6 argued that it was only necessary to test two of the three inbound ball velocities. It was shown in chapter 5 that a player moves the racket primarily in the local y and z direction. For this reason the experiment varied the inbound ball velocity in only these two directions.

Two multi-variate fits were generated; a fit to the outbound ball velocity in the local y direction (i.e. across the face of the racket) and a fit to the outbound ball velocity in the local z direction (i.e. normal to the racket). As such, the velocity in the x direction could only be monitored as an output. i.e. it is possible to alter a parameter to assess its affect on the velocity in the x direction. It is not possible to significantly vary the velocity in the x direction in order to assess its affect on another parameter.

Chapter 7 showed the experimental response of a change in each parameter using the multi-variate fit. The predictive model will be validated by using the same sets of parameters input to the predictive model and comparing their outcomes.

The spin values were measured manually from the impact images. As such they were not included in chapter 7. The time necessary to obtain all spin values was too great, and the accuracy of the spin values was too low to generate a reliable relationship. The spin model will be validated by manually counting a number of experimental spin values and compare them to the predictive model.

Comparing the model output to the results seen in Chapter 7 tests impacts both perpendicular and oblique to the racket face. It tests impacts that are offset and at varying positions on the longitudinal axis, and impacts with varying torque values at the handle. The validation will test the individual deformation and spin sub-models and the accuracy of their response. It will also test how they interact as a coherent whole. In order for the model to behave like the experiment, it is vital that the correct physical parameters of the racket and ball are used.

9.3.2 Physical Parameters

A Head Ti S6 racket was used in the laboratory testing, strung at 272 N tension. The appropriate spring and damper coefficients were put into the deformation model for a racket strung at 272 N lbs, as measured by Goodwill **2002**. The racket's mass and moments of inertia were measured according to the procedures outlined in Brody et al. **2002**. The main physical properties of the racket input into the predictive model are shown in table 9.3.

Head ti S6 Tennis Racket	
Mass (kg)	0.243
Twistweight, MOI about x axis (kgm^{-2})	0.00158
Swingweight, MOI about y axis (kgm^{-2})	0.0106
Spinweight, MOI about z axis (kgm^{-2})	0.0121

Table 9.3. The physical parameters of the Head ti S6 racket used in the laboratory testing.

Wimbledon Slazenger tennis balls were used in the testing. The standard data was input to the deformation model and the physical properties were measured as in table 9.4. The mass and radius were taken as averages from a sample of the balls used in testing. The wall thickness was taken from standard measurements of a pressurised ball's wall thickness.

Wimbledon Slazenger Tennis Ball	
Mass (kg)	0.0571
Radius (m)	0.0335
Wall thickness (m)	0.003

Table 9.4. The physical parameters of the Wimbledon Slazenger tennis balls used in the laboratory testing.

9.3.3 Wrist Rig Mass

The wrist rig used to generate a restrictive torque about the racket handle adds significant mass and inertia to the racket. This was not included in the predictive model. Testing by Baker and Putnam **1979** has shown the conditions of clamping have no affect on the post impact behaviour of the ball.

Initial validation tests were performed in which the extra mass and inertia were included in the predictive model. These tests showed it to be significantly less accurate at predicting post-impact ball properties compared to disregarding the extra mass and inertia. A rigid body model, of infinite stiffness is affected by any change in mass or inertia at any point on the racket. This greatly differs from reality, hence why the extra mass was disregarded. In reality, a racket frame flexes upon impact. In most cases, impacts on the stringbed are sufficiently far enough away from the handle such that clamping conditions have no effect on the post impact ball properties. The stiffness of a racket frame is such, that by the time the displacements and deformations resulting from the impact have travelled to the racket handle and back to the impact point, the ball has left the racket stringbed, unaffected by the conditions of clamping. In a rigid body model this effect is instantaneous, any change in the clamping conditions is immediately apparent. A similar effect has been observed in modern, very stiff racket frames for impacts towards the throat (close to the handle) by Brody et al. **2002**, the deformations and displacements travel to the handle and back before the ball has left the racket stringbed

9.3.4 Comparison

Figure 9.5 shows an example of predicted results versus experimental results. The dotted line shows the $y = x$ line indicating a perfect fit. Plotting the experimental results and the results from the predictive model on a single set of axes gives a visual indication of how well the two correlate and whether the predicted model results fall within the accepted experimental error. Another measure of the quality of fit is the R^2 value. The R^2 value of the plot seen in figure 9.5 gives a good estimation of the quality of prediction.

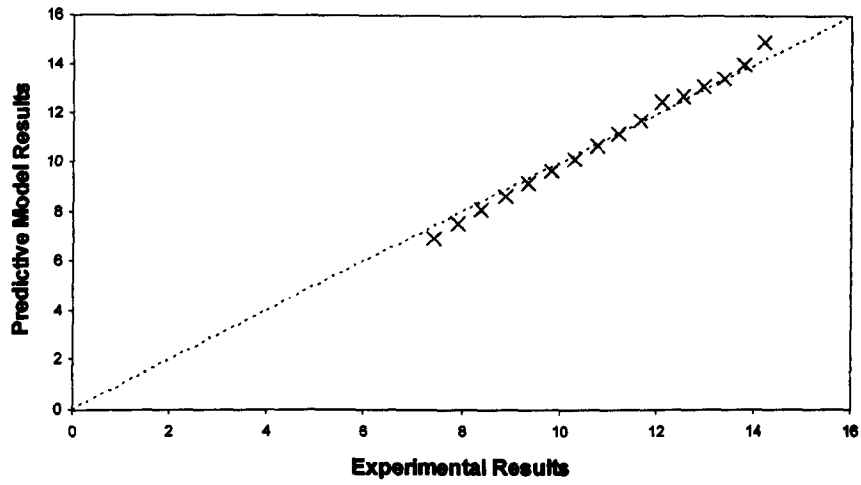

Figure 9.5. Sample experimental and predicted results against the line $y = x$. The correlation to the line $y = x$ indicates the quality of the predictions.

The R^2 value is an indicator of linear fit and lies between 0 and 1. The closer the R^2 value is to 1, the better the quality of fit. Algebraically it is defined as:

$$R^2 = 1 - \frac{SSE}{SST} \quad [9.1]$$

where

$$SSE = \sum \left(Y_i - \hat{Y}_i\right)^2 \quad [9.2]$$

and

$$SST = \left(\sum Y_i^2\right) - \frac{\left(\sum Y_i\right)^2}{n} \quad [9.3]$$

where, $\hat{Y}_i$ is the equivalent value from the line of fit for a given data point Y_i. By setting the Y_i values to the experimental data and attempting to fit them to the predicted values $\hat{Y}_i$, one is able to ascertain how well the data fits the $y = x$ line. *SSE* is the sum of square errors, *SST* is the sum of square deviations from the mean.

A graphical plot and equivalent R^2 value will be given in each validation exercise listed above.

9.4 Results

The model and multi-variate outputs are shown on a single plot in each case, along with the specific input parameters used.

9.4.1 Impact Velocity

Figure 9.6 shows the parameters and comparison plot between the experimental and model outputs for a change in the inbound z velocity. It can be seen on the plot, and is

reflected in the R^2 value, that the model predictions are very close to the experimental values. The predictions are generally within the experimental scatter, which is illustrated by the two solid lines and represents two standard deviations from the mean.

Inbound x velocity (ms^{-1})	Inbound y velocity (ms^{-1})	Inbound z velocity (ms^{-1})	Impact position x direction (mm)	Impact position y direction (mm)	Torque (Nm)
0	0	-15 to -40	0	0	0

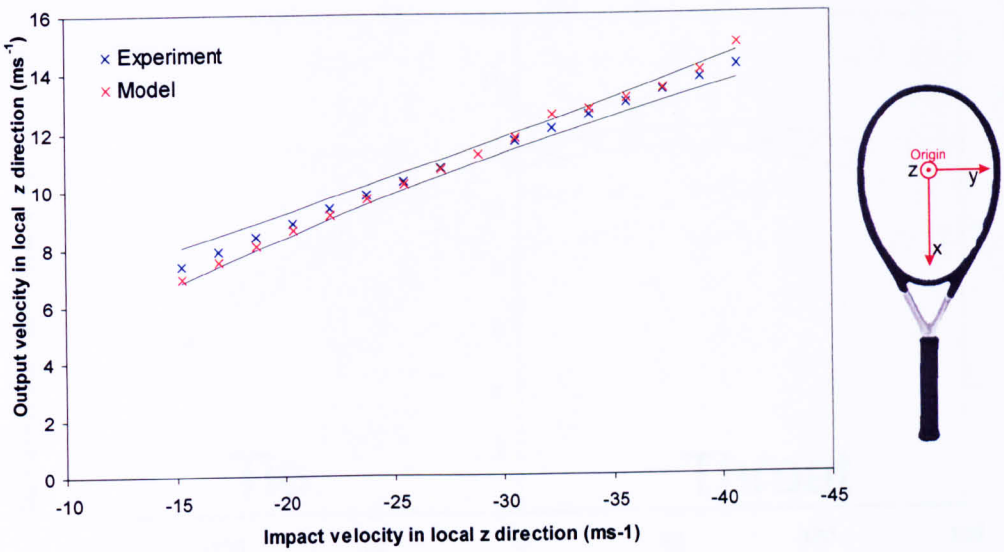

R^2 Fit of model to experimental data: 0.999

Figure 9.6. The parameters of the experiment and model, the plot of the respective results and the R^2 value of the model to the experimental data with regards to inbound velocity in the z direction.

This validation exercise tests the interaction between the spring damper model and the racket frame model. In this case the ball impacts the stringbed centre causing frame rotation and translation. At the stringbed centre, the model produces very accurate results for a variety of impact speeds. At this point on the stringbed very little frame vibrations are excited. The ability of the model to predict ball velocities at a variety of impact locations along the racket frame was also tested and is included below. This validation exercise has shown that impacts at around 30 ms^{-1} produce the most accurate results. This value will be used where appropriate in future validation exercises.

9.4.2 Longitudinal Impact Location

Figure 9.7 shows the model and experimental results for a series of input parameters as the longitudinal impact position changes. The zero impact position while corresponds to an impact on the stringbed centre. Negative values denote impacts toward the tip and positive values denote impacts toward the racket throat. As can be seen from the plot of results,

impacts toward the throat become increasingly poor at modelling the experiment, whilst predicted values remain within (or close to) the experimental error at the tip of the racket.

Inbound x velocity (ms^{-1})	Inbound y velocity (ms^{-1})	Inbound z velocity (ms^{-1})	Impact position x direction (mm)	Impact position y direction (mm)	Torque (Nm)
0	0	-30	-110 to 115	0	0

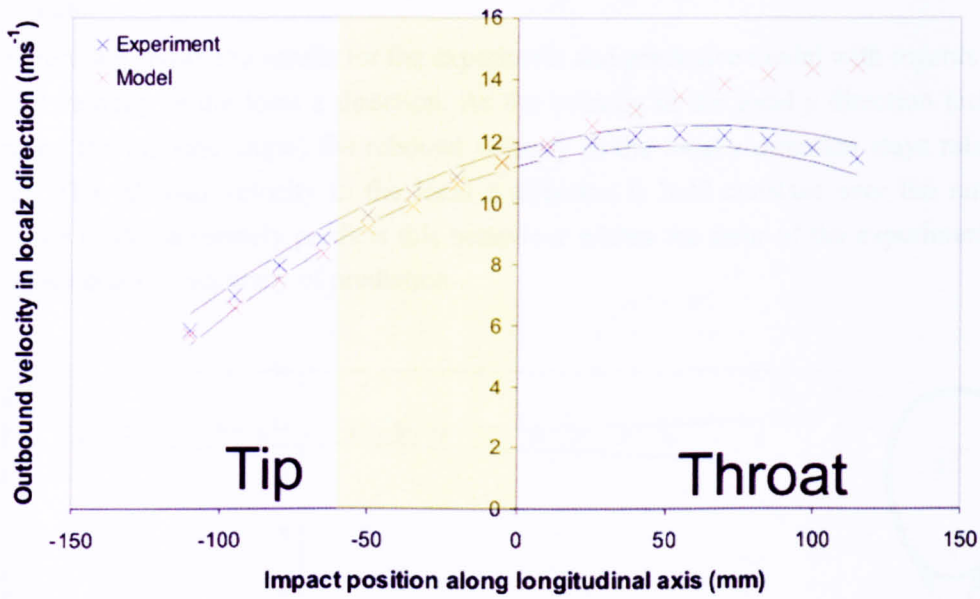

R^2 Fit of model to experimental data: 0.985

Figure 9.7. The parameters of the experiment and model, the plot of the respective results and the R^2 value of the model to the experimental data with regards to longitudinal impact position. The shaded region shows the range of impact positions obtained in player shot analysis (the mean ± a standard deviation).

The limits of the rigid body approach become clear in this validation exercise. In a rigid body model, the rebound velocity gradually increases as the impacts move further toward the throat. In reality, the frame vibrations constitute an increasingly large proportion of the impact energy. This is reflected in the results. The model rebound velocity continually increases, whilst the experimental results show a decrease in rebound ball velocity further toward the throat.

For impacts toward the tip of the racket, the energy loss through vibration does not greatly affect the rebound velocity due to the lower effective mass of the impact point. A smaller proportion of energy is lost through vibration. The plot in figure 9.7 includes a shaded region displaying the range of impact positions obtained in the player shot analysis. This shows that the rigid body assumption of the racket frame is capable of predicting outbound ball velocities within the experimental error for the range of impact positions shown in chapter 5.

9.4.3 Impact Angle

Table 9.8 shows the input parameters used when validating the inbound and outbound impact angle. This corresponds to an inbound angle of -30 to 15 degrees.

Inbound x velocity (ms^{-1})	Inbound y velocity (ms^{-1})	Inbound z velocity (ms^{-1})	Impact position x direction (mm)	Impact position y direction (mm)	Torque (Nm)
0	-8 to 17	-30	0	0	0

Table 9.8. The range of input parameters used when validating the inbound and outbound impact angle.

Figure 9.9 shows the results for the experiment and predictive model with regards to the outbound velocity in the local z direction. As the velocity in the local y direction increases (increasing the inbound angle) the rebound velocity in the local z direction stays relatively constant. The inbound velocity in the local z direction is held constant over the range of inputs. The model accurately predicts this behaviour within the error of the experiment. The R^2 value reflects this accuracy of prediction.

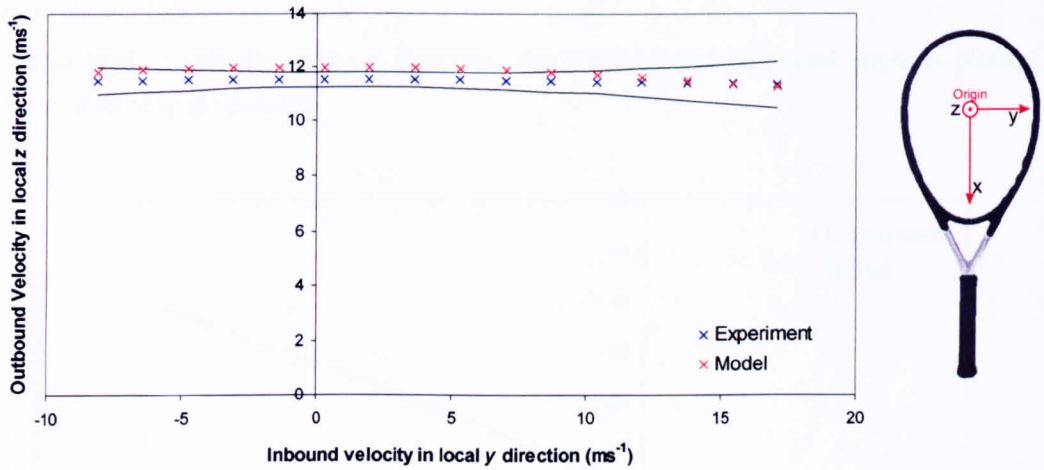

R^2 Fit of model to experimental data: 0.999

Figure 9.9. A comparison of the model and experimental data with regards to inbound angle and outbound velocity in the z direction. The R^2 fit of the experimental data to the predicted values is shown below.

Figure 9.10 shows the results with respect to the outbound velocity in the local y direction. As the inbound velocity in the y direction increases, the predicted values increasingly deviate from the experimental values. Both the experimental and predicted values show a linear relationship between the inbound and outbound velocity in the y direction, with the intersection at around 0, as expected. The magnitude of the outbound velocity is over-predicted in every case. This magnitude is primarily due to the response of the spin sub-model described in chapter 8.

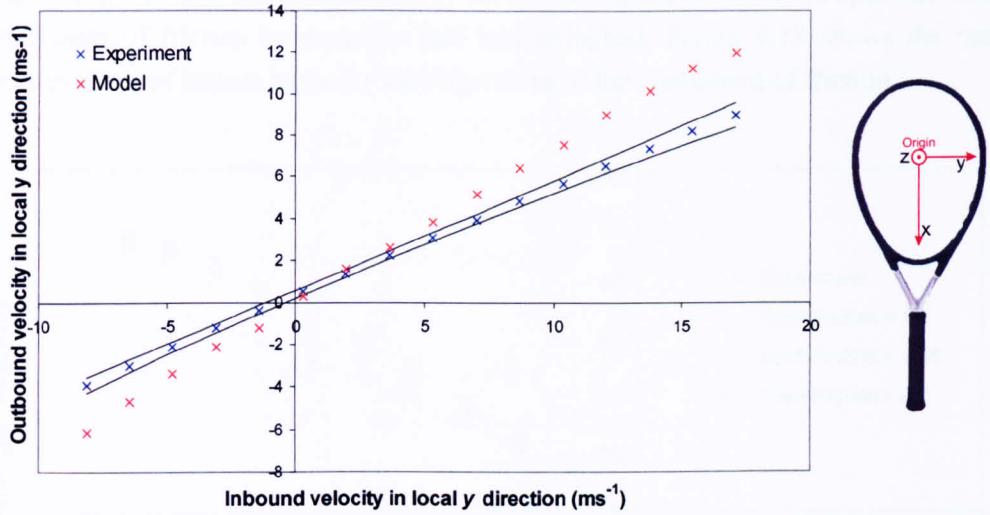

R^2 Fit of model to experimental data: 0.850

Figure 9.10. A comparison of the model and experimental data with regards to inbound and outbound velocity in the y direction. The R^2 fit of the experimental data to the predicted values is shown below.

If instead of velocity in the y direction, the inbound and outbound angle is plotted, a similar relationship is revealed.

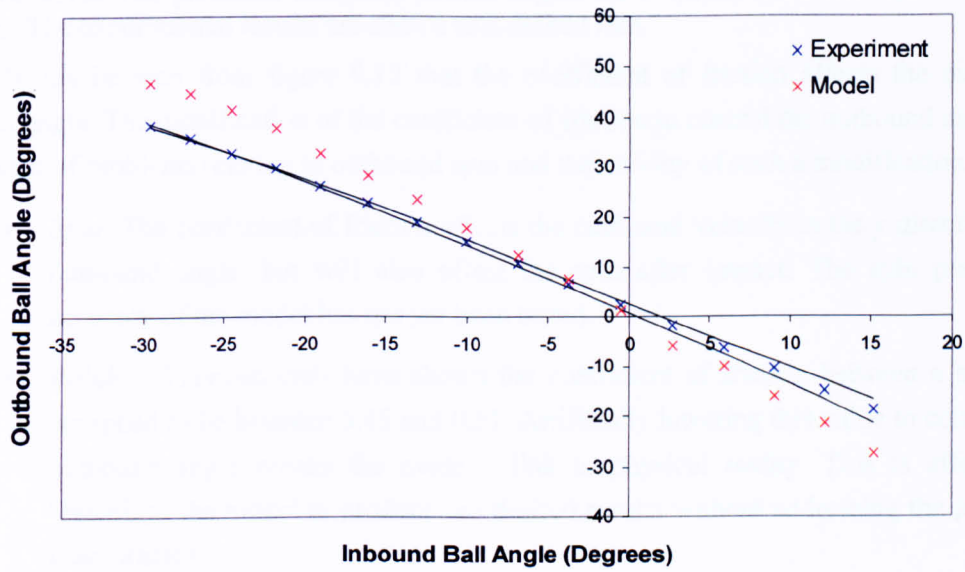

R^2 Fit of model to experimental data: 0.917

Figure 9.11. A plot which compares the model and experimental data with regards to inbound and outbound angle. The R^2 fit of the experimental data to the predicted values is shown below.

The model predicts that the ball leaves the stringbed with a higher velocity in the y direction, compared to the experimental data. The magnitude of this velocity is governed by

the response of the spin sub-model. One of the governing variables of the spin sub-model is the coefficient of friction between the ball and stringbed. Figure 9.12 shows the model's response in terms of impact angle for varying values of the coefficient of friction.

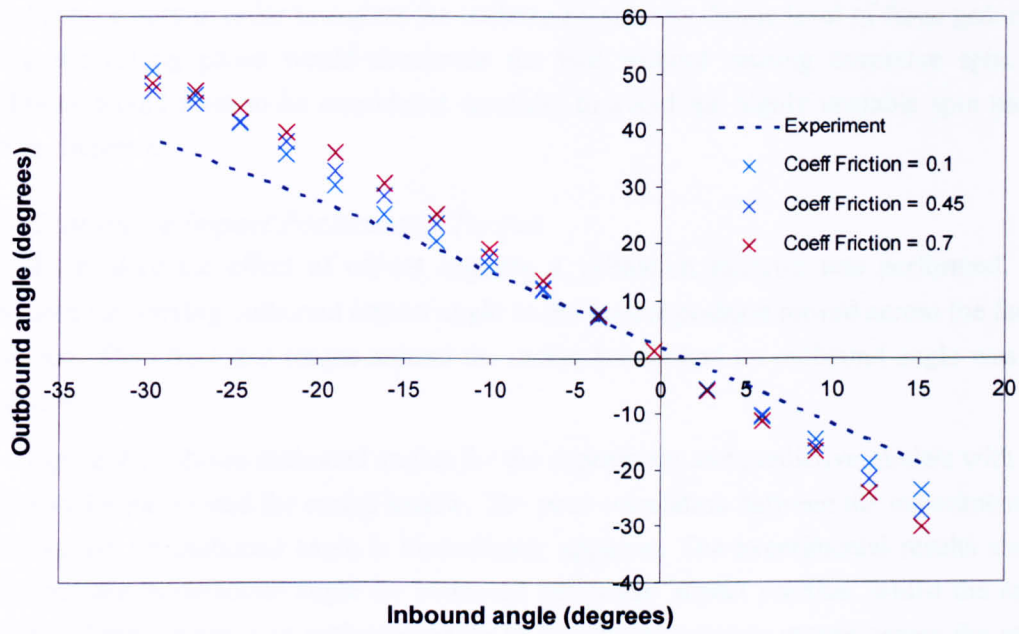

Figure 9.12. The predicted outbound impact angles for a variety of coefficient of friction values. The experimental results are shown as a dashed line.

It can be seen from figure 9.12 that the coefficient of friction affects the outbound impact angle. The modification of the coefficient of friction to control the outbound angle has a number of problems relating to outbound spin and the validity of such a modification.

- *Spin:* The coefficient of friction affects the outbound velocity in the y direction and outbound angle, but will also affect the spin after impact. The spin prediction accuracy of the model has not yet been tested.
- *Validity:* Previous tests have shown the coefficient of friction between a ball and stringbed to be between 0.45 and 0.51. Artificially lowering this value to control the outbound angle breaks the model's link to physical reality. This is effectively 'patching' the model to produce the desired results without addressing the physical inaccuracies.

Changing the coefficient of friction does not directly change the outbound velocities and angles. It alters the force that is generated during ball slip, changes the rate at which the ball decelerates, and changes the transition point between rolling and slip. Lowering the value of the coefficient of friction extends the period of slip on the racket stringbed. Higher coefficients of friction trigger the rolling phase of spin sooner, causing much less deceleration, and accordingly high outbound y velocities and impact angles.

It is clear that modification of the friction coefficient is not sufficient to correct the error in the spin model. The over-prediction of this sub-model with regards to y velocity and outbound angle is due to insufficient deceleration of the ball on the stringbed. This is in turn due to lower than necessary force generation. Modification of the mechanics of the spin model is necessary in order to correct the outbound y velocity. Some level of force generation during the rolling phase would decelerate the ball without causing excessive spin. The conditions would have to be considered carefully to avoid the highly unstable spin models seen in chapter 8.

9.4.4 Transverse Impact Position and Torque

To explore the effect of off-set impacts, a validation exercise was performed. This monitored the varying outbound impact angle as the impact position moved across the face of the racket. The effect that torque around the racket handle had on outbound angle was also monitored.

Figure 9.13 shows outbound angles for the experiment and predictive models with zero restrictive torque around the racket handle. The poor correlation between the experiment and model values for outbound angle is immediately apparent. The experimental results show a slight increase in outbound angle for increased transverse impact position, whilst the model predicts a linear increase in outbound angle as the impact position moves across the racket transverse axis.

Inbound x velocity (ms^{-1})	Inbound y velocity (ms^{-1})	Inbound z velocity (ms^{-1})	Impact position x direction (mm)	Impact position y direction (mm)	Torque (Nm)
0	0	-30	0	0 to 64	0

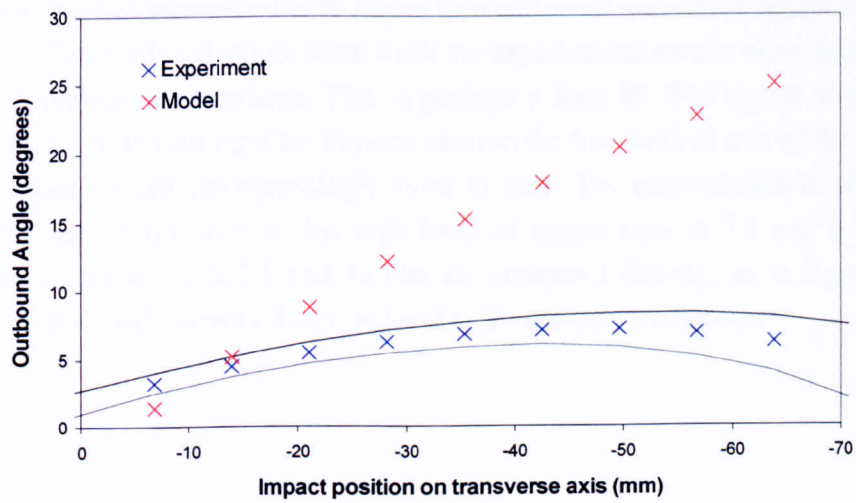

Figure 9.13. The experimental and predictive model results of the outbound angle for impacts along the transverse y axis of the racket face for no restrictive torque.

Figure 9.14 shows the same experimental and model results as figure 9.13, but with a restrictive torque around the handle of 7.5 Nm. A slightly better correlation is seen with these results but the model still displays a linear increase.

Inbound x velocity (ms^{-1})	Inbound y velocity (ms^{-1})	Inbound z velocity (ms^{-1})	Impact position x direction (mm)	Impact position y direction (mm)	Torque (Nm)
0	0	-30	0	0 to -64	7.5

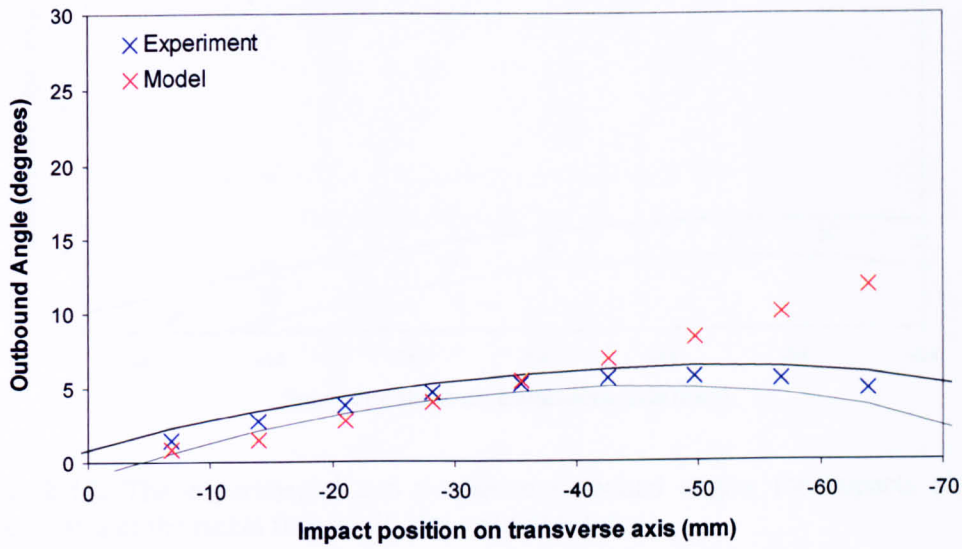

Figure 9.14. The experimental and predictive outbound angles for impacts along the transverse axis of the racket face for a 7.5 Nm restrictive torque.

Figure 9.15 shows the experimental and model results for a restrictive torque of 15 Nm. This torque value was ascertained to be higher than one could reasonably expect from a tennis player's grip. The predicted values seem to fit the experimental results more accurately than either of the previous comparisons. This is perhaps a false fit. The higher level of torque causes the racket to remain rigid for impacts close to the longitudinal axis of the racket. The outbound angles remain correspondingly close to zero. The experimental results however show a very similar response at this high level of torque than at 7.5 and 0 Nm. If the experimental responses at 0, 7.5 and 15 Nm are compared directly, as in figure 9.16, the torque has a surprisingly minor effect compared to the model's predictions.

Inbound x velocity (ms^{-1})	Inbound y velocity (ms^{-1})	Inbound z velocity (ms^{-1})	Impact position x direction (mm)	Impact position y direction (mm)	Torque (Nm)
0	0	-30	0	0 to -64	15

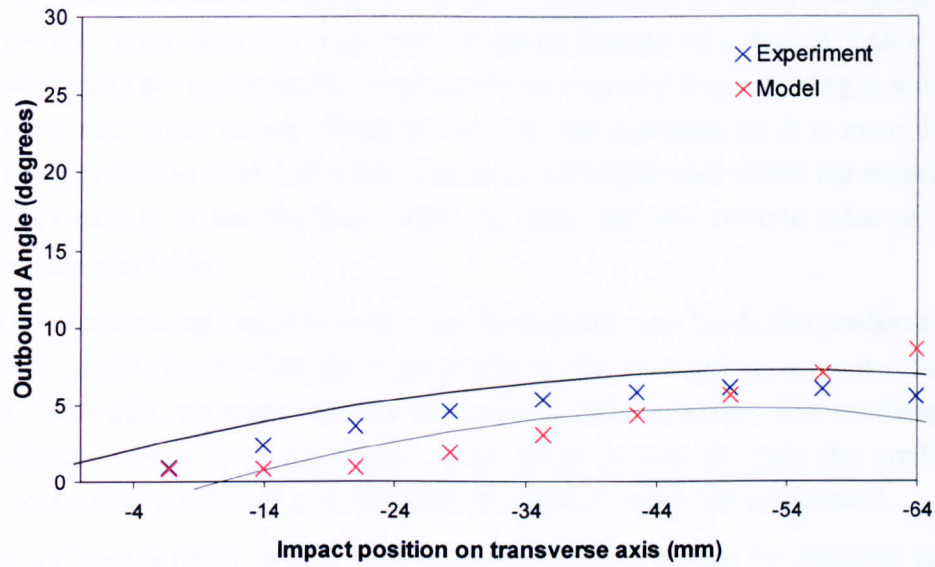

Figure 9.15. The experimental and predictive outbound angles for impacts along the transverse axis of the racket face for 15 Nm restrictive torque.

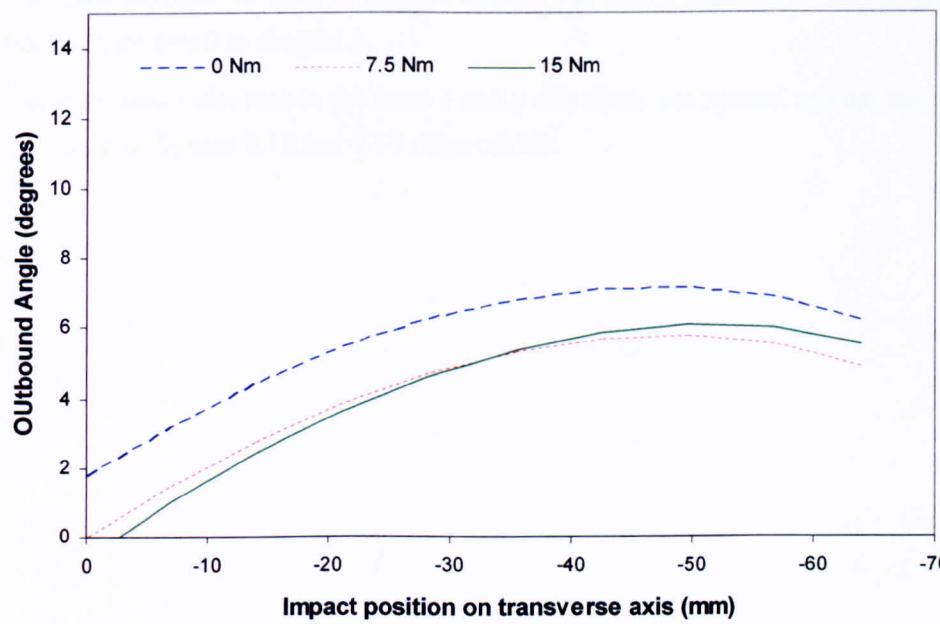

Figure 9.16. A comparison of the experimental response at three levels of torque.

From figure 9.16, a reduction in outbound angle with the addition of a restrictive torque can be seen. The reduction in outbound angle is consistently around 2 degrees at all positions

along the tennis racket. Although this seems quite small, over the length of a tennis court this could be several metres, certainly the difference between a ball landing in or out.

The experimental results show very little difference between 7.5, or 15 Nm of torque. This in itself may be due to the experimental apparatus used in testing. When measuring the torque applied by the variable clutch, it was done with a torque wrench at low speed. How this measurement varies from the high speed dynamic loading of a typical tennis impact is unknown. It may be more valuable to reduce the experimental torque loading to a situation of 'no torque' and 'some torque'. When taking this into consideration it is more difficult to validate the predictive model response. The levels of torque used within the model may not correspond exactly to the physical reality. As such, the only reliable value of torque to validate against is 0 Nm.

Given that the only reliable results may be at zero torque levels, the predicted values in figure 9.13 quickly deviate from the experimental results. As a ball impact moves further into the transverse axis, the torque causing the racket to twist increases. The resulting rebound angle deviates away from the normal. This result is seen in both the predicted and experimental values, although experimentally the effect is much less pronounced.

In an internal report, Whyld **2004** performed impacts against the stringbed centre of a head clamped racket and 50 mm offset. It was found that, in isolation the stringbed acts to correct transverse impacts. The ball leaves the stringbed with a trajectory back towards the stringbed centre. It is clear that the stringbed is not simply a level surface throughout impact, but its surface deforms in such a way to correct the ball's trajectory. This experiment is described in more detail in chapter 2.

The outbound velocities in the local z and y directions are plotted against the transverse impact position in figures 9.17 and 9.18 respectively.

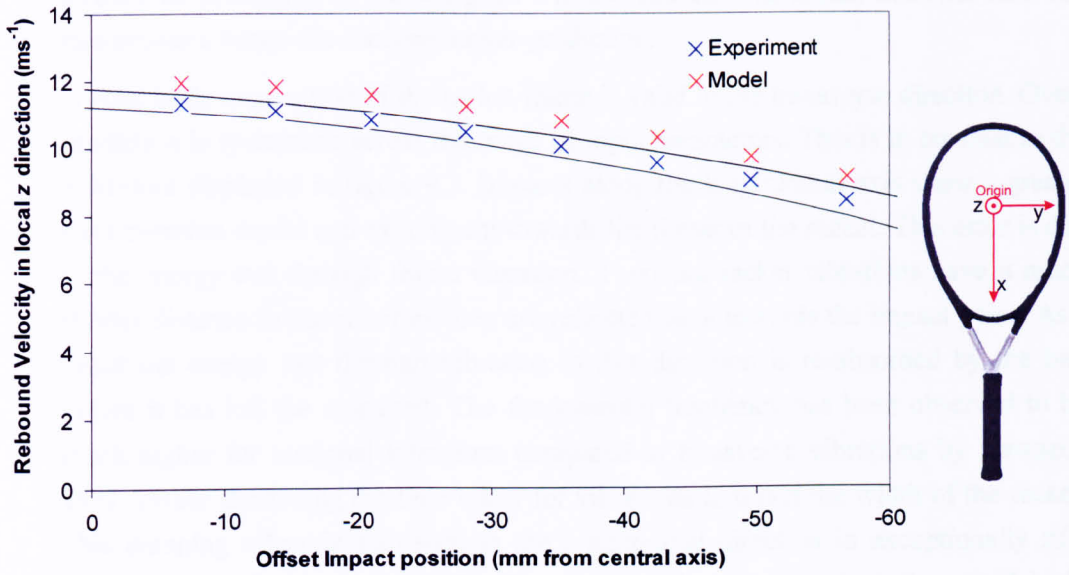

Figure 9.17. The outbound velocity in the local z direction as the impact moves along the transverse axis.

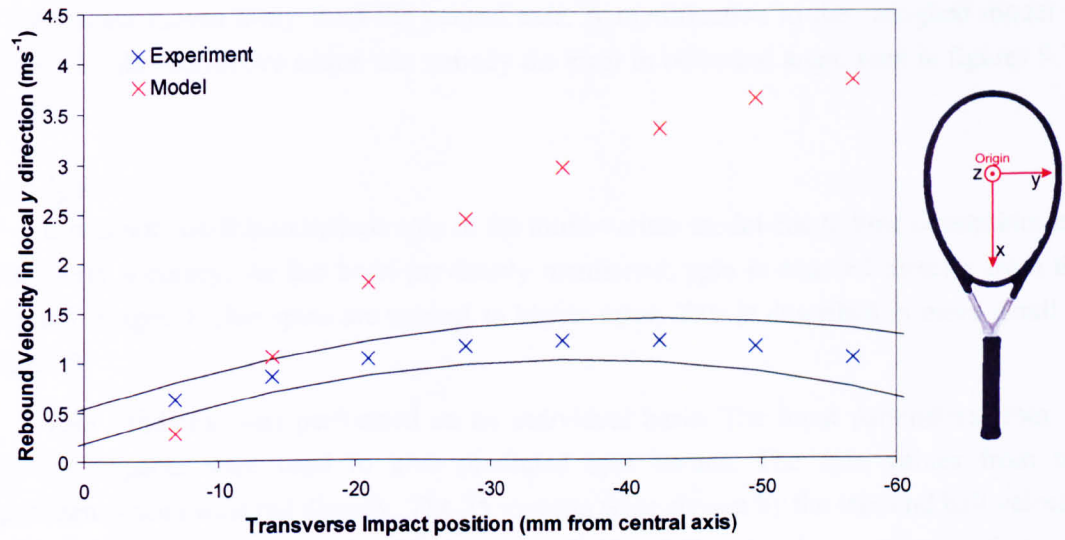

Figure 9.18. The outbound velocity in the local y direction as the ball impact moves along the racket's transverse axis.

Figure 9.17 shows that the model over-predicts the experimental results. Despite this, they closely follow the trend of the experiment as the impact moves away from the central axis. This discrepancy reveals two things:

1. The consistent over-prediction is further evidence that the stringbed deformation may change the trajectory of the ball. Stringbed deformation generates a reactive force. If a portion of this force acts to force the ball towards the centre of the racket, the velocity

directly perpendicular to the stringbed will be reduced. The model does not take this into account, hence the consistent over-prediction.

2. A rigid body assumption of the racket frame is valid in the transverse direction. Over-prediction is systematic across the range of input parameters. This is in contrast to the behaviour displayed in figure 9.7. Impacts along the longitudinal axis show a greater error between model and experiment towards the throat of the racket. This error is due to the energy lost through frame vibration. Torsional racket vibrations have a much shorter distance to travel before they are reflected back towards the impact point. As a result the energy lost through vibration in this direction is re-absorbed by the ball before it has left the stringbed. The fundamental frequency has been observed to be much higher for torsional vibrations compared to transverse vibrations by Kawazoe **1997** further shortening the time taken for vibrations to travel the width of the racket. This damping effect is also seen in the longitudinal direction in exceptionally stiff tennis rackets (Brody et al. **2002**). The results tally very closely with a rigid body assumption.

The frame modelled as a rigid body is a valid assumption for impacts in the transverse direction. The deformation model does not account for the corrective action of the stringbed as the impact moves away from the central axis. A modification to the stringbed model to account for this corrective action can remedy the error in outbound angle seen in figures 9.13 to 9.15.

9.4.5 Spin

It was not possible to include spin in the multi-variate model due to time constraints and issues with accuracy. As has been previously mentioned, spin is counted directly from the recorded images, higher spins are subject to higher error. This is described in more detail in chapter 5.

Spin validation was performed on an individual basis. The input parameters from 25 different impacts were used to give predicted spin values. The spin values from the experiment were measured directly. The 25 impacts were chosen by the inbound ball velocity in the y direction. It was previously shown in chapter 5 that this is a governing factor in outbound spin. A range of y velocity values were chosen to give a range of spin values. The input parameters for all 25 impacts are shown in table 9.19, in descending order of outbound spin. The impacts were chosen to best represent the entire input domain.

Without a multi-variate fit, the experimental and predicted values must be compared directly and equated to a line of $y = x$. Figure 9.20 shows such a comparison. A line $x = y$ is included for comparison and error bars of ± 3.33% are included on the experimental values. This error value is according to an error of a single frame at 2000 rpm, and is meant as a guideline to an expected error value.

Inbound x velocity (ms^{-1})	Inbound y velocity (ms^{-1})	Inbound z velocity (ms^{-1})	Impact position x direction (mm)	Impact position y direction (mm)	Torque (Nm)
-0.01	23.7	-30.5	-74.26	-1.72	0
-0.1	20.53	-28.8	43.91	6.73	12.5
0.2	18.36	-29.43	-37.59	-9.54	0
0.0	18.58	-34.1	69.00	19.61	12.5
-0.2	21.78	-38.9	49.43	-3.92	7.5
0.4	18.67	-29.0	-9.8	7.59	0
0.3	18.18	-31.24	19.79	10.50	0
-0.7	13.84	-27.4	-36.84	-2.62	0
-0.1	14.50	-26.1	-3.81	4.25	0
0.7	13.38	-30.6	58.67	4.94	0
-0.4	14.77	-34.3	-90.71	4.71	0
-0.4	14.05	-27.6	7.64	16.54	7.5
-0.3	13.88	-26.72	-93.29	-22.33	0
-0.5	8.75	-23.66	4.21	-5.41	0
-0.2	14.32	-33.78	29.05	5.00	12.5
-0.4	8.65	-20.89	-107.76	-12.33	0
0.0	13.83	-34.67	40.11	11.16	0
-0.3	8.82	-26.12	30.01	2.59	0
-0.56	8.58	-22.91	85.83	-13.67	0
0.02	8.73	-29.74	58.69	2.58	0
-0.16	8.59	-21.19	51.70	6.03	12.5
0.68	7.09	-21.73	64.58	0.71	12.5
-0.47	6.39	-21.36	70.07	-0.99	0
-0.29	6.68	-21.41	34.95	-2.15	0
-0.26	6.95	-20.75	-63.98	-3.79	0

Table 9.19. The input parameters for all 25 impacts tested in the spin validation exercise. The parameters are in descending order according to outbound spin.

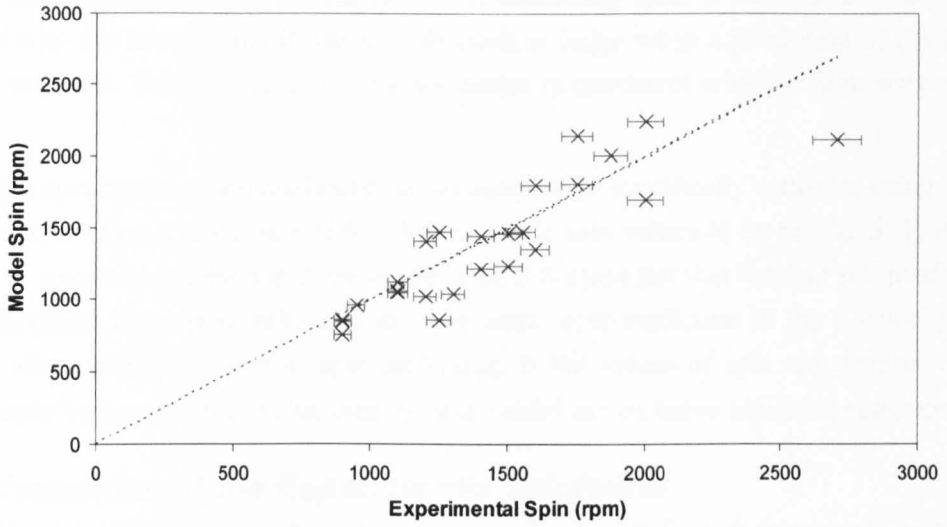

R^2 Fit of model to experimental data: 0.976

Figure 9.20. The predicted and experimental spin values for 25 separate impacts.

The results generally show good correlation other than a single experimental spin value of 2700 rpm. An R^2 value of 0.9764 suggests a good fit. The input parameters in this case cover the entire input domain, with a range of input positions, torques and inbound ball velocities. The magnitude and scatter in the difference between prediction and experiment seems to increase as the measured spin value increases. An upward linear trend in error is associated with an increase in spin measurement.

The validation of the spin prediction aspect of the model includes a number of problems. It was not possible to include spin as an aspect of the multi-variate fit. This made it impossible to test particular aspects of the spin model by keeping other parameters constant. As a result, 25 individual impacts were tested with a variety and range of input parameters. Although this increases the robustness of the validation, it does not facilitate an easy analysis of any resulting discrepancies between model and experiment.

The differences seen in the results are due to a combination of spin measurement error and the predictive model. An error of ± 1 frame of video was quoted in chapter 5 when discussing the error in spin measurement. This is perhaps an accurate assumption when the spin values are below around 1000 rpm. When the magnitude of spin increased the difficulty of measurement and associated error increased significantly. It was shown earlier in this chapter that the spin sub-model over-predicts outbound y velocity due to a systematic error in the assumption of ball rolling. It is clear from figure 9.22 that this error is also manifest in the predicted spin value. This is to be expected, the outbound spin and velocity in the y direction are directly related.

The predictive model gave a spin value with an associated axis of spin described in three dimensions. The spin measured from the recorded video images is given as a scalar

value measured using a single camera. When measuring spin, if the axis of spin was not aligned with the image plane it was very difficult to judge when a revolution of the ball had been completed. This uncertainty in measurement is consistent with the high scatter of the error.

The spin aspect of the predictive model needs to be specifically validated using video at a higher resolution and frame rate to allow accurate spin values to be recorded. This would allow the spin to be resolved in three dimensions. It is also clear that the spin sub-model needs to be modified in order to minimise the systematic over-prediction in the y velocity which should also correct the error in spin prediction. If the values of spin are measured with a sufficiently high confidence value then the spin model can be better validated and improved.

9.5 Discussion of the Experimental Validation

The model has been validated against experimental results and shows varying levels of fit for different experimental parameters.

A number of assumptions were made in producing the predictive model, each of which has been implemented with varying levels of success. The assumptions and the associated discussion of their validity are discussed below.

9.5.1 Rigid Body Model

The racket frame was assumed to be a rigid body. This simplifies the calculations involved with its translations and rotations by assuming that it does not deform. For impacts along the longitudinal axis, this assumption is inaccurate towards the throat of the racket. In reality, the racket frame vibrates considerably toward the throat of the racket, and this accounts for some fraction of the total energy. The model over-predicts the outbound velocity compared to the experimental values for impacts at the throat of the racket, as shown in figure 9.7. At the node point of the racket and further toward the tip, the model predictions are much more accurate. In this region, the vibrations are much smaller in amplitude and do not affect the outbound ball velocity as significantly.

The region of impact exhibited by players in the player shot analysis is also shown in figure 9.7. This reveals that frame vibration is not a significant problem in the area of the racket most commonly hit.

For impacts along the racket's transverse axis, the rigid body model is a good assumption. Figure 9.17 shows a good correlation between the experimental and predicted results. Impacts away from the racket's central axis still result in frame vibrations. The shorter distances that torsional vibrations have to travel along the transverse axis means that the energy dissipated by vibration is re-absorbed by the ball before it leaves the stringbed. In this situation the rigid body model is a good representation of reality.

A rigid body assumption does have some role to play in a predictive model. Goodwill **2002** overcame the problem of frame vibration by using a one dimensional finite element

beam model. This model was restricted to impacts along the longitudinal axis and would have required considerable added complexity to include impacts along the transverse axis. With the knowledge that a rigid body assumption is valid along the transverse axis, this could be used as a valid expansion of the finite element frame model.

9.5.2 Point Contact

The point contact assumption is primarily associated with the ball spin model. Several concessions have been made to satisfy this assumption. Point contact assumes that all force acts at a point on the ball and racket stringbed. The rolling and slipping phases of the ball spin model have been modified to tally with this point contact assumption. This has resulted in the quasi-rolling phase outlined in chapter 8. When rolling, although the ball deforms, the ball does not increase in angular velocity. This concession is linked with the over-prediction of the outbound angle seen in figure 9.11. The lack of a retarding force during the rolling phase of spin results in insufficient deceleration of the ball's COM. This results in the over-prediction compared to the experimental results.

A distributed contact assumption would better reflect reality, but increase complexity greatly. In a distributed loading scenario, the force is greatest at the centre of the ball and reduces towards the edges. This is compared to point contact when a single force acts through the ball's COM. The two cases are illustrated in figure 9.23.

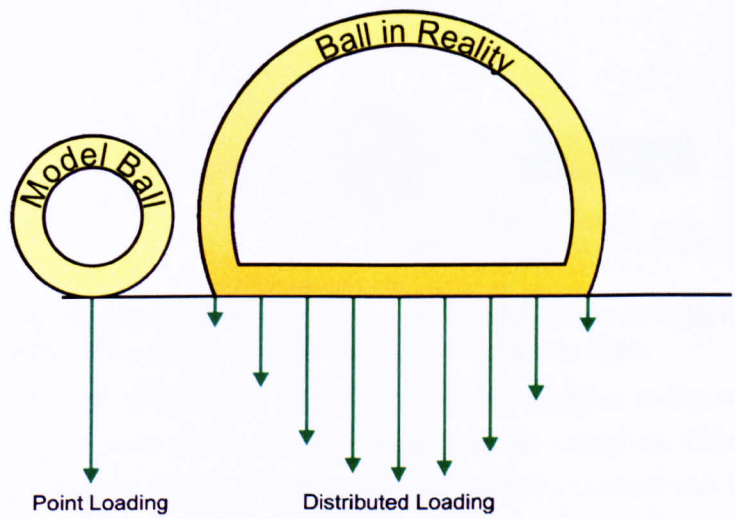

Figure 9.23. A comparison of the model's point loading assumption and the more realistic distributed loading seen in reality.

In a 3D model, the distributed loading would form a circle of contact rather than the single line seen in figure 9.23. A distributed loading assumption allows variable distributions of force to be used. This could be used to accommodate off set forces which generate overspin and allow more complex spin behaviours to be modelled. Cross **2002a** and Goodwill et al. **2005** noticed that during oblique impacts, ball deformation causes the resultant reactive impact force to act behind the COM, increasing the torque and spin. At present the ball is

rigid in the tangential direction, this would have to be modified to account for this effect. Using a distributed load would also require a more complex modelling of the stringbed to account for the distributed contact. The response of the racket frame and outbound ball trajectory would also much better represent reality.

9.5.3 Stringbed Deformation

It was assumed that during impact, the stringbed deforms uniformly across the contact surface. As a result of this, the force due to deformation acts perpendicularly to the racket frame. It was shown in an internal report by Whyld **2004** that the stringbed acts to correct the ball trajectory when the ball impacts off the central axis. This corrective action becomes greater the further the impact moves away from the centre of the racket.

This corrective action comes from an increase in the stringbed stiffness away from the racket's central axis. The coefficients of stringbed stiffness can be modified by a correction function, which varies with the impact position y along the transverse axis:

$$K' = K \times C \quad | \quad C = f(y) \qquad \textbf{[9.1]}$$

If $f(y)$ is an exponential function, it will be 1 at the centre of the racket and approach infinity away from the edge, as illustrated in figure 9.24.

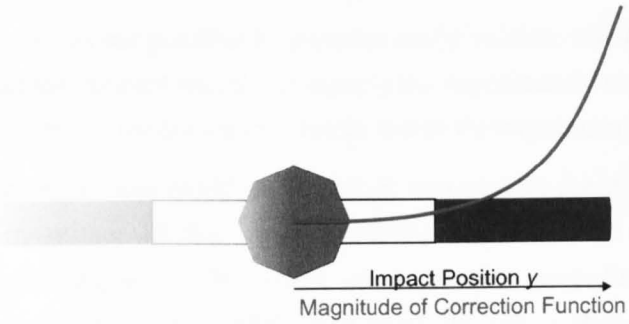

Figure 9.24. If an exponential correction function is used, it has no effect on the stringbed stiffness at the centre of the racket and a large effect towards the edge.

The ball/stringbed deformation model includes an effective radius term. This is the radius of the circle of contact that the ball makes with the stringbed. Using the correction factor, the stringbed deformation at both edges of the ball's contact can be calculated, as shown in figure 9.25. The stringbed deformation at the edge of the ball closest to the racket's centre is more than that closest to the edge. By assuming that the stringbed is linear across the ball's surface, an angular effect is created. If the force resulting from ball/stringbed deformation acts perpendicularly to the stringbed's surface then the trajectory is corrected towards the racket's centre. This is illustrated in figure 9.25.

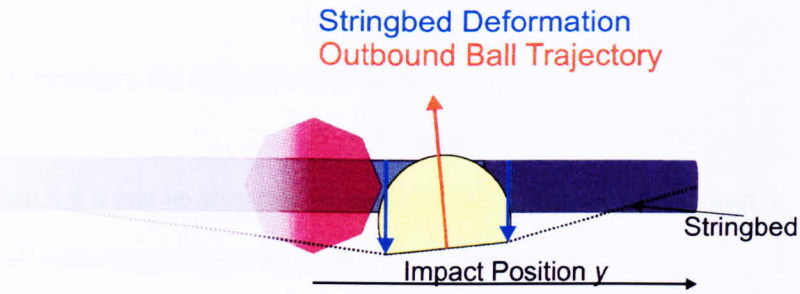

Figure 9.25. When the stringbed deforms to different amounts along the transverse axis, the force acts to correct the balls trajectory towards the racket's centre.

An exponential correction function of the form seen below was used to modify the stringbed stiffness coefficients.

$$C = a \cdot y \times e^{(b \cdot y - c)} + 1 \qquad [9.2]$$

The coefficients *a, b* and *c* control the shape and scaling of the exponential function.

It is possible to determine the coefficients *a, b* and *c* experimentally by testing the deformations under load at different areas of a racket stringbed. It is likely that the correction factor *C* would be a function of the longitudinal *and* transverse position. For the purposes of this discussion, it has been limited to the transverse direction.

With limited time it was not possible to experimentally validate this modification to the stringbed model. Instead the concept was tested against the experimental results by modifying the values of *a, b* and *c* until the model results closely match the experimental values.

The ball/stringbed model was modified to include a corrective force which changes the ball's trajectory. The magnitude of this corrective force was calculated at each time step according to a corrective angle θ. The value of θ changes according to the relative deformations of the stringbed at the edge of the ball, using the values shown in figure 9.25, θ is calculated as below:

$$\theta = \sin^{-1}\left(\frac{Def_A - Def_B}{r_E}\right) \qquad [9.3]$$

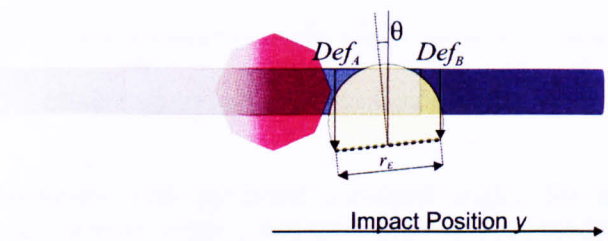

Figure 9.26. The values used in the calculation of a corrective angle θ.

The force from the deformation model usually acts in the local *z* direction only. The corrective angle θ was used to modify the deformation force and to calculate its vertical and horizontal components. The force in the local *z* direction becomes:

$$F_z = F \cdot \cos(\theta) \quad [9.4]$$

In the local y direction, the magnitude of the force is:

$$F_y = F \cdot \sin(\theta) \quad [9.5]$$

From equation 9.4 it can be seen that impacts off the central axis will result in:

1) An overall reduction of force in the local z direction

2) An increase in force back towards the centre of the racket in the local y direction.

This is reflected in the systematic over-prediction of outbound velocity in the z direction seen in figure 9.18 and the lack of correlation of the velocity in the y direction as seen in figure 9.19.

An iterative process was used to generate values for a, b and c as seen in equation 9.2. The values used are shown in table 9.27.

a	b	c
3	97	-3

Table 9.27. The values used in the correction function C as seen in equation 9.2.

When implemented into the stringbed deformation model, the correction factor reduces the outbound angle across the face of the racket as seen in figure 9.28.

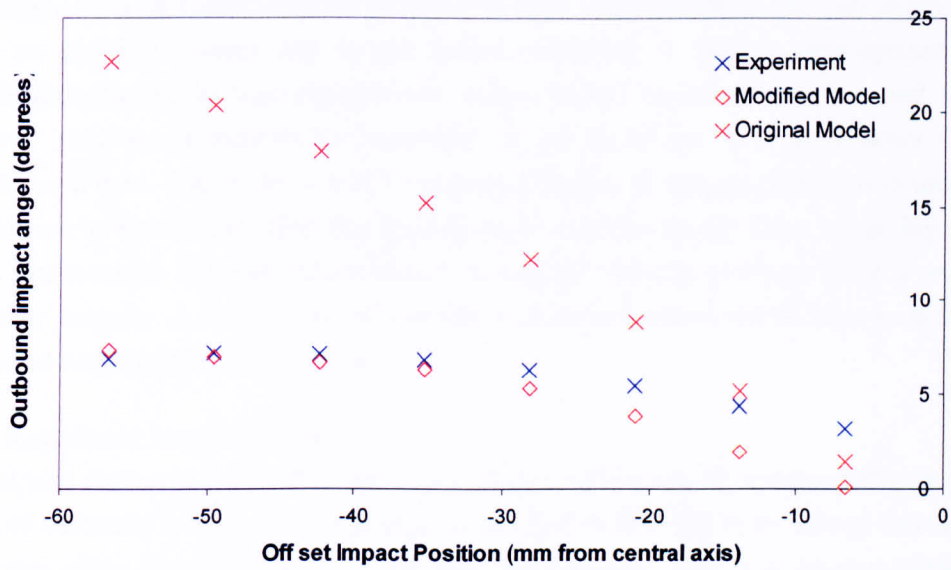

Figure 9.28. The experimental and predicted outbound angles for impacts along the transverse racket axis. In this case the original and modified stringbed models are shown.

The iterative process used to obtain the coefficients of C has produced a good correlation between the experimental and predicted results.

The corrective action of C is shown in figure 9.29 as a percentage value.

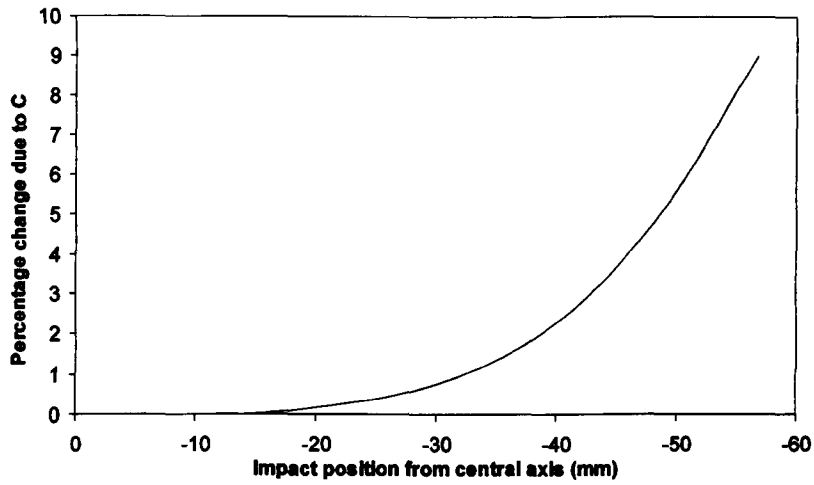

Figure 9.29. The percentage magnitude by which C alters the spring constant values to produce a corrective action.

It can be seen that even at the extremities of the racket face, the spring constants used in the deformation model are only increased by around 9%. An advantage of this approach is that relatively small changes in the spring constants produce the required corrective action without significantly affecting the outbound velocity.

The iterative exercise has shown that this approach is valid for correcting the outbound ball angle. Without calculating the coefficients of C experimentally, the correction function bears no physical relationship to the actual stringbed. A further development of this modification should include experimental values linked to impact position and stringbed stiffness. This would increase the versatility of the model and provide a better fit to the experimental data. The model would be improved further if dynamic testing was used. It has been shown by Cross et al. **2000** that the behaviour of tennis strings alters at varying dynamic loads. The example in figure 9.28 is at an inbound ball velocity of 30 ms^{-1} and is untested at any other velocity. A fully validated corrective stringbed model would have to account for impacts at varying inbound velocities.

9.5.4 Restrictive Handle Torque

It was shown in figure 9.16 that a torque around the handle has a stabilising effect in terms of outbound ball angle. It was also shown that as the restrictive torque increases, this stabilising effect does not change by any significant amount. This is in contrast to the model results, which show a systematic decrease in outbound angle as the restrictive torque increases.

It was assumed in this validation exercise that the experimental torque value directly coincides with the constant restrictive torque applied in the predictive model. It is unknown whether the high impulse resulting from impact generates a constant restrictive torque and

whether this torque corresponds to the level used in the model. As such it is not possible to ascertain whether the lack of correlation comes from the experiment or predictive model.

A better method of applying a restrictive torque is necessary in order to validate the predictive model. Torque is the only experimental variable not measured directly; the velocity and impact position was measured directly from the impact images. The torque was measured prior to impact and as such is the only variable set at artificial intervals.

A torque gauge using strain gauges and high frequency sampling equipment could be used to measure the effective torque around the handle. The clutch used to restrict the movement about the handle could be set within rough intervals and measured directly during impact. This eliminates any ambiguity between the experimental torque values and those used in the predictive model.

With a direct reading of the experimental restrictive torque value, the response of the model could be better validated. Exactly how this torque affects the post-impact ball and racket behaviour could be ascertained.

9.6 Player Shot Validation

The predictive model was used to predict the outcome of shots recorded during the player shot analysis outlined in chapters 4 and 5. The player shot analysis includes the full racket and ball movement prior to impact. This provides the necessary initial conditions to input into the predictive model. The physical characteristics of the ball and racket are also required, including the moment of inertia of the racket around all three of the global axes. This information was only available in three cases.

Ten individual shots were chosen at random from a possible thirty two. The initial conditions from each shot were put into the predictive model. The local outbound velocities in the y and z directions and the outbound spin were compared with the results given from the player shot analysis. The specific parameters used in the model are shown in table 9.30.

Racket

Velocity of Racket COM (ms^{-1})				Angular Velocity of Racket ($rads^{-1}$)		
Test	x	y	z	Swingwise (about *x*)	Spinwise (about *z*)	Twistwise (about *y*)
1	9.5	-3.1	12.5	22.3	-17.1	-10.7
2	9.1	-6.0	15.7	31.1	-13.6	10.6
3	-3.6	10.3	13.5	37.3	9.6	9.3
4	-5.7	7.8	13.0	36.5	32.3	8.5
5	12.7	-6.0	16.3	31.1	-6.4	-8.8
6	11.4	-8.0	15.3	24.7	-10.2	-7.4
7	14.3	-5.5	19.8	27.6	-20.4	-14.0
8	6.3	-0.4	15.5	23.7	-14.4	-13.5
9	8.6	-11.0	14.4	23.9	-15.3	-12.0
10	-2.2	-9.0	11.4	23.3	-11.0	1.3

Ball

Velocity of Ball COM (ms^{-1})				Impact Position (mm)		Inbound Spin (rpm)
Test	x	y	z	x	y	
1	-2.8	1.1	-7.5	-10.4	11.8	2860
2	-3.7	1.2	-10.7	-121.5	47.3	3000
3	0.4	-0.5	-8.4	-93.9	-30.8	2860
4	2.8	-1.3	-11.3	-79.9	24.0	3750
5	-2.7	-0.7	-6.7	-65.9	-38.2	3000
6	-3.0	1.3	-6.5	-46.7	-13.3	2860
7	-2.4	-0.3	-6.5	-55.8	18.4	2610
8	-2.8	-1.5	-10.5	-50.9	26.6	3330
9	-2.2	-1.9	-10.6	-109.2	33.9	3750
10	1.7	1.9	-10.1	-35.8	20.2	2400

Table 9.30. The input parameters of the racket and ball used in the predictive model when modelling player shot results.

Comparisons of the predicted and measured resultant ball velocity and outbound angle are shown in figures 9.31 and 9.32. A $y = x$ line is shown to indicate the ideal comparison. For velocity values, an error of $\pm$ 3 ms^{-1} has been included to reflect experimental error. An error of 5° is included on experimental angle values.

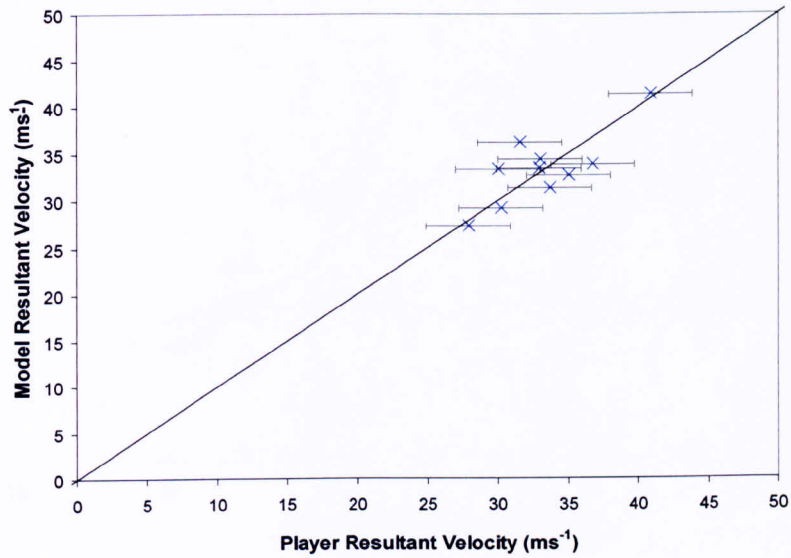

Figure 9.31. A comparison between the resultant outbound ball velocity of the model and measured experimental values.

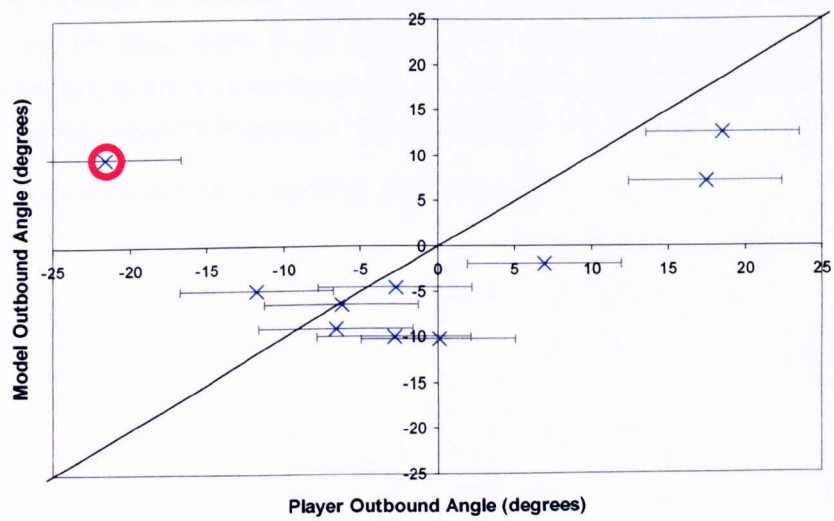

Figure 9.32. A comparison between the outbound ball angle given by the predictive model and player shot analysis.

Figure 9.31 shows that resultant velocities are mostly predicted within experimental error. Predicted values for outbound angle are generally close to experiment other than a single anomalous value.

Figure 9.33 shows the component velocity values including experimental error.

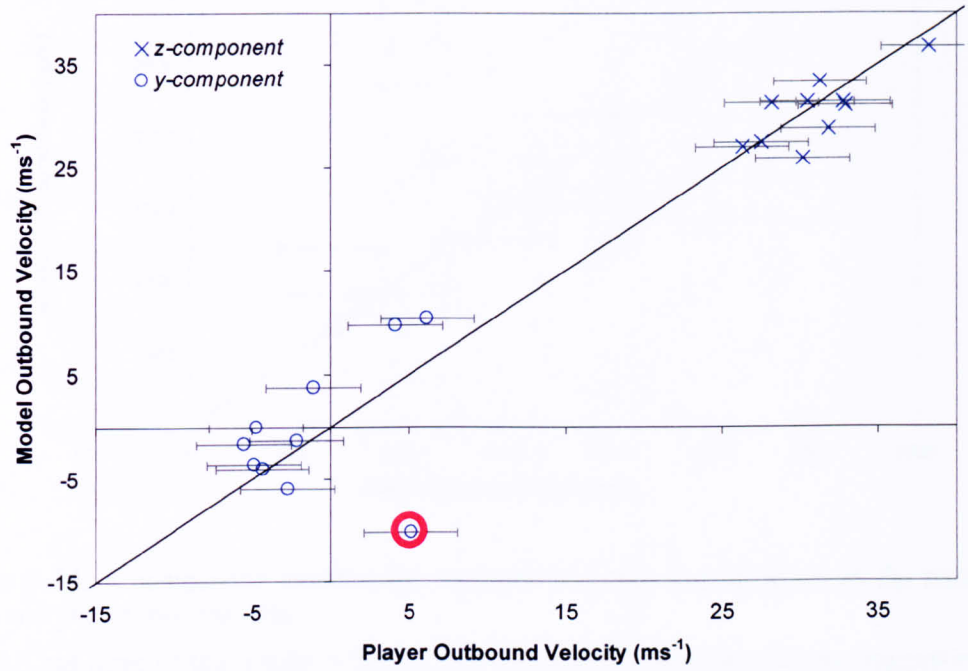

Figure 9.33. A comparison between the component velocities given by the model and experiment.

The z-component of velocity shows a better correlation than the y-component. It has been mentioned that weaknesses in the spin model result in differences between model and reality. Despite this, in many cases the results are within or close to the limits of experimental error, reflecting the general robustness of the model itself.

A comparison of spin value is shown in figure 9.34.

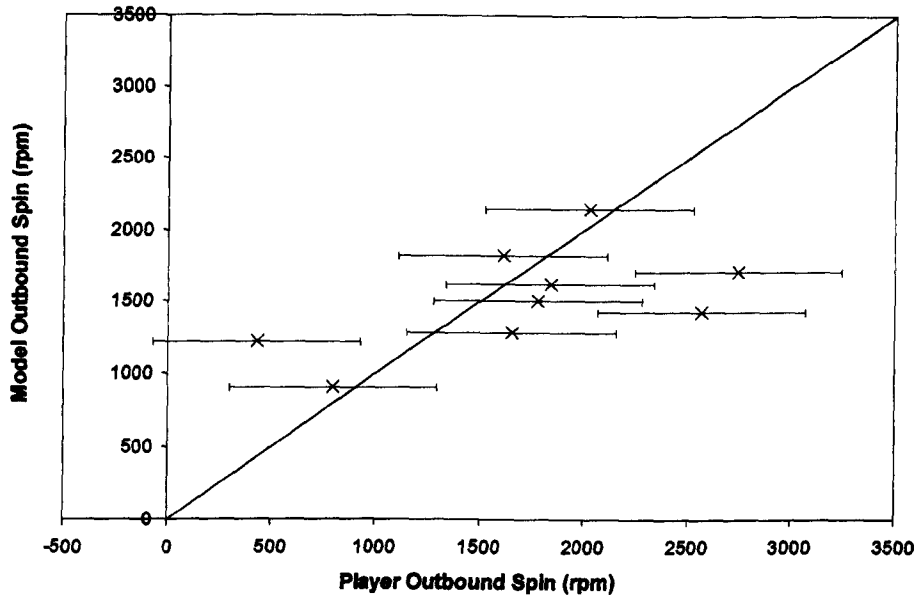

Figure 9.34. A comparison between the outbound ball spin outputs given by the predictive model and player shot analysis.

All but three of the results in figure 9.34 fall within experimental error suggesting that the model is generally an adequate predictor at outbound spin. This is despite recognised problems with experimentally measuring spin values and the predictive model.

The player shot validation represents a subtly different approach to the experimental validation process occupying much of this chapter. The experimental validation was performed to test each aspect of the model individually and uncover possible oversights and problems with the predictive model. By validating the model against actual player shot data every aspect of the model is tested simultaneously using realistic values.

The results shown within this section show that the model is capable of predicting outbound velocity and spin from a variety of different shots with acceptable levels of accuracy. A single anomalous result, shown in figures 9.32 and 9.33 could be the result of an experimental processing error. Development of the spin model to more closely match the physical reality may yield more reliable spin prediction.

The player shot validation has reinforced the points discussed in the previous section. Areas of the model which have shown a good correlation with the experimental results continue to do so when compared with a player's shots. Areas of the model which show a weaker correlation have a larger scatter. Accurate predictions of velocity in the y direction will give an associated launch angle of the ball, on a tennis court. Outbound spin in 3D could be used to calculate the associated flight path and increase the scope of the model, such as the complete tennis shot simulator Tennis GUT as developed at the University of Sheffield (Haake **2007**). In this way the predictive model is a powerful tool for investigating the effect of changes in shot and racket type.

9.7 Chapter Summary

This chapter has outlined the validation of a predictive model, the development of which was described in chapter 8. The predicted results given by the model were compared with experimental results generated through a multi-variate fit. The experiment and its multi-variate fit were described in chapters 6 and 7.

The multi-variate fit method was used to validate the predictive model for a change in five parameters:

1) The inbound velocity in the y direction.
2) The inbound velocity in the z direction.
3) The impact position along the longitudinal direction.
4) The impact position along the transverse direction.
5) The restrictive torque around the handle.

It was found that the model was accurate at predicting outbound z velocities for a change in each of the five parameters above. The rigid body assumption meant that the greatest inaccuracies came from impacts towards the racket throat. In reality, frame vibrations account for a fraction of the total energy which is not accounted for in the predictive model. This results in an over-prediction of the ball velocity. However, the longitudinal impact positions observed in the player shot analysis are in the region of minimum racket vibration, hence the rigid body model produced accurate predictions.

Predicted outbound velocities in the y direction showed consistent over-prediction for impacts off the transverse axis and for a range of inbound y velocities. This over-prediction was due to the rolling condition of the spin model and the lack of retardation force.

The outbound impact angle was formed from the outbound velocities in the y and z direction. It was seen that as impacts moved away from the central axis, the model over-predicted the outbound angle. A racket stringbed generates a corrective action for off-set impacts which moves the ball trajectory back towards the racket centre. This corrective action was modelled using an exponential curve which increased the stringbed stiffness away from the central axis. Although not experimentally validated, this method was shown to produce more accurate results.

The spin was validated using a smaller scale exercise in which the spin values of 25 impacts were measured manually. The input parameters of each impact were put into the predictive model and the results compared with the manually recorded values. A direct comparison showed inherent scatter which increased as the measured spin value increased.

The predictive model was validated against ten shots from the player shot analysis. The possible number of shots to test against was reduced as the full inertial properties of each

racket were required. This validation exercise showed that the model is capable of giving values within experimental error for a complex combination of realistic input parameters.

This validation exercise has shown the predictive model to be usable at predicting post-impact ball characteristics. In combination with a suitable trajectory model, this model could be used to investigate the effect of varying shot and racket combinations.

10 Model Applications

10.1 Introduction

The previous chapter outlined the validation of a predictive model capable of predicting the outcome of a realistic tennis shot. This chapter demonstrates possible model applications as a series of case studies. A predictive model allows one to observe the effect of a change in tightly controlled parameters which may be difficult to observe experimentally. In this way the effect of a change in shot or racket type can be assessed without ever having to swing a racket. Accurate racket/ball motion is provided by the player data outlined in chapter 5. A series of case studies will also give a good indication of whether the model reacts as expected physically.

10.2 Aim

To illustrate the use of the predictive model shown in chapter 9.

10.3 Chapter Structure

This chapter involves two main case study areas:

1. *Effect of Shot Type:* This case study investigates the effect (velocity, angle and spin) of changing the swing and weight characteristics of the racket during impact.
2. *Effect of Shot Accuracy:* This case study assesses how a change in impact position affects the trajectory according to different levels of impact accuracy.

10.4 Effect of Shot Type: Methodology

The predictive model was used to consider how the output of a shot changes according to particular input parameters in which the following methodological steps were used:

- The movement of the racket was altered by varying its swing speed around all three local axes.
    - Appropriate values of racket swing speed were obtained from the player testing data.
- The weighting of the racket was altered by varying its moment of inertia around the longitudinal and transverse axes.
    - Appropriate racket weightings were obtained from the paper by Haake et al. **2007**. This paper provides a large sample of racket data from all eras of the game and was used to assess typical minimum and maximum values for rackets of the current era.

10.4.1 Racket Movement

Four separate impact points were used in the case of swing speed; the throat, centre, tip and off set. The three swinging movements were defined as *swinging*, *twisting* and *spinning*. The location of each of these impact points and the directions of the swinging movements are described in figure 10.1.

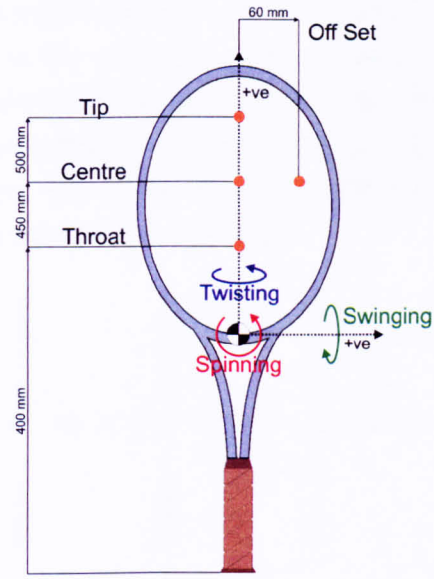

Figure 10.1. The impact locations and swinging directions used in the first case study.

The characteristics of the racket used in the study were as follows:

Mass:	243 g
Swingweight:	0.012 kgm^{-2}
Twistweight:	0.0015 kgm^{-2}
Spinweight:	0.0135 kgm^{-2}

These values are typical of a modern racket and those used by the players in the player testing analysis.

Swinging

Swingwise rotation is associated with a standard racket swing. A racket swung with zero swingwise rotation will be moving at the same speed at all points along the racket's length. The tip of a racket swung with high amounts of swingwise rotation will be moving comparatively faster than the throat. This is according to the convention described in figure 10.1 and assuming that the racket's linear velocity is directly out of the page. Shots with large amounts of swingwise rotation are often described as *wristy*. This is due to a large amount of racket rotation being about the wrist. More traditional tennis shots with lower amounts of swingwise rotation consist of a set elbow/wrist and rotation about the shoulder. This is backed up by a quote from Knudson **2006**: *"Classic technique tended to be dominated by shoulder*

motions. The more sequential coordination that is often called the 'modern' forehand adds elbow flexion and wrist rotation to assist in the creation of racket speed and upward motion." The closer the centre of rotation to the racket COM, the greater the amount of swingwise rotation.

In order to represent these separate situations, four cases were used in which the racket movement was due purely to rotation about a point a specified distance from the racket COM. The centres of rotation used in this case study were at distances of 0.3, 0.45 0.95 m from the COM and at infinity (zero rotation). The amount of rotation about each point was calculated so as to give the COM an instantaneous linear velocity of 18 m/s. This value is typical of those obtained from the player testing analysis. This is illustrated in figure 10.2. The racket had zero rotation in the twist and spinwise directions.

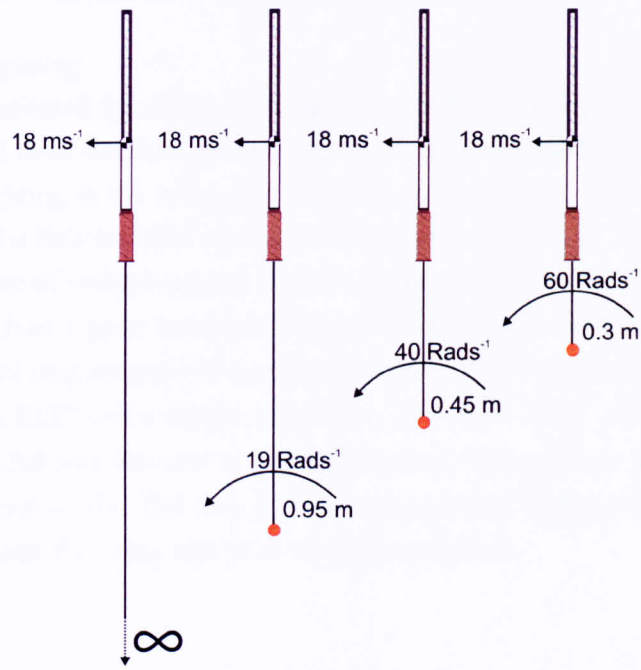

Figure 10.2. The instantaneous centres of rotation and angular velocities used in the first case study.

Twisting

Twistwise rotation is about the longitudinal axis of the racket. Twisting the racket will *open* or *close* the racket face at impact, i.e. increase or decrease the angle between the ball and racket. Twisting motion during impact has an effect on the ball depending on the location of impact. It can increase or decrease the rebound velocity of an off set impact depending on whether the twisting action increases or decreases the relative ball/racket velocity at impact. It may also alter the angle at which the ball leaves the stringbed. The values of twistwise rotation used in this study were 0, 9 and 18 $rads^{-1}$, representing the range of measured impacts from the player testing study. In order to simulate positive and negative twisting motion the offset impact location was set at 60 mm either side of the longitudinal axis. In every case the

racket had 40 $rads^{-1}$ of swingwise rotation in order to represent a typical shot from the player shot analysis. The racket had zero rotation in the spinwise direction.

Spinning

Racket spin is associated with movement about an axis perpendicular to the racket face. Hence, rotation in this direction increases the velocity of the racket perpendicular to the stringbed of the racket face. Chapter 5 showed that velocity in this direction (planar velocity) is associated with increased ball spin. Whilst increased spinwise rotation can increase the spin on the ball, it can also change the angle at which the ball leaves the stringbed and make it more difficult to hit the ball as desired. Values of 0, 15 and 30 $rads^{-1}$ were used in this case study to reflect those obtained in player testing. No rotation was added in the Twistwise direction but 40 $rads^{-1}$ was present in the swingwise direction.

10.4.2 Racket Weighting

This study monitored the effect of changing the racket weighting on shot output. In this case only swing and twist weight were considered. Haake et al. **2007** gives a good account of modern racket weighting in the swing and twist directions as RDC units. The RDC unit is a proprietary unit to the Babolat RDC machine (described in chapter 7). The RDC unit is given in $kgcm^{-2}$. In the case of swingweight, it is given 10 cm from the handle tip. This convention is used because it gives a good impression of how hard a racket is to swing from the wrist. The predictive model uses moment of inertia values around the racket COM and in kgm^{-2}. In order to convert the RDC unit a simple conversion from cm^{-2} to m^{-2} and a shift in reference point using the parallel axis theorem is required. In each case a racket mass of 300 gm was used, heavier than previously. This was intended to represent a light racket with added lead tape used to manipulate the swing and twist weight as required.

Swingweighting

Haake et al. **2007** showed that a modern racket has a swingweight between 260 and 360 RDC units. A balance point of 30 cm from the racket tip was used (also obtained from Haake et al. **2007**). Using the parallel axis theorem the point of reference was shifted to the COM as follows:

$$I_{COM} = I_{RDC} + md^2 \qquad [10.1]$$

where I_{COM} is the swingweight around the racket COM, I_{RDC} is the given RDC swingweight value, m is the mass of the racket (0.3 kg) and d is the distance through which the reference point was shifted (0.4 m). RDC values of 260, 310 and 360 gave transformed values of 0.014, 0.019 and 0.024 kgm^{-2}. Changing the swingweight of the racket alters the maximum swingspeed the player is able to generate. For this reason this case study uses a flat shot (zero swingwise rotation) at the impact locations shown in figure 10.1. The twistweight was set at 0.00125 kgm^{-2}, the spinweight of the racket was equal to *swingweight* +

twistweight according to the perpendicular axis theorem. The change in swingweight was used to illustrate how a racket resists rotation, altering the rebound velocity and angle.

Twistweighting

The twistweight of the racket was set at 0.0005, 0.00125 and 0.002 kgm^{-2} according to the values in Haake et al. **2007**. A higher twistweight is associated with a high *stability*, a value which in itself is difficult to define. Head **1975** claimed that his oversize racket design increased twistweight and therefore reduced rotation (and error) when hitting a ball off the longitudinal axis. For this reason the impact locations used in this study start at the stringbed centre (450 mm from butt) and move in 20 mm increments along the transverse axis up to 80 mm off set. The swingweight used was 0.019 kgm^{-2}.

10.5 Effect of Shot Type: Results

The results presented are those deemed to be most relevant for each study. In most cases this is the resultant velocity after impact and the angle at which the ball leaves the stringbed. This will be appropriately described in each case.

Swinging

The effect of swingwise rotation on absolute velocity is shown in figure 10.6. The results are categorised in order of location of the instantaneous centre of rotation. The speed of rotation increases as the centre of rotation moves toward the COM.

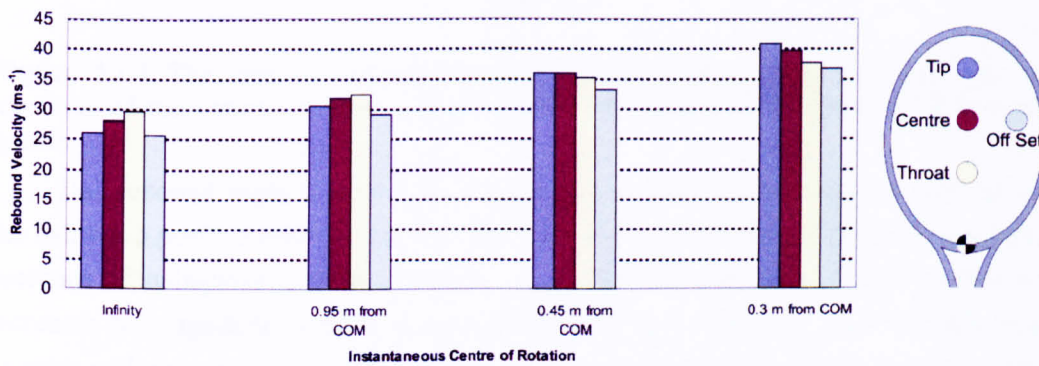

Figure 10.3. The absolute rebound velocity values for four impact locations with varying locations of the centre of rotation.

It can be seen from figure 10.3 that increased swingwise rotation increases the relative inbound velocity between the ball and racket. This results in an increased rebound velocity for all impact locations. However, it can be seen that when the centre of rotation is closer to the COM, it is more beneficial to hit towards the tip of the racket, whilst the converse is true for as the centre of rotation moves away from the COM.

The speed of swingwise rotation will alter the rebound angle along the longitudinal axis. For this reason this angle has been monitored, and is shown in figure 10.4. Angle convention is also shown.

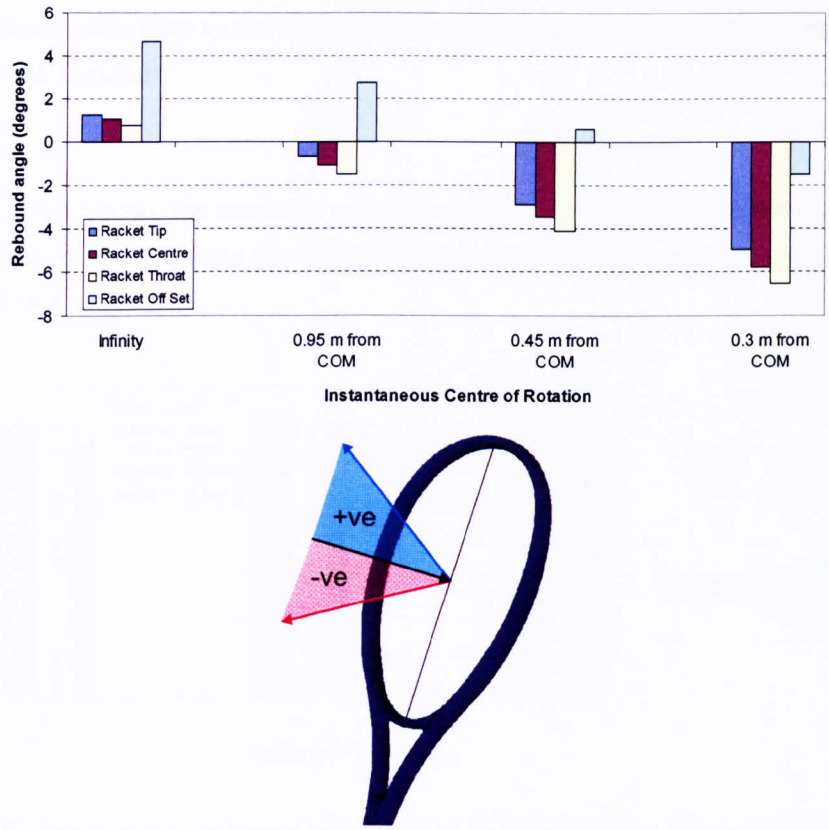

Figure 10.4. The rebound angle of the ball for four different impact locations with varying locations of the centre of rotation, equivalent to a number of different swingwise rotation speeds.

Ball rebound angle is largest for impacts towards the tip. With zero swingwise rotation the ball has a positive rebound angle in all cases. For impacts along the longitudinal axis, the presence of swingwise rotation produces a negative rebound angle. Increasing this rotation increases the magnitude of the rebound angle. For off set impacts the rebound angle is largely positive with zero swingwise rotation. The addition of swingwise rotation decreases this angle such that it becomes negative in the most extreme case. Rebound angle in this case is due to racket rotation during impact (the ball is perpendicular to the racket face). With zero swingwise rotation the racket rotates such that the ball leaves the stringbed with a positive rebound angle. The presence of swingwise rotation reverses the racket rotation during impact causing the ball to leave the stringbed with a negative rebound angle. For impacts off the longitudinal axis, racket rotation is much larger during impact and requires a significant amount of swingwise rotation to reverse the effect. In terms of a standard groundstroke, the addition of swingwise rotation means that the shot location should be moved towards the tip of the racket in order the achieve maximum velocity. For a flat shot, the trajectory of the ball

is such that it leaves the racket face moving away from the player (towards the tip of the racket). Increased swingwise rotation alters the trajectory of the ball such that it moves towards the player, or towards the throat of the racket. In a standard forehand shot these angular deviations would serve to alter the trajectory of the ball to either side of the court. How these deviations relate to the flight of the ball is dependent on the stance and positioning of the player on the court.

Twisting

Figure 10.5 shows the resultant rebound velocity of a tennis ball for three values of twistwise rotation. In this case the off set impact location is at 60 mm either side of the longitudinal axis.

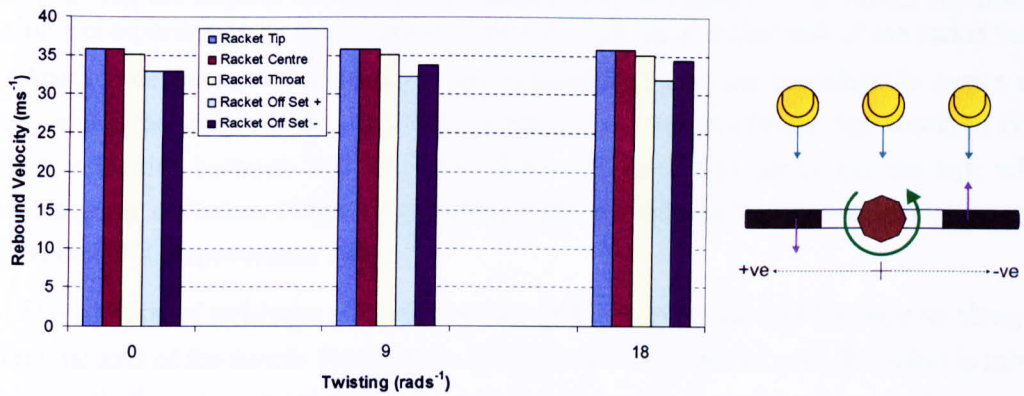

Figure 10.5. The resultant rebound velocities of the ball for five different impact locations with varying values of twistwise rotation.

As might be expected, very little effect is observed for impacts along the longitudinal axis. In the case of off set impacts, if the racket is rotating towards the ball, the relative inbound velocity between ball and racket increases, increasing rebound velocity. Where the racket rotates away from the ball, relative inbound velocity decreases and rebound velocity drops. This is illustrated alongside the chart in figure 10.5.

Figure 10.6 shows the horizontal rebound angle of the ball off the racket face for the same conditions as figure 10.5. In this case the values are absolute allowing a comparison to be made between impact locations on either side of the racket face. The relative directions are shown diagrammatically alongside the chart.

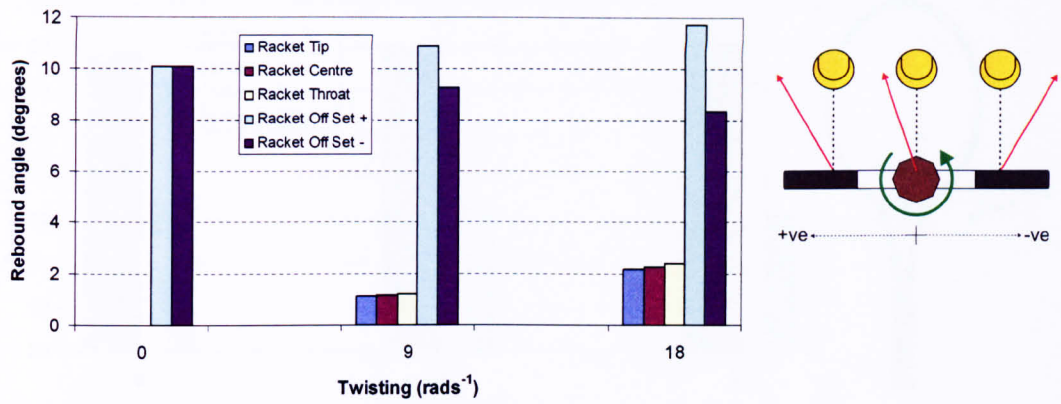

Figure 10.6. The horizontal rebound angles of the ball for a number of twistwise rotation values showing the relative directions according to impact location. The values are absolute allowing a comparison to be made between impact locations on either side of the racket face.

Angular deviation for impacts off the longitudinal axis are considerably larger than impacts along the longitudinal axis. Positive twistwise rotations (those that result in larger resultant velocities between ball and racket) have a correcting action on the ball which reduces angular deviation. Negative twistwise rotations enlarge the angular deviation away from the racket's perpendicular axis.

The addition of twistwise rotation has very little effect on the ball for impacts along the longitudinal axis of the racket. For impacts off set to the longitudinal axis, the effect is mixed. If hit correctly the rebound velocity is increased and angular deviation reduced. However, on the opposite side of the racket the penalty for hitting the ball off set is great. Rebound velocity is further reduced and the angular deviation increased.

The angular deviations observed in this section would alter the vertical trajectory of the ball when a racket is held in the standard orientation. An impact off the racket's longitudinal axis incurs a significant deviation change which may result in the ball hitting the net or bouncing outside the court's boundary. It can be seen that the penalty for hitting off the longitudinal axis can be minimised if the twistwise rotation increases relative ball velocity. However the player testing analysis suggests that most players are not capable of this level of control, not a tactic to be encouraged.

Spinning

The resultant rebound velocities for a variety of spinwise rotation values are shown in figure 10.7.

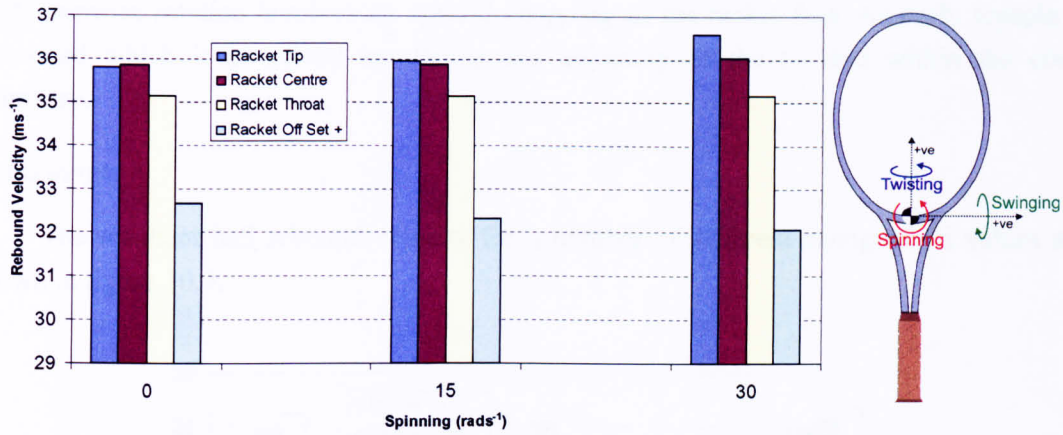

Figure 10.7. The resultant rebound velocities of the ball for four different impact locations with varying values of spinwise rotation.

It is apparent from figure 10.7 that the ball rebound velocity increases as Spinwise rotation increases. Although this effect is small it is due to the ball being accelerated away from the racket perpendicular.

Figure 10.8 shows the post-impact ball spin for a number of different spinwise rotation values.

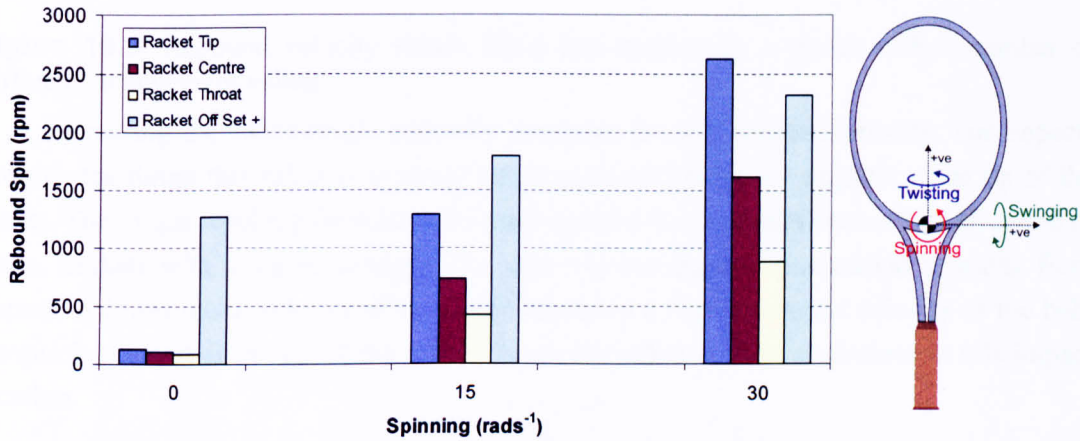

Figure 10.8. Post-impact spin rates of the ball for a number of spinwise rotation values.

Impacts off the longitudinal axis produce a high amount of spin even at zero spinwise rotation values. As mentioned previously, off set impacts produce significant racket rotation during impact, this results in high spin levels. Along the longitudinal axis, increasing spinwise rotation increases the magnitude of spin. This is more significant towards the tip of the racket as the relative inbound velocity between ball and racket is maximised.

Spinwise rotations have the largest effect for impacts towards the tip of the racket. This movement of the racket is directly associated with spin generation. The larger the magnitude of spinwise rotation the greater the amount of spin which is generated. In a standard forehand

shot, spinwise rotation involves an upward *chopping* of the racket face. As such, topspin is generated which is beneficial in altering the trajectory of the to land within the court boundary.

Swingweight

The resultant ball rebound velocity for a number of different swingweight values are shown in figure 10.9.

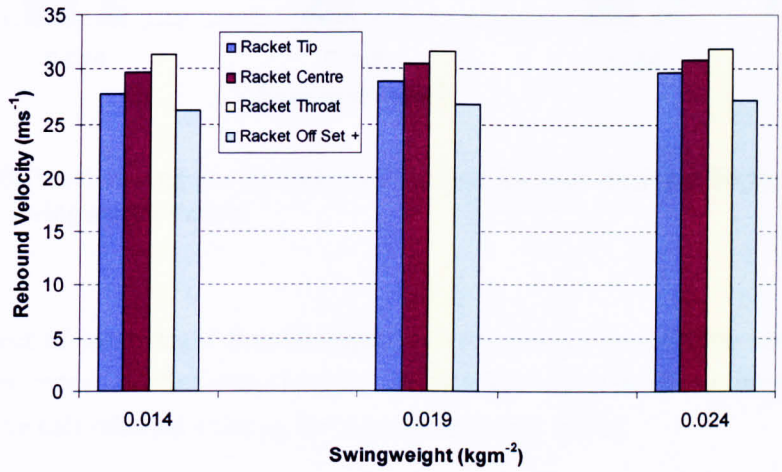

Figure 10.9. Rebound velocity values for a ball incident to a racket with a number of different swingweight values.

Increasing the swingweight generally increases the ball rebound velocity. For impacts towards the throat this effect is minimal but is more noticeable for impacts at the tip of the racket. The torque resulting from impact causes a racket to rotate accelerate about its centre of mass. Rackets with a higher swingweight have a lower angular acceleration resulting from impact. A lower recoil velocity of the racket results in a higher rebound velocity of the ball. Torque is greatest at the tip of the racket, hence the effect is most noticeable at this impact location.

For the same reason, vertical angular deviation (as shown in figure 10.4) is reduced with increased swingweight. Racket rotation is reduced during impact and this is seen in figure 10.10.

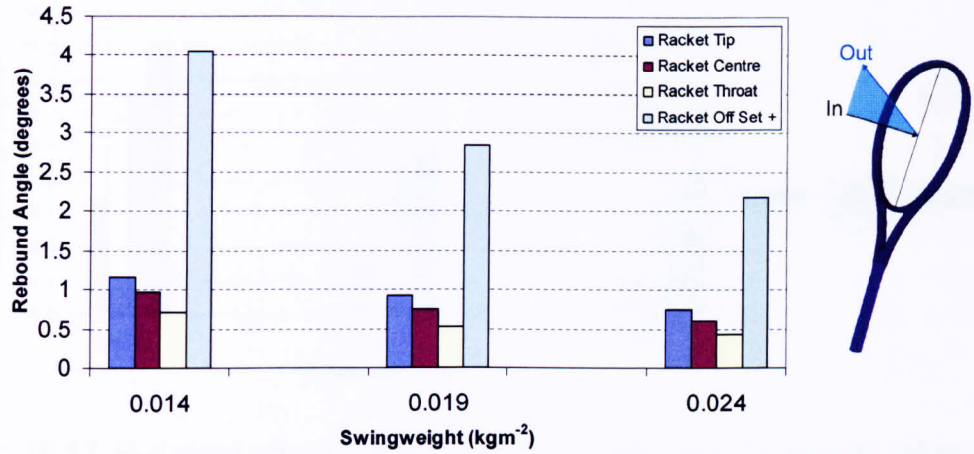

Figure 10.10. Vertical Angular deviation of the ball for four different impact locations and three separate swingweight values.

Twistweight

The effect of twistweight is most apparent for impacts along off the longitudinal axis. For this reason impact location was along the width of the racket in 20 mm increments. Figure 10.11 shows the ball rebound velocity for three twistweight values.

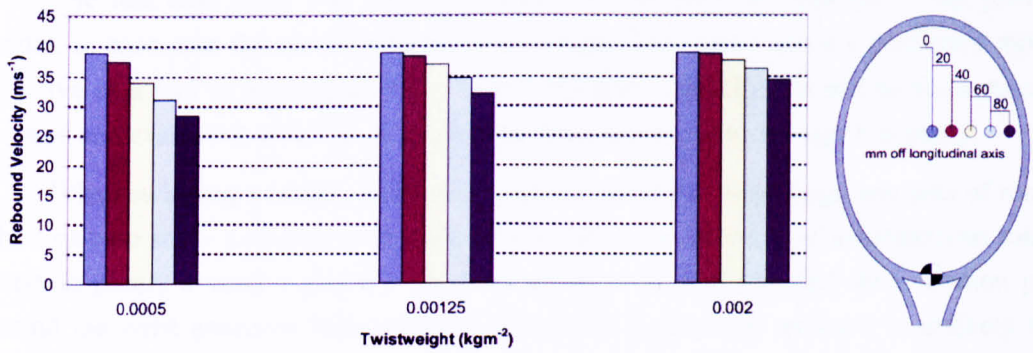

Figure 10.11. Rebound ball velocity for three twistweight values, impact locations are along the racket's width.

For the lowest twistweight value the difference between impacts along the longitudinal axis and off set impacts is greatest. At higher twistweight values the racket resists rotation significantly, the penalty for hitting in the off set is significantly reduced as a result. Due to the decreased racket rotation, horizontal rebound angle is reduced also, as shown in figure 10.12.

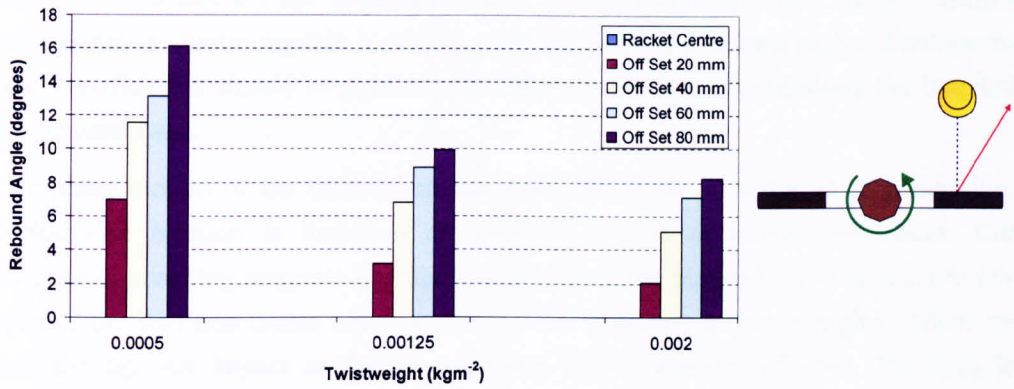

Figure 10.12. Horizontal rebound angle of the ball for a number of twistweight values.

In terms of an actual shot, increasing the twistweight of a racket significantly decreases the penalty for hitting off of the longitudinal axis of the racket. The decrease in rebound velocity is minimised, as is angular deviation. Modern widebody rackets have significantly higher twistweights than their older wooden counterparts. As such, a modern player can swing quicker and less accurately as impact location is no longer as crucial to the ball's rebound trajectory.

10.6 Effect of Shot Type: Discussion

The first case study was an investigation into the physical response of the predictive model. In each case the model behaves as expected. This shows that the predictive model is effective as a tool to investigate player shot technique. Individual racket movements can be isolated and evaluated, which is difficult to perform realistically and experimentally.

When swinging a racket, impacts toward the tip benefit from large amounts of rotation. The first case study looked at swingwise rotation in terms of centre of instantaneous rotation. Rotation purely around a player's shoulder produces a relatively flat shot, rotation purely around the wrist produces high levels of swingwise rotation. In reality it is unlikely that a player would be able to generate the velocity necessary purely through movement of the wrist. The instantaneous centre of rotation will most likely lie somewhere between the shoulder and wrist as illustrated in the intermediate case of 40 $rads^{-1}$. The player has been shown to hit the ball in the stringbed centre, the ideal point of impact when swinging at around 40 $rads^{-1}$.

Chapter 5 showed that many players had a degree of twistwise rotation present in their swing at impact. It is possible that this rotation was a result of the player rotating the racket to the desired angle for impact. Twistwise rotation has very little effect on the ball when hitting along the longitudinal axis. However, chapter 5 shows that a proportion of shots will always lie off the longitudinal axis off the racket. At one side of the racket twistwise rotations are beneficial compared to an impact off the longitudinal axis in which no twistwise rotation is present. Rebound velocity is increased and angular deviations are reduced. For an impact on the other side of the racket the opposite is true. It is unknown whether a player can choose

explicitly to hit a ball off the longitudinal axis and therefore benefit from the addition of twistwise rotation. Assuming this is not the case, eliminating rotations in this direction would be most beneficial. It should be pointed out that in every case hitting along the longitudinal axis is the ideal case.

In-plane motion of the racket face has been shown to be essential in generating ball spin. Spinwise rotation is therefore an essential aspect of racket movement. Current biomechanical coaching suggests that upward motion in the stroke is vital in order to reverse the spin of the ball and create top-spin. Swingwise rotations generate higher racket speeds towards the tip. An impact at the tip generates larger amounts of spin. The spin levels predicted by the model correlate with those observed in chapter 5, although are slightly higher in the extreme cases. For high racket rotations it becomes much more difficult to hit the ball at the desired location, especially at the tip where relative velocities are much larger. Off set impacts generate high spins even at low swingwise rotation values. These spin values are associated with the larger angular deviations also resulting from an off set impact. As a result the ball will have side-spin predominantly, causing the ball to deviate from its already deviated path. An off set impact is not an effective way to generate ball spin.

Many players augment the characteristics of their racket using lead tape. Altering the swingweight of a racket makes it more resistant to angular accelerations about the racket's width. As a result a ball impacting towards the tip rebounds with more velocity and deviates less from the normal. It is still unknown what relationship exists between swingweight and swing speed. In order to avoid such complications the case study was performed with a flat shot. It is apparent that if a player were to train with a racket with a high swingweight then an advantage can be gained hitting towards the tip providing that the player is able to generate sufficient swingspeed.

Racket Twisting can be greatly reduced by increasing twistweight (or polar moment of inertia). This was first recognised by Head **1975** who proposed a racket with a larger, wider head. Modern players have access to much lighter rackets than the wooden ones available at the time. As a result lead tape at either side of the head is used to increase twistweight. The penalty for hitting off set is greatly reduced by increasing twistweight; the ball rebound velocity increases and angular deviation of the ball from its intended trajectory decreases. It was mentioned previously that minimal twistwise rotation is desirable at the point of impact. As such increased twistweight is not a penalty in generating the movement at impact. However it could cause problems in moving the racket around the court. The fast paced modern game requires swift racket movement and frequent switches from backhand to forehand. In this respect a high twistweight could tire a player more than a lighter weighted racket.

10.7 Effect of Shot Accuracy: Methodology

The impact location on the racket face has considerable implications regarding impact location on the court. For a specific racket swing, varying the impact location alters the rebound velocity and angle of the ball off the racket face. Chapter 5 revealed that certain players are more capable of repeatedly hitting a desired point on the racket face than others. A higher skilled player can hit the ball more consistently in the desired location on the racket. Three arbitrary levels of playing ability were assessed; low, medium and high. A standard deviation in both horizontal and vertical impact accuracy was assigned using the data from chapter 5. These standard deviation values are shown in figure 10.13.

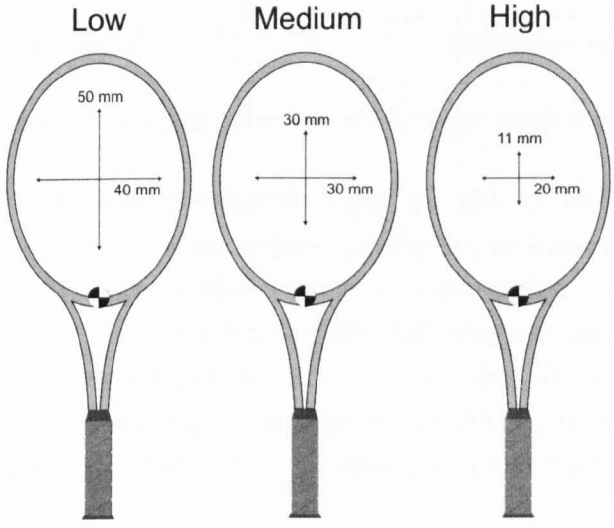

Figure 10.13. The standard deviation values used for low, medium and high levels of player accuracy.

A trajectory model developed internally was used to calculate the impact point on the tennis court. The model used an absolute velocity, spin, elevation and azimuth trajectory angle to calculate the ball's flight using mechanical and aerodynamic calculations.

A shot which was calculated to land on the court's baseline was used to judge the effect of shot accuracy. The pre-impact shot conditions and racket physical characteristics are shown in table 10.14. Each shot was taken from 1.5 m behind the centre of the baseline.

Ball Velocity (ms^{-1})			**Racket Velocity** (ms^{-1})			**Racket Angular Velocity** ($rads^{-1}$)		
x	*y*	*z*	*x*	*y*	*z*	*swing*	*twist*	*spin*
0	0	-8	0	9	14	40	0	0

Ball Spin	**Impact From Butt**	**Impact from longitudinal axis**	**Racket Mass**	**Swingweight** (kgm^{-2})	**Twistweight** (kgm^{-2})	**Spinweight** (kgm^{-2})
0 rpm	450 mm	0 mm	300 g	0.019	0.00125	0.02025

Table 10.14. The Shot and physical characteristics of the ball and racket.

A cumulative probability distribution was generated which corresponded to a normally distributed data set. The cumulative impact location probability distribution in the longitudinal direction is shown in figure 10.15.

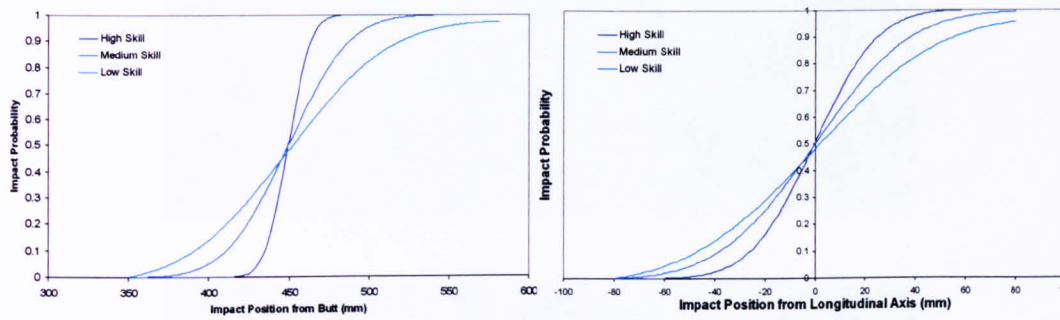

Figure 10.15. The cumulative impact distributions for high, medium and low skill along the longitudinal axis.

It can be seen from figure 10.5 that the higher the skill of the player the smaller the range of impact locations. A random number generator was used to generate 8 random numbers between 0 and 1. The cumulative probability distribution was used to calculate 8 separate impact locations for high, medium and low skill. This was done by finding the point of intersection between the random number and cumulative distribution. The modified impact locations for each skill level were used in the predictive model to give the required outputs for the trajectory simulation. This gave eight court impact locations for high, medium and low skill levels.

10.8 Effect of Shot Accuracy: Results

The results of are shown as the point at which the ball hits the tennis court. An area of several metres around the tennis court is shown as many shots landed outside the court boundary. Figure 10.16 shows the impact locations for all three levels of assumed accuracy (low, medium and high). A black cross designates the point from which each shot was made. Each skill level is associated with the repeatability at which the player is able to make an impact on the racket face.

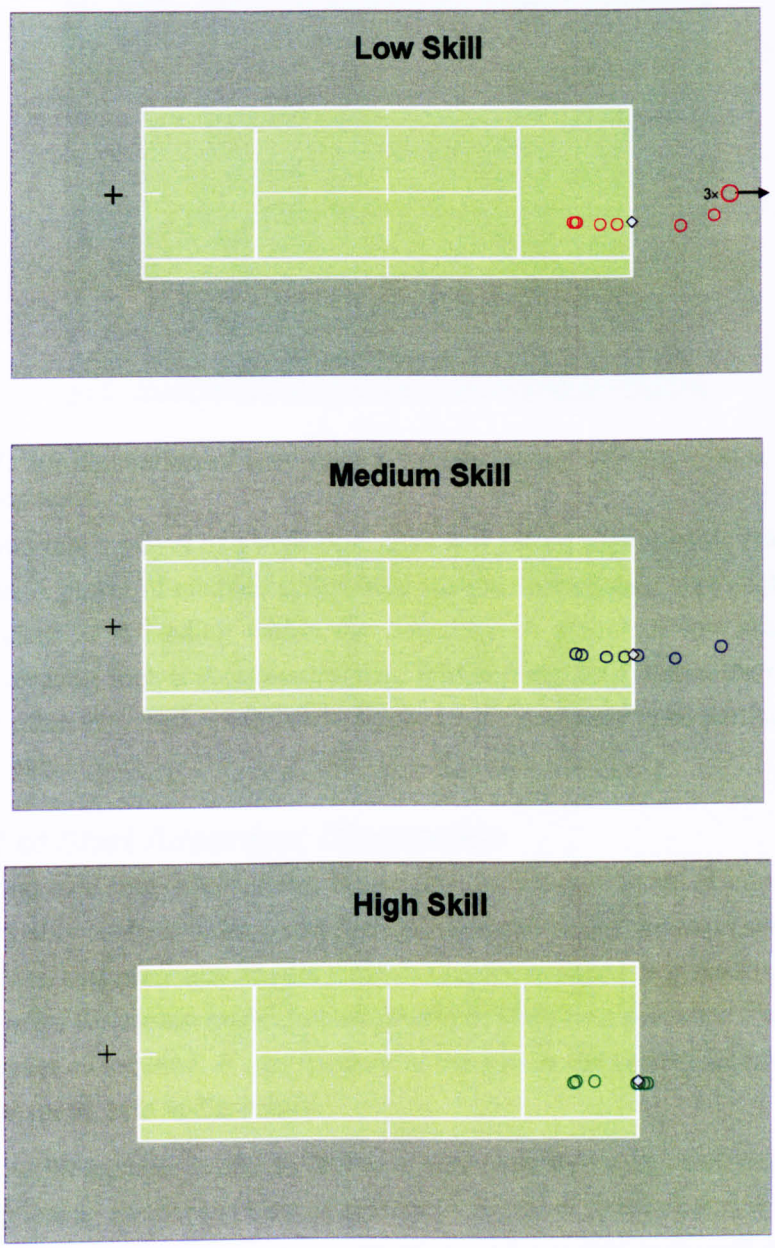

Figure 10.16. The court impact locations for three different skill levels as defined in the previous section. For the low skill level three shots did not land within the extended court boundary.

The previous results section showed that the greatest penalty in trajectory and velocity result from impacts off set from the longitudinal axis. This may result in a much higher or lower trajectory than normal. This results in the very linear spread of impacts seen in figure 10.16. The wide variety of vertical trajectories, velocities and spins result in a large spread for the low skill value as illustrated in figure 10.17. High skill shows very little deviation, concentrated around the baseline. At a high skill level the impact points are concentrated around the desired location. The medium skill level shows an intermediary amount of spread.

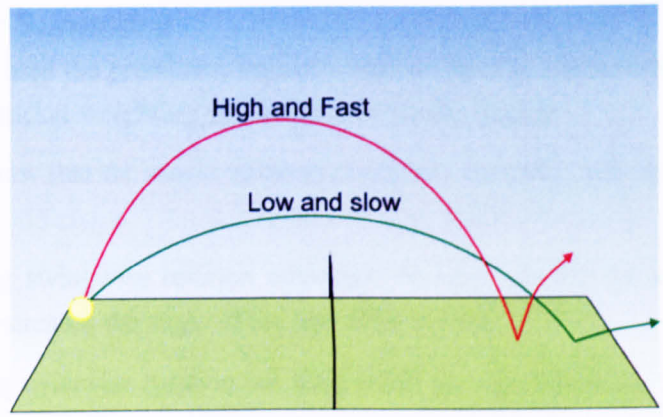

Figure 10.17. An illustration of how vertical trajectory and velocity results in a spread of court impact positions.

This shows that a player of a high skill level will have a high success rate when aiming for the baseline. A player of medium skill would have to shorten their shot slightly in order to be more confident of it landing within the boundary. A player of low skill would have difficulty in executing such a shot successfully. Whilst many land within the court boundary these shots are often very high, as shown in figure 10.17, not likely to be particularly effective in competitive play.

10.9 Effect of Shot Accuracy: Discussion

The second case study showed that higher shot accuracy in terms of impact location on the racket invariably leads to more consistent impact locations on the court surface. The first case study showed that particular impact locations are more suited at generating ball rebound velocities and spins for certain racket impact positions. It follows that even if a player is able to move the racket as required, if they cannot hit the ball in the correct location a penalty is paid in terms of speed, spin and accuracy.

A highly skilled player is able to deliver a shot with high speed and spin, in a location deemed appropriate by the player, very repeatedly. A player of lower skill may have to reduce the speed of the racket, or aim more conservatively in order to deliver the ball within the court boundary with a sufficiently high success rate.

The case studies discussed above represent a handful of possible scenarios and uses for the predictive model described in chapters 8 and 9. As might be expected, there is no *ideal* way to swing or weight a racket. Each is a compromise of player ability and player style. This model represents a powerful method of assessing player styles and racket types. This could be used to develop a player's swing, or create a racket particularly suited to an individual. This becomes particularly powerful when coupled with the player analysis technique discussed in chapter 4 and 5, in which the full movement of a player's racket at impact can be assessed.

10.10 Chapter Summary

This chapter used the predictive impact model outlined in chapters 8 and 9 to assess the effect of changing racket weighting and movement during impact.

All results show that the model behaves physically correctly, and can be summarised as follows:

- Increasing swingwise rotation increases rebound velocity for impacts towards the tip, and increases the angle of the ball after impact.
- Increasing twistwise rotation has little effect on a ball impact along the longitudinal axis. The effect for impacts off the longitudinal axis is either positive or negative depending on which side of the racket the ball hits.
- Spinwise rotation is essential for spin generation; the maximum spin is obtained for impacts at the tip although impact becomes more difficult as relative inbound ball/racket velocities increase.
- Increasing swingweight increases the racket's resistance to rotation along its length. Impacts towards the tip rebound with more velocity for a given impact speed. This is counteracted by the fact that the racket is harder to swing.
- Increasing twistweight decreases the negative effect resulting from off set impacts. Twisting is generally not desirable at impact. As such a high twistweight is not a great disadvantage in swinging the racket, but it may inhibit its movement around the court between shots.

Generally, there is no ideal shot or racket but the predictive model presented in this study provides a method in which every feasible shot or weight combination can be tested accurately and reliably.

11 Conclusions

11.1 Introduction

This chapter lists the conclusions and major findings of each chapter included in this study. The findings are categorised according to the objectives outlined in Chapter 1. Possible further investigations are given at the end of this chapter.

11.2 Player Shot Characteristics

It was established from the literature review that accurate shot characteristics of elite level players were necessary in order to robustly validate a predictive model. Experiments to find out such information were subsequently carried out, the conclusions for which are shown below.

11.2.1 Methodology Development

In order to obtain data-points in 3D space, a 2-camera 3D system with checkerboard calibration was chosen to be used throughout this study. The accuracy of the system was assessed by reprojecting points using automatic and manual point selection techniques. It was concluded that:

- Reprojection error is associated with the quality of calibration, specifically the size of the calibration object within the recorded images.
- The variability of reprojection error increased as the size of the calibration object decreased within the recorded images.
- A manually selected point had an error of around ± 0.5 pixel within each 2D image.
- Pixel error within each image translated to mm error within 3D space according to the relative size of the object within the recorded images.
- Generally, a recorded object should be as large as feasibly possible within each recorded image. It must also be captured frequently enough to obtain a confident assessment of velocity etc.

The calibration method was used as a basis on which to develop a player testing methodology. Two cameras positioned at each end of the net were focused onto the centre of the baseline and used to record each shot. Five markers on the player's racket and a marked ball were used to calculate racket and ball movement and impact position. In developing this methodology it was concluded that:

- A 2 × 2 × 2 metre volume was small enough to accurately calibrate the system, yet large enough to capture the entire area of interest for each shot.
- A sufficiently small recorded time frame can be used to linearise racket movement and obtain the shot conditions immediately prior to and post-impact. A camera speed of 1000 frames per second was sufficient to accurately linearise shot movement.
- At present, manual point selection provided the most accurate and versatile method of obtaining the required 2D data points.

11.2.2 Shot Recording and Analysis

The fully developed analysis methodology was used at the 2006 Wimbledon Qualifying Tournament to record 106 shots from 13 internationally ranked players. Custom-written software was used to analyse the data. In executing this methodology and analysis, the following conclusions were made:

- The player testing methodology in the configuration used was accurate to within 2.5 mm regarding position and around 1.7% regarding spin at a typical value of 1000 rpm.
- A male player swung the racket faster than a female player and generated higher post-impact ball velocities. However, racket angular velocities and impact positions were typically very similar.
- All players aimed to hit the node point of the racket. For each shot, an *ideal point* exists for which ball rebound velocity will be a maximum. Players were not observed to aim for this point.

This methodology has a large amount of potential for shot analysis far outreaching the applications demonstrated in this study.

11.3 Repeatable Impact Experiment

Detailed knowledge of the ball and racket movements close to impact during play enabled an impact experiment to be designed around typical values. In order to validate a predictive model.

11.3.1 Experimental Methodology Development

In developing the methodology it was found that:

- The accuracy of the BOLA ball projection device was not sufficient to create incrementally varied impact conditions.
- The camera tracking system was able to obtain ball velocities and impact positions to within 3 mm.
- It was judged that 2880 experimental results were needed to fully represent the velocities angles and grip torques seen in play.

11.3.2 Experimental Data-Fitting and Results

Experimental restrictions resulted in the number of recorded data points falling to 900. Analysis of the obtained data points revealed that:

- The raw data was well distributed within the input domain for each variable.
- A simple multi-variate polynomial regression technique could be used to model the recorded data points.

The multi-variate modelling technique enabled individual variables to be altered and observed. In observing the recorded data it was found that:

- For impacts at the centre of the racket, inbound ball velocity was linearly related to outbound ball velocity.

- Impact velocity increased as impact position moved from the tip towards the throat of the racket. Impact velocity began to decrease as the impact moved very close to the racket throat. It was concluded that this was due to high frame vibrations.
- Inbound angle and outbound angle are linearly related. Outbound angle was consistently higher than inbound angle. This was concluded to be due to racket rotation during impact.
- A reduction in ball deviation was observed with the addition of restrictive torque about the racket handle. However, no significant decrease in ball deviation was observed from 7.5 to 15 Nm.
- Rebound velocity decreased as the impact position moved away from the racket's longitudinal axis. Ball deviation from the perpendicular increased as the impact position moved away from the racket's central axis.

11.4 Predictive Model

11.4.1 Predictive Model Validation

In validating the predictive model it was concluded that:

- The model was accurate at predicting outbound velocities perpendicular to the racket face for varying inbound ball angles, velocities and grip torques. The rigid body assumption meant that the greatest inaccuracies came from impacts towards the racket throat. In this location, energy losses due to frame vibration caused the model results to deviate from reality.
- Predicted outbound velocities across the racket face showed consistent over-prediction for impacts off the transverse axis and for a range of inbound angles. This over-prediction was due to the rolling condition of the spin model and the lack of retardation force.
- As impacts moved away from the central axis, the model over-predicted the outbound angle. A racket stringbed generates a corrective action for off-set impacts which moves the ball trajectory back towards the racket centre. This corrective action was modelled using an exponential force acting tangentially to the stringbed.
- The validation of the spin model showed larger errors at large spin values. It was concluded that whilst the spin model could be improved, the spin values obtained from experiment were subject to an error which increased with spin value.

Ten shots were chosen from the player shot analysis and simulated within the predictive model it was concluded that:

- The outbound velocity and rebound angle showed good correlation between observed and predicted results.
- Ball spin showed adequate correlation within the accepted experimental error values.

11.4.2 Predictive Model Application

The final chapter of this section used the validated model to perform two specific case studies. The first monitored how the type of shot or racket affected the rebound ball velocity and spin. The second case study investigated how the accuracy of a player can affect the ball's impact position on the court. Both of these case studies were performed by inputting specific

data into the predictive model. Typical values of a player's shot were obtained from the player shot analysis. Typical racket characteristics were obtained from Haake et al. **2007**. It was found that:

- Ball rebound velocity is maximised by adapting the impact location to shot type.
- When the racket has low amounts of swingwise rotation, impacts towards the racket throat maximise ball rebound velocity.
- When the racket has high amounts of swingwise rotation, impacts towards the tip maximise ball rebound velocity.
- Twistwise rotation can be used to minimise the effects of an impact off the longitudinal axis. However, if the impact is at the wrong side of the longitudinal axis, the negative effects are increased.
- Spinwise rotation can be used to generate large amounts of spin, particularly for impacts towards the racket tip.
- A racket with a high swingweight resists rotations along its length. Impacts towards the racket tip rebound with a higher velocity and deviate less from the perpendicular. However, a racket with a high swingweight is harder to rotate and accelerate to high speed.
- A racket with a high twistweight resists rotations about its length. In this way the negative effects of impacts off the longitudinal axis are minimised. Twistwise rotations are generally low at the instant of impact. For this reason a racket with a high twistweight is not necessarily a disadvantage.
- A player with an impact variability of 20 mm on the racket face can expect to have a variability of impact on the court of around 1.45 m. A player with an impact variability of 50 mm on the racket face can expect to have a variability of impact on the court of around 4 m.

It was concluded that the predictive model represented an accurate and versatile method of investigating how shot type and racket characteristics can affect ball rebound trajectory, velocity and spin.

11.5 Future Research

Each section of this study has shown potential for further research. A number of possible expansions are shown below.

11.5.1 Development of the player testing methodology

A main tenet of the player testing methodology was minimal intrusion into the player's environment. A compromise was reached in which small markers were added to the racket frame. For this reason all recorded player characteristics were obtained in practice conditions. It is still unknown how a player swings a racket when in competition conditions. In order to achieve this, development of the existing methodology is necessary. In competition conditions no additional markers can be present on the racket and no modifications to the ball markings can be made. It follows that one of two possible developments must be made:

1) A method in which racket orientation and position can be obtained without distinctive racket markers being present. For example, a method in which the entire racket face is equated to a calculated ellipse. In this way position, orientation and velocity can be calculated from the position and skewing of the equated ellipse.
2) Racket markers could be built into the racket paint. Collaborating with a specific player and sponsor may enable distinct markings to be built into the decoration of the racket frame. In this way, no further modification of the racket frame or analysis methodology is necessary.

With regards to ball markings, Goodwill et al. **2007** was able to track ball spin from high speed video images using only the ball logo. A development of this method could be used in order to obtain accurate values of ball spin. A major advance in the analysis methodology would be the inclusion of an accurate automatic tracking method. Removing the requirement to manually track each data point would significantly decrease the required analysis time. This would increase the number of players able to be recorded and therefore the amount of data which could be obtained.

11.5.2 Development of the Repeatable Experiment Methodology

The repeatable impact experiment was limited in that inbound ball velocity was not varied in the local x direction. This was due to limitations in the apparatus and possible orientations of the racket relative to the BOLA cannon. Ball spin was also not accounted for in the resulting multi-variate fit. As a result, the outbound ball spin given by the predictive model could not be validated in the same way as every other input parameter. The primary reason for this was that ball spin was not tracked automatically along with ball position. Developing an automatic method of counting ball spin would enable it to be included as a variable in the multi-variate fit.

11.5.3 Development of the Predictive Model

Validation of the predictive model showed that it is accurate when predictions are compared to measured experimental values. However the validation exercise revealed a number of possible areas of development.

- The spin model must be modified to better agree with experimental results. The physical behaviour of the model may still not best represent actual behaviour of the ball. Further investigation into the tangential contact behaviour of a ball on a racket stringbed is necessary.
- Corrective action of the stringbed must be experimentally validated. A viable method of producing a corrective stringbed action was shown in this study. However, the force values used to generate this action were not related to any experimentally obtained data. A clear need to investigate the magnitude and direction of the stringbed reaction force is necessary.
- The racket frame was modelled as a rigid body. Goodwill **2002** modelled a racket impact using a multi-section flexible beam model. An obvious next step would be to integrate the flexible beam model into the current predictive model

12 References

Abdel-Aziz, Y I and Karara, H M (1971), Direct Linear Transformation from Comparator Coordinates into Object Space Coordinates in Close-Range Photogrammetry. In: *Proceedings of the Symposium on Close-Range Photogrammetry*, Falls Church, VA, USA, pp 1-18, (American Society of Photogrammetry)

Abdi, H (2003) In *Encyclopedia for Research Methods for the Social Sciences*(Eds, Lewis-Beck, M., Bryman, A. and Futing, T.) Sage, Thousand Oaks, pp. 792-795.

About.com (2007) http://tennis.about.com/cs/yourgame/a/hitonrise.htm

Adrian, M J and Enberg, M L (1971) Sequential Timing of Three Overhead Serving Patterns, *Kinesiology Review*, 1-9.

Allen, T, Goodwill, S R and Haake, S J (2007), Experimental Validation of a Tennis Ball Finite-Element Model. In: *Tennis Science and Technology 3*, Roehampton University, London, UK,

Ashcroft, A D C and Stronge, W J (2002), Putting Spin on a Tennis Ball: Friction Between Tennis Ball and Racket String-Bed. In: *The Engineering of Sport 4*, Kyoto Japan,

Bahamonde, R E (1989) Kinetic Analysis of the Serving Arm During the Performance of the Tennis Serve, *Journal of Biomechanics*, **22**, 983.

Baker, J A W and Putnam, C A (1979) Tennis Racket and Ball Responses During Impact Under Clamped and Freestanding Conditions, *The Research Quarterly*, **50**, 164-170.

Barrass, D F, Jones, R and Dickens, P (2005), Structured Relationship Model of Tennis Player Perception from Tennis Grips and Handles. In: *The Impact of Technology on Sport*, Tokyo, Japan,

Bartlett, R (1997) *Introduction to Sports Biomechanics.*

Bishop, C M (1995) *Neural Networks for Pattern Recognition*, Oxford.

Blanksby, B, Elliott, B and Ellis, R (1979) Selecting the Right Racquet - Performance Characteristics of Regular Sized and Over-Sized Tennis Racquets, *The Australian Journal for Health, Physical Education and Recreation*, **(December)**, 21-25.

BOLA (2007) http://www.bola.co.uk

BoschRexroth (2007) http://www.boschrexroth.co.uk

Bridge, J N (1998a) The Way Balls Bounce, *Physical Education*, **33**, 174-181.

Bridge, J N (1998b) The Way Balls Really Bounce, *Physical Education*, **33**, 236-241.

Brody, H (1979) Physics of the Tennis Racket, *American Journal of Physics*, **47**, 482-487.

Brody, H (1981) Physics of the Tennis Racket II: the 'sweet spot', *American Journal of Physics*, **49**, 816-819.

Brody, H (1987a) Models of Tennis Racket Impacts, *International Journal of Sport Biomechanics*, 293-296.

Brody, H (1987b) *Tennis Science for Tennis Players,* University of Pennsylvania Press, Philadelphia.

Brody, H (1995), How Would a Physicist Design a Tennis Racket. In: *Physics Today,*

Brody, H (1997) The Physics of Tennis III: The ball-racket interaction, *American Journal of Physics,* **65(10),** 981-987.

Brody, H (2000), A Limit On Spin. In: *International Tennis Federation Technical Commission Meeting,* Brussels,

Brody, H, Lindsey, C and Cross, R (2002) *The Physics and Technology of Tennis,* Racquet Tech Publishing.

Brody, H and Roetert, P (2004) In *Biomedical Engineering Principles in Sports*(Eds, Hung.G.K and Pallis.J.M.) Kluwer Academic/Plenum Publishers, New York.

Broer, M R (1973) W.B. Saunders, London, pp. 245.

Calder, C A, Holmes, J G and Mastny, L L (1987), Static and Dynamic Characteristics of Tennis String Performance. In: *Progs 1987 Sem Conference on Experimental Mechanics,* Houston, USA, pp 613-616

Capel-Davies, J (2007), Effects of tennis ball type on the speed of the game. In: *Tennis Science and Technology 3*, Roehampton University, London, Uk,

Capel-Davies, J and Miller, S (2007), Evaluation of automated line-calling systems. In: *Tennis Science and Technology 3*, The International Tennis Federation, London, UK,

Carré, M (2000), The Dynamics of Cricket Ball Impacts and the Effect of Pitch Construction, Department of Mechanical Engineering, *The University of Sheffield*

Carré, M, Haake, S J, Baker, S W and Newell, A J (1998), The Analyisis of Cricket Ball Impacts Using Digital Stroboscopic Photography. In: *The Engineering of Sport 2*, pp 23-29, (Blackwell Science)

Chadwick, S G and Haake, S J (2000), Methods to Determine the Aerodynamic Forces Acting on Tennis Balls in Flight. In: *Tennis Science and Technology*, London, UK,

Coe, A O (2000), The Balance Between Technology and Tradition in Tennis. In: *Tennis Science & Technology*, The International Tennis Federation, London, UK, pp 3-40, (Blackwell Publishing)

Crespo, M, Reid, M and Miley, D (2003), Analysis of Stroke Production in Tennis: A review. In: *Tennis Science & Technology 2*, The International Tennis Federation, London, UK, pp 179 - 183

Cross, R (1997) The Dead Spot of a Tennis Racket, *American Journal of Physics,* **8(65),** 754-764.

Cross, R (1998) The Sweet Spots of a Tennis Racket, *Sports Engineering,* **1,** 63-78.

Cross, R (1999a) The Bounce of a Ball, *American Journal of Physics,* **67,** 222-227.

Cross, R (1999b) Impact of a Ball with a Bat or Racket, *American Journal of Physics,* **67,** 692-702.

Cross, R (2000a) The Coefficient of Restitution for Collisions of Happy Balls, Unhappy Balls, and Tennis Balls, *American Journal of Physics,* **68(11),** 1025-1031.

Cross, R (2000b), Dynamic Properties of Tennis Strings. In: *Tennis Science and Technology,* International Tennis Federation, London, Uk, pp 119-126

Cross, R (2000c) Effects of Friction Between the Ball and Strings in Tennis, *Sports Engineering,* **3,** 85-97.

Cross, R (2000d) Flexible Beam Analysis of the Effects of String Tension and Frame Stiffness on Racket Performance, *Sports Engineering,* **3,** 111-122.

Cross, R (2001a) Customising a Tennis Racket by Adding Weights, *Sports Engineering,* **4,** 1-14.

Cross, R (2001b) Measurements of the Horizontal Coefficient of Restitution for a superball and a tennis ball, *American Journal of Physics,* **70,** 482-489.

Cross, R (2001c) Why Bows Get Stiffer and Racquets get Softer when the Strings are added, *American Journal of Physics,* **69,** 907-910.

Cross, R (2002a) Grip-Slip behaviour of a bouncing ball, *American Journal of Physics,* **11(70),** 1093-1102.

Cross, R (2002b) Measurements of the Horizontal Coefficient of Restitution for a Superball and a Tennis Ball, *American Journal of Physics,* **70,** 482-489.

Cross, R (2003), Properties of Tennis Equipment: Balls that bite, rackets that don't vibrate and strings don't make any difference. In: *Tennis Science and Technology 2,* The International Tennis Federation, London, UK,

Cross, R (2005) Bounce of a spinning ball near normal incidence, *American Journal of Physics,* **73(10),** 914-920.

Cross, R, Lindsey, C and Andruczyk, D (2000) Laboratory Testing of Tennis Strings, *Sports Engineering,* **3,** 219-230.

Cross+Morse (2007) http://www.cross-morse.co.uk

Daish, C B (1972) *The Physics of Ball Games,* English Universities Press London.

Davies, G, Rothberg, S J, Jones, R and Roberts, J R (2003), Player Perception Evaluation of 'Feel' in Tennis Ball Impacts. In: *Tennis Science and Technology 2,* The International Tennis Federation, London, (ITF Publishing)

D'Errico, J (2006) http://www.mathworks.com/matlabcentral/fileexchange/loadFile.do?objectId=9577&objectType=FILE

Dignall, R J and Haake, S J (2000), Analytical Modelling of the Impact of Tennis Balls on Court Surfaces. In: *Tennis Science and Technology*, Roehampton University, London, UK, pp 155-162, (Blackwell Science)

Dignall, R J, Haake, S J and Chadwick, S G (2000), Modelling of an Oblique Tennis Ball Impact on a Court Surface. In: *The Engineering of Sport*, Sydney, Ausrtalia, (Blackwell Science Ltd, Oxford)

DTI (1998) *ADULTDATA, The Handbook of Adult Anthropometric and Strength Measurements.*

Elliott, B C (1982) Tennis: The Influence of Grip Tightness on Reaction Impulse and Rebound Velocity, *Medicine and Science in Sports and Exercise,* **14,** 348-352.

Elliott, B C (1983) Spin and the Power Serve in Tennis, *Journal of Human Movement Studies,* **9,** 97-103.

Elliott, B C and Blanksby, B (1980) Vibration and Rebound Velocity Characteristics of Conventional and Oversized Tennis Rackets, *Research Quarterly for Exercise and Sport,* **51,** 608-615.

Elliott, B C, Marsh, A P and Blanksby, B (1986) A Three-Dimensional Cinematographic Analysis of the Tennis Serve, *International journal of Sport Biomechanics,* **2,** 260-271.

Elliott, B C, Marsh, A P and Overheu, P R (1989) The Topspin Backhand Drive in Tennis: A Biomechanical Analysis, *The Journal of Human Movement Studies,* **(16),** 1-16.

Elliott, B C and Marsh, T (1989) A Biomechanical Comparison of the Topspin and Backspin Forehand Approach Shots in Tennis, *Journal of Sports Science,* **7,** 215-227.

Fischer, W (1977) Tennis Racket, *US Patent 4273331*

Goldstein, H (1980) *Classical Mechanics,* Addison-Wesley.

Goodwill, S R (2002), The Dynamics of Tennis Ball Impacts on Tennis Rackets, The Department of Mechanical Engineering, *The University of Sheffield*

Goodwill, S R, Capel-Davies, J, Haake, S J and Miller, S (2007), Ball Spin Generation By Elite Players During Match Play. In: *Tennis Science & Technology 3*, The University of Roehampton, London, (The International Tennis Federation)

Goodwill, S R, Douglas, J, Miller, S and Haake, S J (2006), Measuring Ball Spin Off a Tennis Racket. In: *The Engineering of Sport 6*, Munich, pp 379-384, (Springer)

Goodwill, S R and Haake, S J (2001) Spring Damper Model of an Impact Between a Tennis Ball and Racket, *Proceedings for The Mechanical Engineers,* **215,** 1331-1341.

Goodwill, S R and Haake, S J (2002a), Modelling of an Impact Between a Tennis Ball and Racket. In: *Tennis Science and Technology 2*, The International Tennis Federation, London, pp 79-86, (ITF)

Goodwill, S R and Haake, S J (2002b), Why were 'Spaghetti String' Rackets Banned in the Game of Tennis? In: *4th International Conference on Sports Engineering*, Kyoto, Japan,

Goodwill, S R and Haake, S J (2004a), Aerodynamics of Tennis Balls - Effect of Wear. In: *The Engineering of Sport 5*, Davis, California, pp 35-48

Goodwill, S R and Haake, S J (2004b) Ball Spin Generation for Oblique Impacts with a Tennis Racket, *Experimental Mechanics,* **44,** 195-206.

Goodwill, S R and Haake, S J (2004c), Effect of String Tension on the Impact between a Tennis Ball and Racket. In: *The Engineering of Sport 5*, Davis, California, pp 3-9

Goodwill, S R, Kirk, R and Haake, S J (2005) Experimental and Finite Element Analysis of a Tennis Ball Impact on a Rigid Surface, *Sports Engineering,* **8,** 145-158.

Groppel, J L, Shin, I, Spotts, J and Hill, B (1987) Effects of Different String Tension Patterns and Racket Motion on Tennis Racket - Ball Impact, *International Journal of Sport Biomechanics,* **3,** 142-158.

Haake, S J (1989), Apparatus and Test Methods for Measuring the Impact of Golf Balls on Turf and their Application in the Field, *University of Aston in Birmingham*

Haake, S J (1996), Oblique Impact Of a Rotating Elastic Solid On a Deformable Surface. In: *International Congress on Experimental Mechanics*, Nashville, Tennessee, U.S.A, pp 376-377

Haake, S J (2007), The Evolution of the Tennis Racket and its Effect on Serve Speed. In: *Tennis Science and Technology 3*, The University of Roehampton,

Haake, S J, Allen, T, Choppin, S B and Goodwill, S R (2007), The Evolution of the Tennis Racket and its Effect on Serve Speed. In: *Tennis Science and Technology 3*, Roehampton University, London, pp 257-271, (International Tennis Federation)

Haake, S J, Carré, M J, Kirk, R and Goodwill, S R (2005) Oblique Impact of Thick Walled Pressurised Spheres as Used in Tennis, *Journal of Mechanical Engineering Science,* **219(11),** 1179-1189.

Hadland, J (1974), A Review of the Current State of the Art (High Speed Cameras). In: *High Speed Photography*, London, UK,

Hatze, H (1976) Forces and Duration of Impact and Grip Tightness During the Tennis Stroke, *Medicine & Science in Sports,* **8,** 88-95.

Hatze, H (1988) High-Precision Three-Dimensional Photogrammetric Calibration and Object Space Reconstruction Using a Modified DLT-Approach, *Journal of Biomechanics,* **21,** 533-538.

Hatze, H (1992) Objective Biomechanical Determination of Tennis Racket Properties, *International jounral of Sport Biomechanics,* **8,** 275-287.

Hatze, H (1993) The Relationship Between the Coefficient of Restitution and Energy Losses in Tennis Rackets, *Journal of Applied Biomechanics 5.*

Hatze, H (1994) Impact Probability Distribution, Sweet Spot, and the Concept of an Effective Power Region in Tennis Rackets, *Journal of Applied Biomechanics,* **10,** 43-50.

Hatze, H (1998) The Centre of Percussion of Tennis Rackets: A Concept of Limited Applicability, *Sports Engineering,* **1,** 17-25.

Hawkeye (2007) http://www.hawkeyeinnovations.co.uk/

Head, H (1975) Oversize Tennis Racket, *United States Patent 3,999,756*

ITF (2007a) http://www.itftennis.com/technical/

ITF (2007b) http://www.itftennis.com/technical/equipment/rackets/history.asp

ITF (2007c) *Rules of Tennis 2007,* The International Tennis Federation.

James, D (2004), Understanding the Playing Performance of Cricket Pitches, Sports Engineering Research Group, *The University of Sheffield*

Jenkins, C and Calder, C A (1990) Transient Analysis of a Tennis Racket Using PC-based Finite Elements and Experimental Techniques, *Experimental Mechanics,* 130-134.

Jenkins, S P R (2005) *Sports Science Handbook.*

Johnson, W, Reid, S R and Trembaczowski-Ryder, R E (1972) The Impact, Rebound and Flight of a Well Inflated Pellicle as Exemplified in Association Football, *The Manchester Association of Engineers,* **5,** 1-25.

JZZ Technologies (2007) http://jzztechnologiesinc.com/default.aspx

Kanda, Y (2004), Estimation of Tennis Racket Power using Three-Dimensional Finite Element Analysis. In: *The Engineering of Sport 4,* Kyoto, Japan, pp 207-214

Kawazoe, Y (1997), Experimental Identification of a Hand-Held Tennis Racket and Prediction of Rebound Ball Velocity in an Impact. In: *46th Japan National Congress for Applied Mechanics,* Japan,

Kirk, R (2003), Oblique Impacts of Tennis Balls on Acrylic Surfaces, The Department of Mechanical Engineering, *The University of Sheffield*

Kirk, R, Carré, M, Haake, S J and Manson, G (2006), Modelling Traction of Studded Footwear on Sports Surfaces using Neural Networks. In: *The Engineering of Sport 6,* Munich, Germany, pp 404-408

Knudson, D (1993) Effect of String Tension and Impact Location on Ball Rebound Accuracy in Static Tennis Impacts, *Journal of Applied Biomechanics,* **9,** 143-148.

Knudson, D (1997), Effect of Grip Models on Rebound Accuracy of Off-Center Tennis Impacts. In: *XV International Symposium on Biomechanics in Sports,*

Knudson, D (2006) *Biomechanical Principles of Tennis Technique,* Racquet Tech Publishing.

Kohavi, R (1995), A study of Cross-Validation and Bootstrap for Accuracy Estimation and Model Selection. In: *International Joint Conference on Artificial Intelligence (IJCAI),*

Kotze, J, Mitchell, S R and Rothberg, S J (2000) The Role of the Racket in High Speed Tennis Serves, *Sports Engineering,* **3,** 67-84.

Koziol, D L and Reed, T F (1978) Tennis Ball, *U.S Patent 4,098,504*

Leigh, D C and Lui, W (1992) Dynamics of the Interactions Between Ball, Strings, and Racket in Tennis, *International journal of Sport Biomechanics,* **8,** 181-206.

Levenburg, K (1944) A method for the Solution of Certain Non-linear Problems in Least Squares, *Quarterly of Applied Mathematics,* **2,** 164-168.

Lewis, J D and Peck, G T (1958) A Method of Flash Synchronization for High-Speed Cinematography, *Journal of Scientific Instruments,* **35,** 338-340.

Lui, K Y (1983) Mechanical Analysis of Racket and Ball During Impact, *medicine and Science in Sports and Exercise,* **15,** 388-392.

Lutwiller, D (2001) In *Photonics Spectra.*

Marquardt, D W (1963) An Algorithm for Least-Squares Estimatin of Nonlinear Parameters, *Journal of the Society for Industrial and Applied Mathematics,* **11,** 431-441.

Mathworks.com (2007) www.mathworks.com/matlabcentral

Maw, N (1975) The Oblique Impact of Elastic Spheres, *Wear,* **38,** 101-114.

Menache, A (2000) *Understanding Motion Capture for Computer Animation and Video Games,* Morgan Kaufmann.

Miller, S (2007), The role of Science & Technical in Evaluating and Regulating Tennis Equipment. In: *Tennis Science & Technology*, The University of Roehampton, London, Uk, pp 1-19, (ITF)

Miller, S and Messner, S (2003), On the Dynamic Coefficient of Restitution of Tennis Balls. In: *Tennis Science and Technology 3*, University of Roehampton, London, Uk,

Mitchell, S R, Jones, R and King, M (2000a) Head Speed vs. Racket Inertia in the Tennis Serve, *Sports Engineering,* **3,** 99-110.

Mitchell, S R, Jones, R and Kotze, J (2000b), The Influence of Racket Moment of Inertia During the Tennis Serve: 3-Dimensional Analysis. In: *Tennis Science & Technology*, The International Tennis Federation, London, (Blackwell Science)

Nave, C R (2005) http://hyperphysics.phy-astr.gsu.edu/hbase/perpx.html

Pallis, J M (2000) http://wings.avkids.com/Tennis/Project/usspin-03.html

Pallis, J M (2004) http://www.tennisserver.com/set/set_04_01.html

Pingali, G S, Jean, Y and Carlbom, I (1998), Real Time Tracking for Enhanced Tennis Broadcasts. In: *Computer Vision and Pattern Recognition*, pp 260-265

Plagenhoef, S (1970) *Fundamentals of Tennis,* Prentice Hall, New Jersey.

Pratt, G W (2000), The Interaction of the Tennis Ball and the Court Surface. In: *Tennis Science and Technology*, Roehampton University, London, UK, pp 163-168, (Blackwell Science)

Prozone (2007) http://www.pzfootball.co.uk

Ratkowsky, D A (1983) *Nonlinear Regression Modelling,* Marcel Dekker.

Rayleigh, F R S (1877) On the Irregular Flight of a Tennis-Ball, *Vortex Motion,* 14-17.

Reid, M and Elliott, B (2002) The One- and Two- Handed Backhands in Tennis, *Sports Biomechanics,* **1,** 47-68.

Roberts, J R, Jones, R, Harwood, C, Mitchell, S R and Rothberg, S J (2001a) Human Perceptions of Sports Equipment Under Playing Conditions, *Journal of Sports Sciences,* **19,** 485-497.

Roberts, J R, Jones, R and Rothberg, S J (2001b) Measurement of Contact Time in Short Duration Sports Ball Impacts: An Experimental Method and Correlation with the Perceptions of Elite Golfers, *Sports Engineering,* **4(191-203).**

Scanlan, T K and Ravizza, K (1989a) An In-depth Study of Former Elite Figure Skaters: I. Introduction to the Project, *Journal of Sport & Exercise Pyschology,* **11,** 54-64.

Scanlan, T K and Ravizza, K (1989b) An In-depth Study of Former Elite Figure Skaters: II. Sources of Enjoyment, *Journal of Sport & Exercise Pyschology,* **11,** 65-83.

Scanlan, T K, Stein, G L and Ravizza, K (1991) An In-depth Study of Former Elite Figure Skaters: III. Sources of Stress, *Journal of Sport & Exercise Pyschology,* **13,** 103-120.

Seber, G A F and Wild, C J (2003) *Nonlinear Regression,* Biddles/IBT Global.

Sharma, S (1996) *Applied Multivariate Techniques,* John Wiley & Sons inc.

Sherry, D and Hawkins, P (2001) Video Processor Systems for Ball Tracking in Ball Games, *U.K Patent*

SMPTE (2007) http://www.smpte.org/home

Strobl, K, Sepp, W, Fuchs, S, Paredes, C and Arbter, K (2007) http://www.vision.caltech.edu/bouguetj/calib_doc/

Svoboda, T, Martinec, D and Pajdla, T (2005) A Convenient Multi-Camera Self-Calibration for Virtual Environments, *PRESENCE: Teleoperators and Virtual Environments,* **14,** 407-422.

Taniguchi, T and Miyazaki, T (2005), Measurement of Aerodynamics Forces Exerted on Baseballs Using a High Speed Video Camera. In: *The Impact of Technology on Sport,* Tokyo, Japan,

Thomson, A (2000), Dynamic Characteristics of Tennis Balls and the Determination of 'Player Feel', Mechanical Engineering, *The University of Sheffield*

Tilmanis (1975) *Advanced Tennis for Coaches, Teachers and Players,* Lea Febiger, Philadelphia, Pennsylvania.

USRSA (2007) http://www.racquettech.com

Van Gheluwe, B and Hebbelinck, M (1985), The Kinematics of the Service Movement in Tennis: A Three-Dimensional Cinematographical Approach. In: *Biomechanics IX-B*, Champaign, IL, USA, pp 521-526

Watanabe, T, Ikegami, Y and Miyashita, M (1979) Tennis: The Effects Of Grip Firmness On Ball Velocity After Impact, *Medicine & Science in Sports,* **11,** 359-61.

Whyld, N M (2004), The Effect of Off Set Racket Impacts - An internal Report, The Department of Mechanical Engineering, *The University of Sheffield*

Widing, M A and Moeinzadeh, M H (1989) Nonlinear Finite Element Analysis of a Frame Stiffened with Tension Members, *Computers and Structures,* **33,** 233-240.

Widing, M A and Moeinzadeh, M H (1990) Finite Element Modeling of a Tennis Racket with Variable String Patterns and Tensions, *International journal of Sport Biomechanics,* **6,** 78-91.

Xsens (2007)
http://www.xsens.com/index.php?mainmenu=technology&submenu=research&subsubmenu=human_motion

Xu, M, Orwell, J and Jones, G (2004), Tracking Football Players with Multiple Cameras. In: *2004 International Conference on Image Processing,*

Yan, F, Christmas, W and Kittler, J (2005) A Tennis Ball Tracking Algorithm for Automatic Annotation of Tennis Match, *BMVC.*

Zhang, Z (1999), Flexible Camera Calibration by Viewing a Plane from Unknown Orientations. In: *International Conference on Computer Vision,* Corfu, Greece, pp 666-673

A. Internal Report: Assessment of Calibration Techniques

The University of Sheffield
Department of Mechanical Engineering
Sports Engineering Research Group

3D Image Reconstruction from a Stereo Camera Pair: Assessment of Calibration Techniques

Neil Whyld

August 2004

1. INTRODUCTION

The use of stereo camera imaging to re-construct points in three-dimensions is well documented. There are several techniques available for camera calibration and position reconstruction. The most suitable method for a given application is very much dependent on the specifics of that situation.

This short report aims to assess the suitability of three different methods of calibration/reconstruction for analysing tennis ball and racket interactions, as well as full scale player testing. It will focus predominantly on accuracy, flexibility and ease of use.

The methods to be assessed are:-

- Grid calibration using:-
  - Standard DLT algorithm (calculates 11 independent camera parameters which are used to relate 2D positions (u,v) in the two camera image planes to the corresponding 3D position (x,y,z) in the global reference frame).
  - Modified DLT algorithm (Development of the Standard algorithm which ensures the three principle axes (x,y,z) are orthogonal).
- Checkerboard calibration (Algorithm uses the image distortions of a checkerboard held in different orientations to calculate the required camera parameters).

2. EXPERIMENTAL PROCEDURE

2.1. Grid Calibration

A planar calibration grid was constructed from "Bosch" extruded aluminium beams. The structure was painted black and 18 highly reflective markers were attached at carefully measured locations. The evenly spaced markers were divided into two groups (numbers and letters) to allow for a variety of different calibration and verification point combinations to be investigated. The x,y and z locations of these markers are given in Appendix 1.

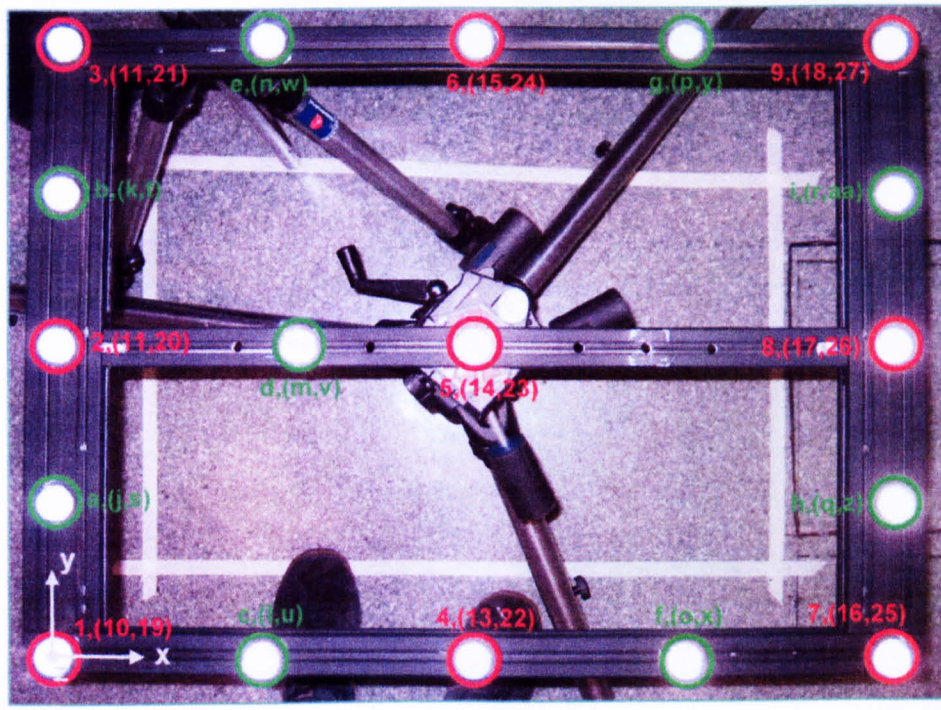

Figure 2.1 Plan view of the calibration grid, showing point labels.

Attaching the calibration grid to a tripod allowed the whole frame to be translated in the z direction. Recording the points at three different heights effectively increased the number of calibration and verification points from two sets of 9 to two sets of 27. The lowest level was taken as a reference height of 0 mm and contained points 1-9 and a-i as illustrated in Figure 2.1. The grid was then raised by 126 mm to produce the second level, containing an identical set of points from 10-18 and j-r. Finally raising the grid to a height of 240 mm above the reference level provided points 19-27 and s-aa.

Taking point 1 (at the reference height) as the origin (0,0,0) the relative position of all other points were calculated by careful measurement from the origin.
Two MotionCorder high speed video cameras were used as the stereo pair. They were orientated at approximately 90° to each other and with the calibration grid in the centre of view for both cameras. See Figure 2.2.

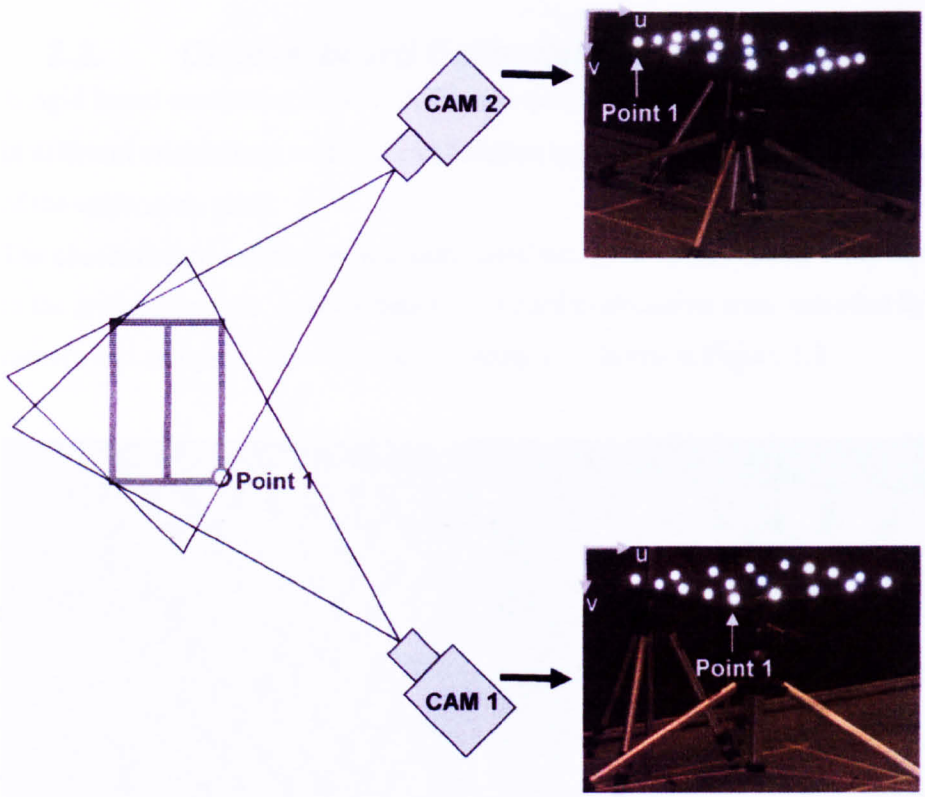

Figure 2.2 Stereo camera setup with views from each camera.

A short amount of footage was taken from both cameras at each of the three grid heights. The footage from each camera was then analysed using Richimas v3.2, and the u,v pixel location of each point (1-27 and a-aa) recorded.

Inputting the u,v data obtained for each calibration point together with their positions relative to the local coordinate system origin (point 1) into routines created in Matlab enabled the calculation of the 11 DLT parameters from both the Standard algorithm and the Modified algorithm. The input of a separate file of u,v data for the verification

points enabled the Matlab routines to reconstruct the positions of the points in the local coordinate system (x,y,z). The difference between the reconstructed positions and the physically measured positions were then compared for accuracy for the two algorithms.

This procedure was repeated using different combinations of calibration and verification points.

2.2. Checkerboard Calibration

A rigid board containing a 14 x 14, 40mm square checkerboard pattern was positioned in different orientations within the calibration area (defined by the previous position of the calibration grid).

The checkerboard calibration was conducted using the same camera setup as that used in the grid calibration. Approximately 20 board orientations were recorded by each camera and analysed. A sample pair of images is shown in Figure 2.3.

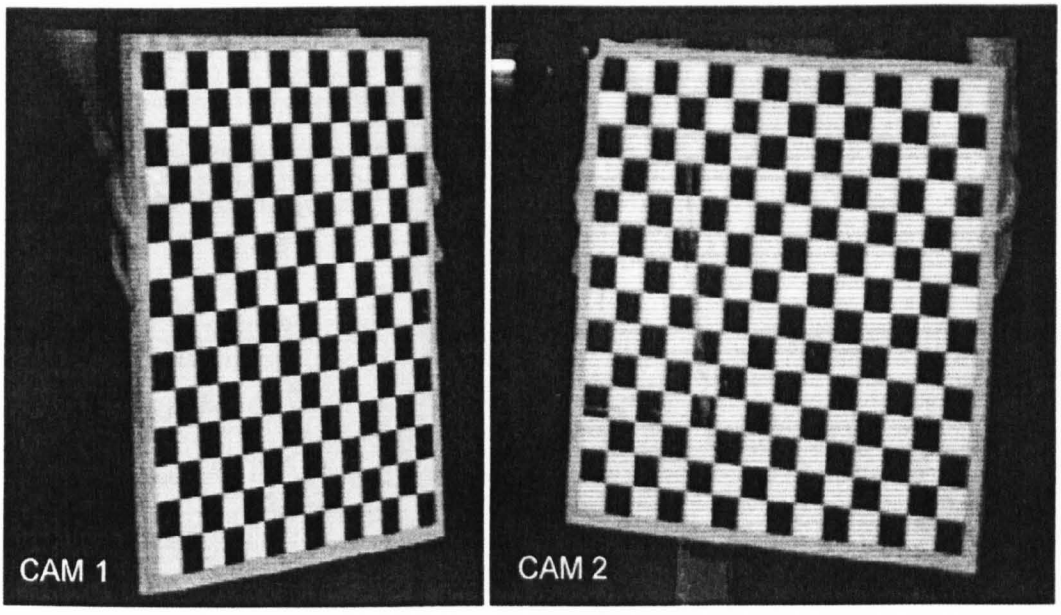

Figure 2.3 Images of the same checkerboard orientation from both stereo cameras.

During the checkerboard analysis, it is possible to define a reference plane in any orientation. The planes used were chosen to correspond with the local coordinates set up by the calibration grid.

The first plane was defined using the xy axis and the second plane was defined with the xz plane, as shown in Figure 2.4.

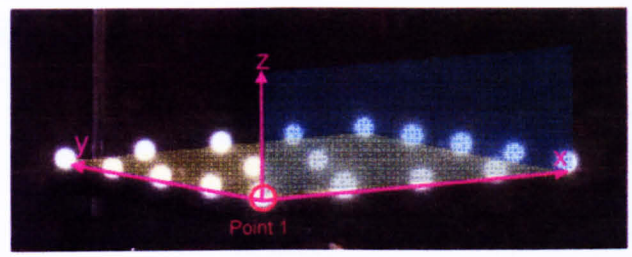

Figure 2.4 Checkerboard reference planes: First plane shown in yellow, second plane in blue.

3. RESULTS

Four combinations of grid calibration and verification points were investigated. Two tests used different sets of points for calibration and verification (i.e. numbers to calibrate the system and letters to check the reconstruction, and vice versa) and the other two sets used the same points for calibration and verification (i.e. numbers to calibrate and also to check reconstruction). These four tests were reconstructed using both the Standard DLT algorithm and the Modified DLT algorithm, and compared to the Checkerboard reconstruction results of the same points.

The results are summarised below:-

Grid calibration

CALIBRATION POINTS	VERIFICATION POINTS	AVERAGE ERROR (mm)		MAXIMUM ERROR (mm)	
		STAND DLT	MOD DLT	STAND DLT	MOD DLT
NUMBER	LETTER	1.07	3.85	2.85	19.50
LETTER	NUMBER	1.26	4.25	2.26	8.20
NUMBER	NUMBER	1.10	4.48	2.87	19.36
LETTER	LETTER	0.92	1.72	2.87	8.18

Table 3.1 Grid calibration results summary.

Checkerboard calibration

VERIFICATION POINTS	AVERAGE ERROR (mm)		MAXIMUM ERROR (mm)	
	XY FIXED	XZ FIXED	XY FIXED	XZ FIXED
NUMBER	2.5	2.04	9.04	7.44
LETTER	1.42		8.86	

Table 3.2 Checkerboard calibration results summary.

The following results focus on the use of number positions for system calibration and letter positions for the checking of re-construction accuracy:-

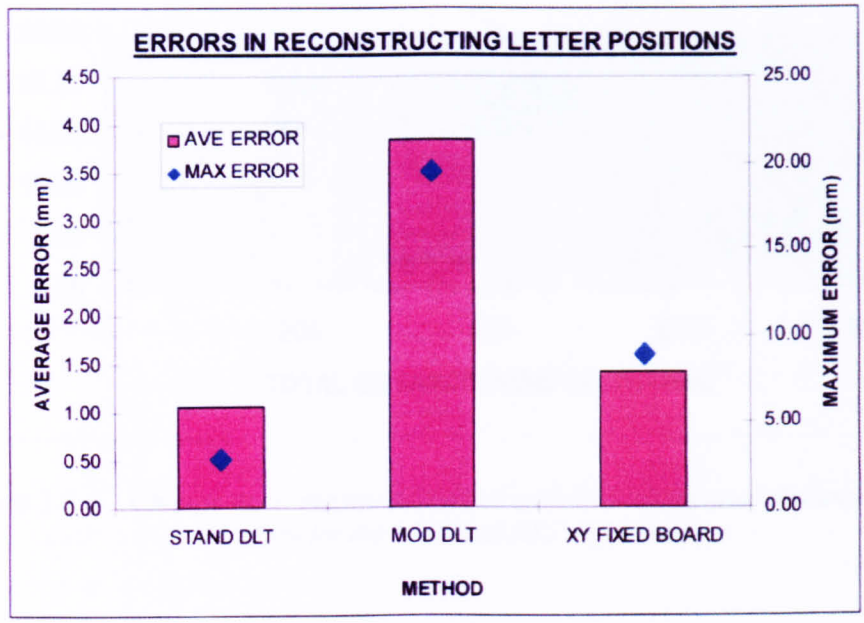

Figure 3.1 Average and maximum letter position reconstruction errors for the three calibration methods, using number positions for system calibration.

Looking at how the error in point reconstruction (in the x, y and z directions) vary with increasing total distance from the origin (point 1), we obtain the following results:-

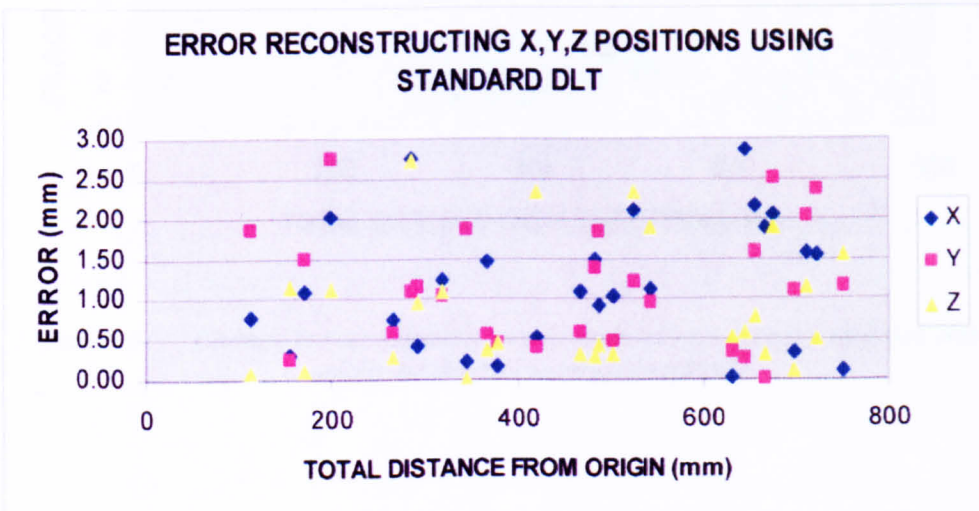

Figure 3.2 Change in reconstruction error with increasing total distance from the origin for the Standard DLT algorithm.

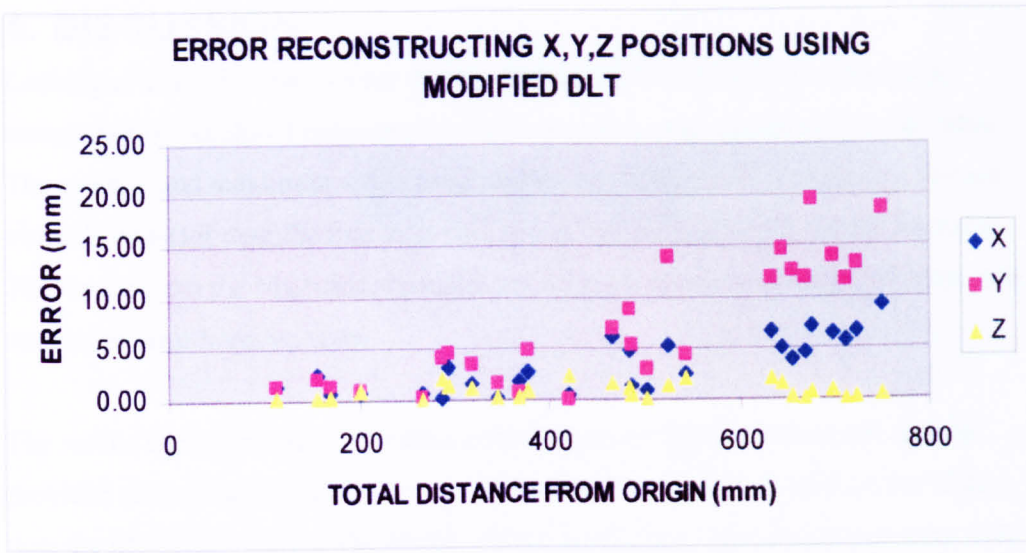

Figure 3.3 *Change in reconstruction error with increasing total distance from the origin for the Modified DLT algorithm.*

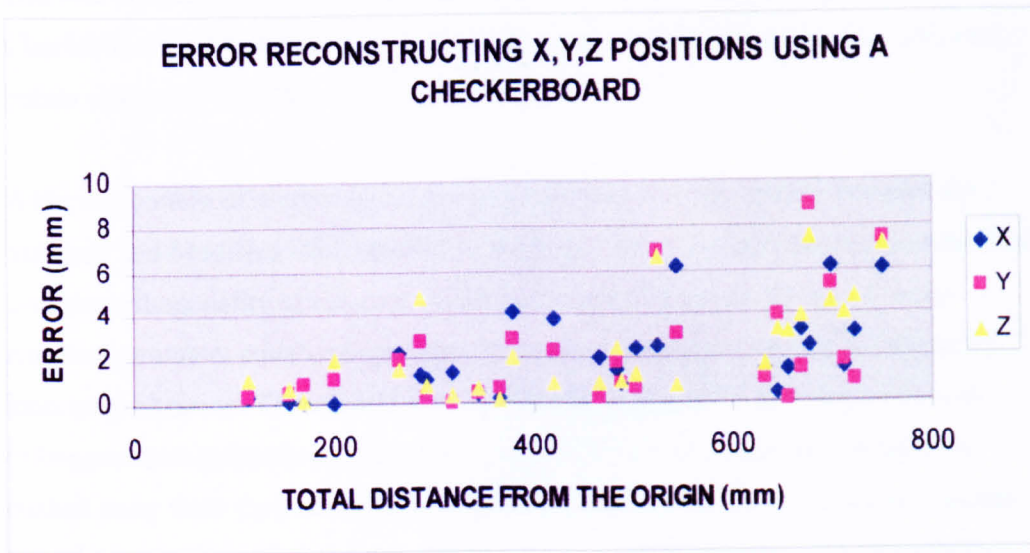

Figure 3.4 *Change in reconstruction error with increasing total distance from the origin for the checkerboard method.*

4. DISCUSSION

Looking at Table 3.1, we can see that the Standard DLT algorithm is producing reconstruction results of considerably higher accuracy than the Modified algorithm. The average and maximum errors produced by the Standard DLT algorithm remain virtually constant over the four tests performed; indicating that the results are valid. The results from the Modified algorithm are far more erratic with large differences in maximum error between tests.

The results shown in Table 3.2 indicate that in general, the Checkerboard method provided reconstruction accuracies lower than the Standard DLT method but higher than the Modified version. The Checkerboard method performed slightly better with the xz axis fixed compared to when the xy axis was fixed. This finding is likely to be specific only to this investigation however, and suggests that there could be significant errors in the true location of the test markers on the calibration grid. If the grid was perfectly square, with markers located in a truly orthogonal pattern, the Checkerboard calibration would provide identical results irrespective of which axis points were used to define the reference plane.

A skewed pattern of marker locations would explain the discrepancy between the Standard and Modified DLT results. As the Standard DLT algorithm has no constraint over the orthogonality of the axes, it merely fits the data points produced to the required parameter equations, giving very accurate results for what is an inherently inaccurate situation. Therefore if the Modified DLT algorithm is trying to fit non-orthogonal data points to an orthogonal model, we would expect the results to be pushed away from their true values, giving what are essentially low accuracy results for a theoretically high accuracy situation. The Checkerboard provides intermediary results as although it doesn't have the orthogonal constraint over the three principle axes of the Modified model, it does have a reference plane defined by the data points. Although the two axes defining this plane are not required to be at 90^{o} to each other, the third axis (normal to the reference plane) is defined by the cross-product of the two other axes, and, must therefore be orthogonal to the reference plane, when in reality it may not be.

In summary: The Standard DLT algorithm allows for all axes to be non-orthogonal. Modified DLT assumes all axes to be orthogonal. The checkerboard method takes one axis to be orthogonal to the plane defined by the other two axes.

If a non-orthogonal grid is responsible for the results described above, one would assume that for the Modified DLT and the Checkerboard methods, the reconstruction errors should increase with distance from the origin. Additionally, due to the level of constraint of each method, the Modified DLT algorithm should be effected the most and thus produce higher errors than the Checkerboard method. Finally, due to the lack of constraints, the error produced by the Standard DLT algorithm should remain independent of the distance from the origin.

Graphs 3.2 to 3.4 support this theory and illustrate all of the trends mentioned above. The errors produced by the Standard DLT algorithm appear totally independent of the distance from the origin. The variation in values will be due to random errors associated with the manual digitisation of the control points. The errors produced by the Modified DLT algorithm clearly increase with distance from the origin, with the y and x positions being effected more than the z reconstruction. The errors associated with the Checkerboard calibration are also shown to be related to the distance away from the origin, but as predicted the level of error is considerably less than that produced by the Modified DLT algorithm.

For the size of test grid used, it is worth noting that the inaccuracy in grid construction needed to produce the levels of error encountered is extremely small.

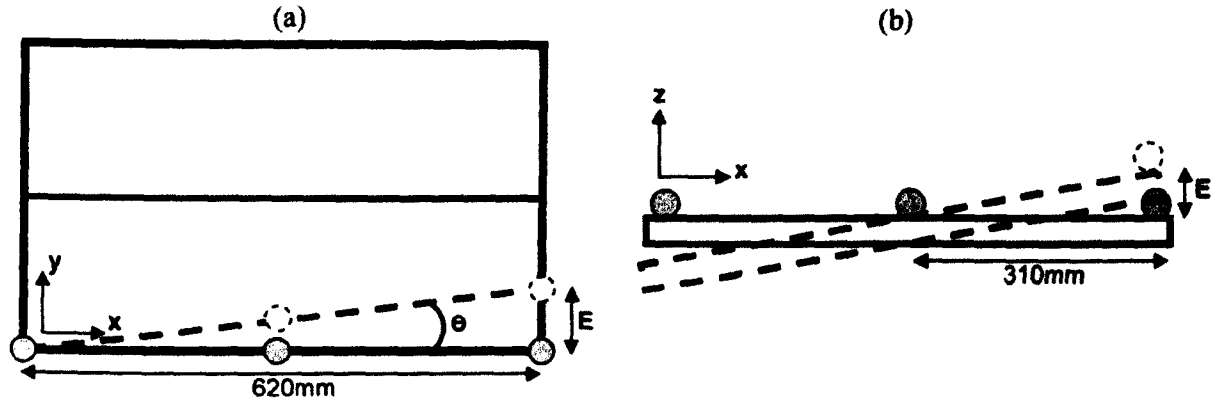

Figure 4.1 *(a); Plan view illustrating error, E, produced in the y direction for a misalignment of markers along the x axis, theta degrees from the true alignment.*

(b); Side view illustrating error, E, produced in the z direction due to misalignment of the calibration grid on the tripod.

Figure 4.1(a) shows that a very small error in the grid construction will produce very large errors in the actual position of the markers. It only requires the line of markers to be aligned 0.46° from the true orientation to offset the end marker by a distance of 5mm in the y direction. Further a rotation of only 0.92° in the line of the markers will provide an error in the y direction of 10mm.

If the grid is in anyway warped and/or not set absolutely level on the tripod, Figure 4.1(b) illustrates that the error in the z direction can be very significant for only small angle deviations. For an error of 5mm the grid alignment need only be 0.92° from its true orientation.

5. CONCLUSIONS

The Standard DLT algorithm proved to be the most "forgiving" to errors in grid construction as it does not constrain the principle axes to be orthogonal. Although this method accurately reconstructed the positions of test points, the true meaning of the results must be carefully considered before this method is used. If it is essential that the results be split into a truly orthogonal reference frame then this method provides no guidance as to the true level of accuracy.

Due to inaccuracies in the grid construction, the Modified DLT algorithm provided the least accurate results. However, the poor reconstruction results did highlight the fundamental problem of the grid not being accurate enough. If a suitably accurate grid were manufactured then this method would provide very accurate and reliable results. Producing this grid would be expensive and time consuming however.

Producing the levels of accuracy required to manufacture a suitable grid is very difficult, especially as its size is increased. The grids are also delicate and difficult to transport.

A far more versatile method of camera calibration is the Checkerboard technique. Its results were of acceptable accuracy given the test situation. A set of markers stuck to the floor of the test area would ensure that that the principle axes remain orthogonal and true to the World reference frame. Perhaps the greatest advantage of this method however is its simplicity. The test object is quick and easy to manufacture and use. It is also relatively small and durable, and hence easy to transport.

Although the relative error associated with the production of a checkerboard is small in comparison to the construction of a calibration grid, it is not zero. Forming the grid from small sections printed on a standard A4 printer allows for the introduction of cutting and alignment errors. These errors can be eliminated relatively cheaply by having a large grid custom printed in one piece.

Appendix 1

Below are details of the measured locations of both sets of marker points. The values are given in millimetres and are measured from the origin (taken as Point 1).

POINT	X	Y	Z
1	0	0	0
2	0	230	0
3	0	461	0
4	311	0	0
5	311	230	0
6	311	461	0
7	622	0	0
8	622	231	0
9	622	462	0
10	0	0	126
11	0	230	126
12	0	461	126
13	311	0	126
14	311	230	126
15	311	461	126
16	622	0	126
17	622	231	126
18	622	462	126
19	0	0	240
20	0	230	240
21	0	461	240
22	311	0	240
23	311	230	240
24	311	461	240
25	622	0	240
26	622	231	240
27	622	462	240

POINT	X	Y	Z
a	0	114	0
b	0	345	0
c	155.5	0	0
d	181	230	0
e	155.5	461	0
f	466.5	0	0
g	466.5	461	0
h	622	114	0
i	622	346	0
j	0	114	126
k	0	345	126
l	155.5	0	126
m	181	230	126
n	155.5	461	126
o	466.5	0	126
p	466.5	461	126
q	622	114	126
r	622	346	126
s	0	114	240
t	0	345	240
u	155.5	0	240
v	181	230	240
w	155.5	461	240
x	466.5	0	240
y	466.5	461	240
z	622	114	240
aa	622	346	240

Tables 5.1 Measured location of the reflective position markers.

B. Multi Variate Fitting Techniques

B.1 Introduction

Regressive fitting techniques are frequently used to ascertain a relationship between a single input and output variable. Even in this simple case the regressed relationship differs from the actual results due to experimental error and other uncontrolled variables. Nevertheless, this regressive relationship can be used to predict experimental outcomes given a single input. The experiment outlined in chapter 6 consists of six input variables and two output variables. Unlike the simpler single variable situation, there is no possible way to visualise the relationship between a single output and all six inputs. It is very difficult and often inaccurate to reduce this situation to a single parameter situation by artificially controlling every other input. Multi variate regressive fitting techniques (Seber and Wild 2003) such as polynomial regression, and neural networks can be used to find algebraic relationships between a single output and a number of different experimental variables. In an experiment with many input parameters, a multi-variate fit allows comparison between a single output variable and a single input variable by keeping all other variables constant. This chapter gives a brief description of multi-variate fit techniques and the particular one used to generate the results seen in chapter 7.

B.2 Aim

This chapter aims to find a suitable multi-variate fitting technique for the results of the experiment described in chapter 6. This multi-variate fit will generate accurate experimental responses for any set of six input parameters.

B.3 Methodology

B.3.1 Experimental Results

The impact test described in chapter 6 was carried out using 3D videogrammetric methods. Two Phantom V4.2 cameras were used to record 900 ball racket impacts of which 878 were successfully recorded. Figure B.1 shows all of the outbound velocities in the z direction plotted according to the inbound velocity in the z direction.

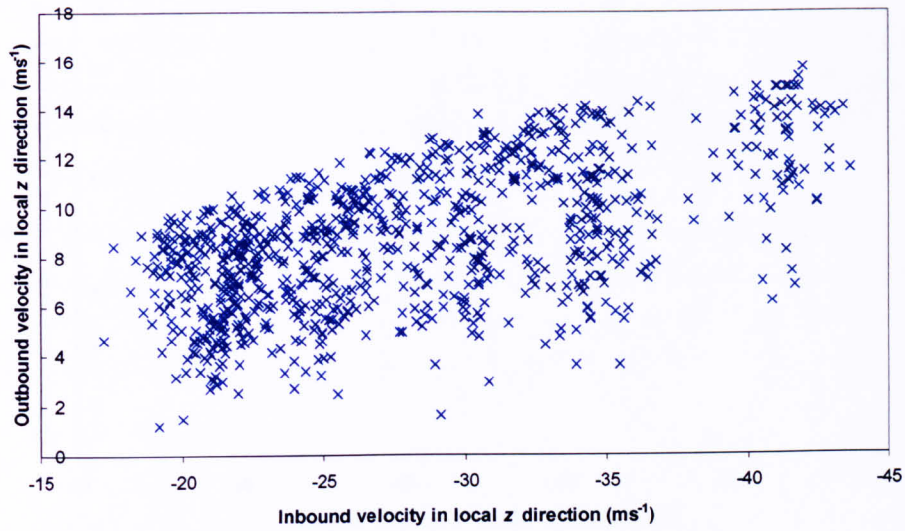

Figure B.1. The experimental outbound velocity in the z direction according to the inbound velocity in the z direction.

Distinct groupings of results can be seen in figure B.1, corresponding to the distinct intervals of inbound velocity used in the experiment. As the inbound velocity increases, the results show a general trend towards an increase in the outbound velocity. The scatter in these results is such that no meaningful relationship can be extracted from the results. The results seen in figure B.1 relate to the full range of five input parameters which are not accounted for in the plot. This includes the velocity in the local x and y direction, the impact position in the local x and y direction and the restrictive torque around the handle.

To obtain a worthwhile comparison between these results and a predictive model, the parameters not accounted for in the plot must be artificially restricted. For example, only impacts within 10 mm of the stringbed centre, ball velocities in the x and y direction within 2 ms^{-1} of zero and a restrictive torque of 0 Nm will be included. These results are shown in figure B.2.

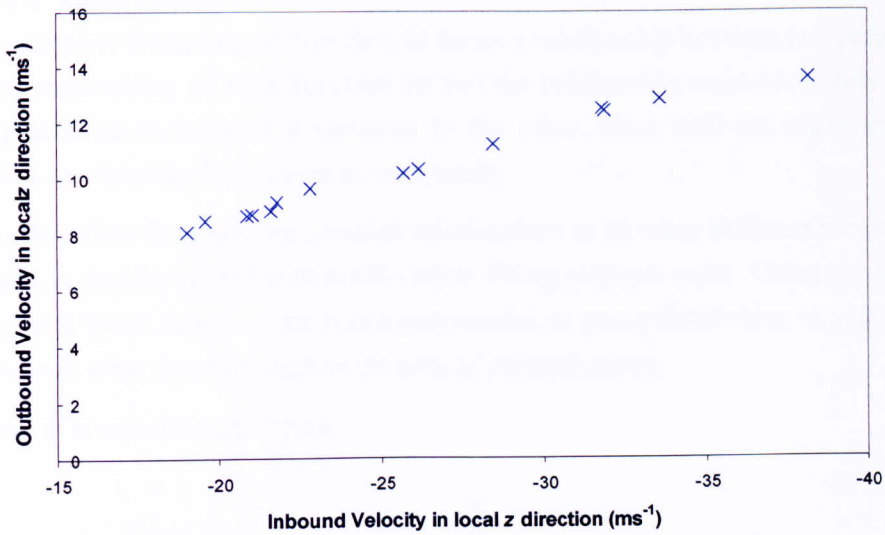

Figure B.2. The experimental outbound velocity in the z direction according to the inbound velocity in the z direction. In this case any results outside of a specific range of parameters for the inbound velocity, impact position and restrictive torque are omitted.

A much clearer correlation is seen in figure B.2. Despite this, there are two immediate problems with this approach.

1) The number of data points is greatly reduced. The points which do not fall within the prescribed range are eliminated. Of the 878 data points recorded, only 17 meet the given criteria. This number could be increased by widening the boundaries used for selecting the data points. This would make the data noisier, introducing more scatter. Not only is the precision decreased by introducing arbitrary data boundaries, but the amount of usable data is severely reduced also.

2) This approach completely defeats the purpose of using accurate videogrammatic tracking techniques. In chapter 6 it was decided to change the input parameters within rough intervals. The values of impact position and ball velocity were then measured very precisely from the impact images. Analysing the data by imposing artificial intervals renders this high level of tracking accuracy redundant. For example, whilst the value of inbound and outbound velocity in the z direction can be accurately obtained from figure B.2, every other parameter can only be ascertained as existing within the intervals stated above.

A regression fit applied to the data in figure B.2 would account only for the data points seen in the plot and would not account for any other experimental parameter. A multi-variate regression fit would account for every recorded data point and also every experimental parameter to the accuracy with which they were originally recorded.

The increased accuracy, versatility and efficiency of a multi-variate means it is an ideal method for analysing the results of the experiment described in chapter 6.

B.3.2 Data Fitting

In its simplest form, a regressive data fit forms a relationship between two parameters. It does this by minimising an error function so that the relationship most accurately describes how one parameter varies with a variation in the other. How well the regressive fit can represent this relationship depends on its complexity.

A multi-variate fit uses more complex relationships to fit many different parameters to a single output. A number of different multi-variate fitting methods exist. Generally they apply commonly used 'base' functions, such as a polynomial, or gauss distribution to a set of data to minimise a basic error function such as the sum of squared errors.

If a set of n experimental inputs:

$$\overset{n}{\underset{i=1}{x_i}} \qquad \textbf{[B.1]}$$

gives n experimental outputs:

$$\overset{n}{\underset{i=1}{y_i}} \qquad \textbf{[B.2]}$$

A fitting function generates a set of n predicted experimental outputs:

$$\overset{n}{\underset{i=1}{y_{pi}}} = f(x_i) \qquad \textbf{[B.3]}$$

An error function can be created which accounts for the difference between the actual, and predicted experimental error function:

$$E = y_p - y \qquad \textbf{[B.4]}$$

This error value can be positive or negative for any particular data point. To avoid the positive and negative error values cancelling out when summed, the sum of *squared* error is calculated instead:

$$SSE = \sum_{i=1}^{n} E_i^2 \qquad \textbf{[B.5]}$$

Coefficients within the function $f(y)$ are altered to minimise the *SSE* value. In this way, an algebraic function can be calculated which fits the distribution of data within a known error value.

This mapping of the experimental data can be used to predict the experimental outcome according to a chosen set of input parameters. These are not limited to the combinations used in the actual experiment. This is especially useful when trying to validate individual aspects of a predictive model.

The literature review outlines the most commonly used multi-variate fit techniques. Whilst more modern and complex methods such as neural networking (Bishop **1995**) automatically refine the base functions and are able to very accurately fit high dimensional

data, it was felt that such an approach is an overly complicated solution. The physical relationships governing the post-impact behaviour of a tennis ball follow generally linear or low order polynomial relationships. Common sense tells us that no small change in ball velocity, impact position or handle grip results in sudden, large changes in post-impact ball velocity. For this reason a simple, polynomial regression method was used.

B.3.3 Polynomial regression

It is impossible to visually represent a data set with a single output parameter dependent of six independent input parameters. For this reason the concepts associated with choosing a suitable polynomial regression will be represented with a single input/output parameter scenario.

Figure B.3 shows a set of nine data points clustered around three distinct data points. Each data point is subject to random error. This is representative of an experiment with three different inputs, each being repeated three times.

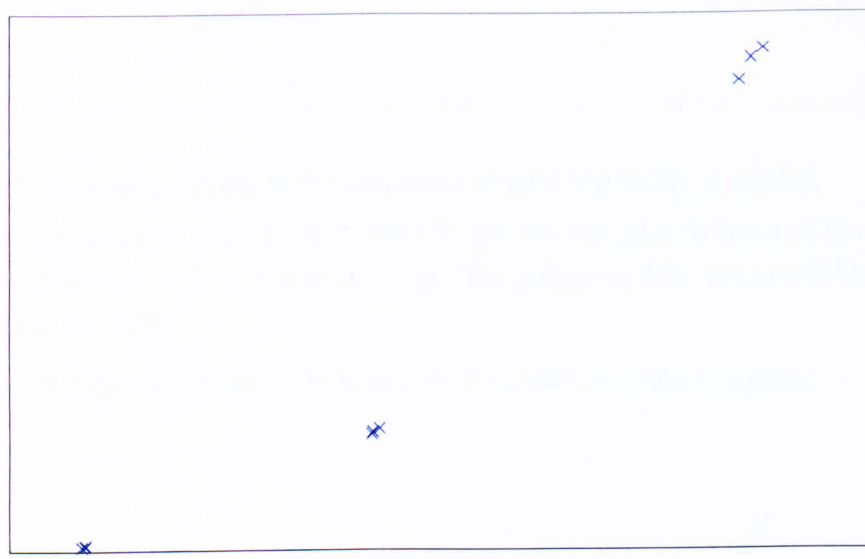

Figure B.3. Nine data points clustered around three distinct data points, each subject to random error.

A polynomial regression fit to the above data is of the form:

$$y_{pi} = (A + Bx_i)^n \qquad \textbf{[B.6]}$$

The higher the value of n, and hence the higher the order of the regressive fit, the more complex the equation becomes. Higher order regressive fits have more coefficients. Whilst a first order equation has two; A and B, a third order equation has four:

$$y_{pi} = A + Bx_i^{\,3} + Cx_i^{\,2} + Dx_i \qquad \textbf{[B.7]}$$

Generally, a more complex polynomial fit is able to provide a better fit to more complex relationships but is at risk of over-fitting.

Using polynomial fits of the first, second and third on the data seen in figure B.3 will reveal the necessary compromise between obtaining a good fit and avoiding over-fitting.

Figure B.4 shows the data with a first order fit applied.

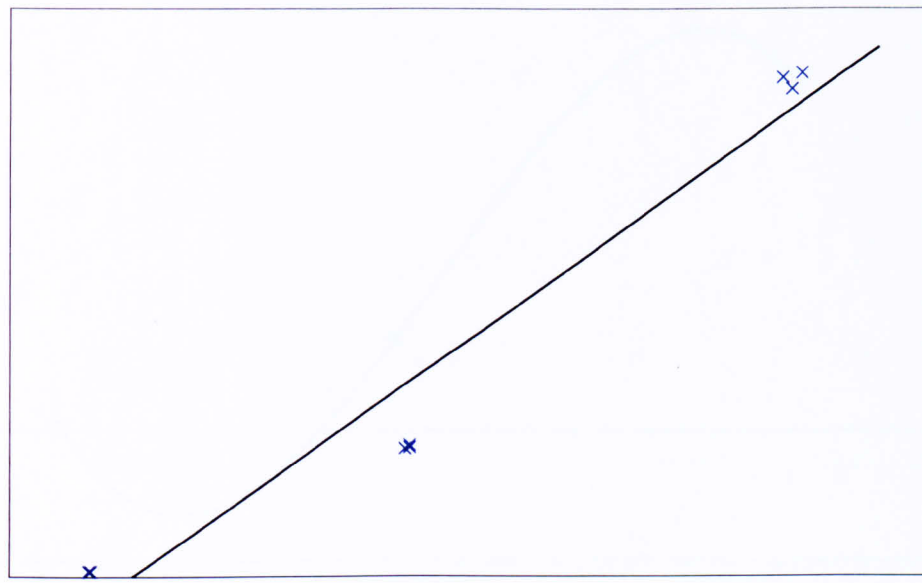

Figure B.4. Experimental data with a first order (linear) regression fit applied.

It can be seen that a linear, first order fit follows the general trend of the data but is perhaps too simplistic a fit to use in this case. The groups of data points still lie some way away from the line of fit.

Figure B.5 shows the same data with a second order quadratic fit applied.

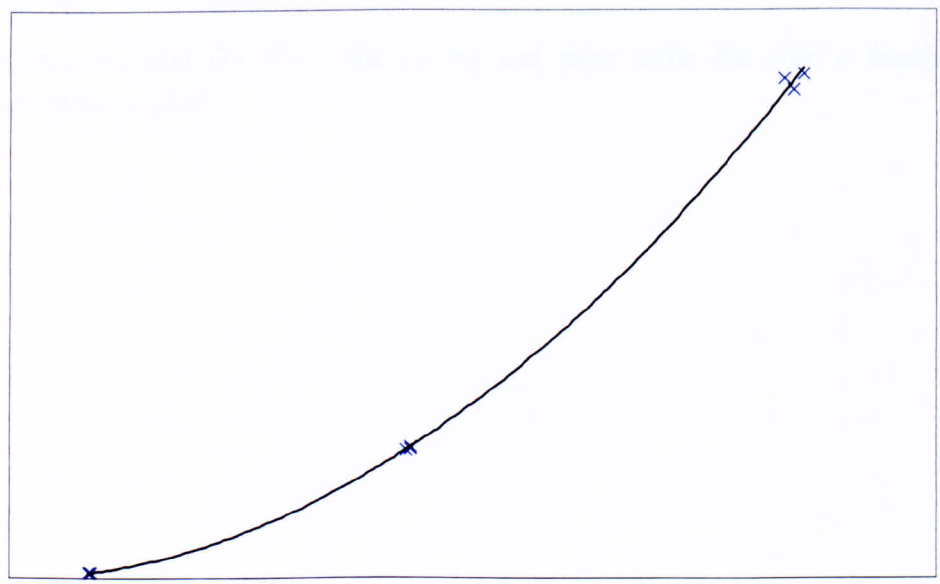

Figure B.5. Experimental data with a second order (quadratic) regression fit applied.

The quadratic fit follows the data very closely clearly following the trend of the data. Figure B.6 shows the same data with a third order cubic fit applied.

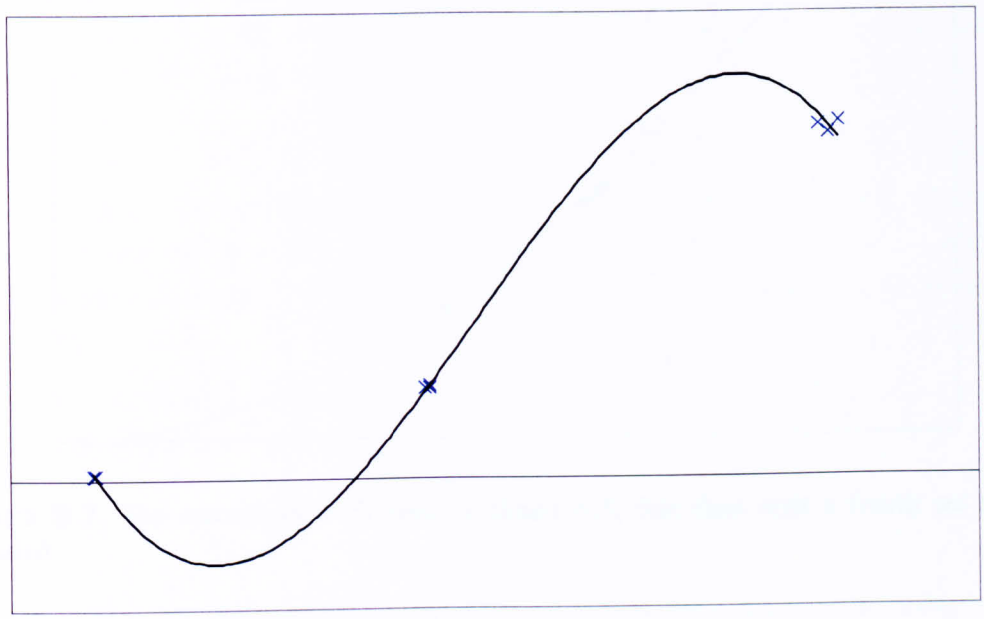

Figure B.6. Experimental data with a third order (cubic) regression fit applied.

The third order fit follows the experimental data equally well but the shape of the line of fit is markedly different. From this data alone it cannot be ascertained whether the data is following a quadratic or cubic relationship.

By omitting a data set from the original fit, a validation can be performed. This data can be used to see how closely a regression follows experimental data which was not used to train the line of fit.

Figures B.7 and B.8 show the second and third order fits with a fourth set of experimental data included.

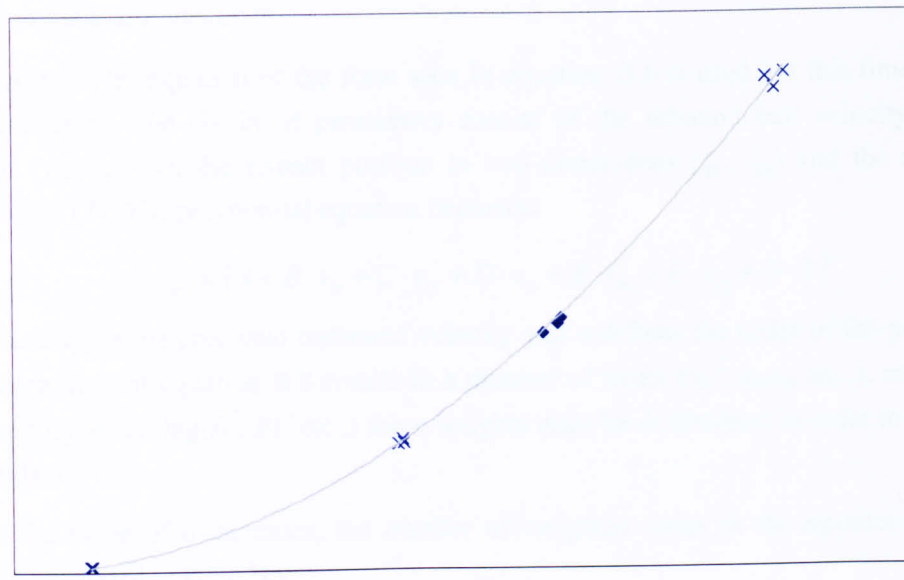

Figure B.7. The second order fit seen in figure B.5, this time with a fourth set of data included.

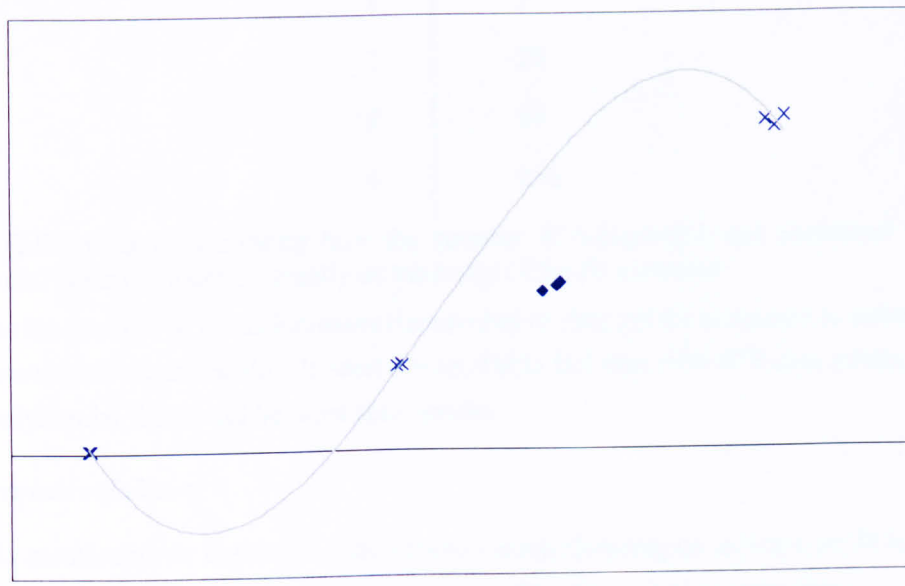

Figure B.8. The third order fit seen in figure B.6, this time with a fourth set of data included.

It can be seen from figure B.7 and B.8 that the original experimental data clearly follows a quadratic relationship. By validating the regression fits against this data, the error associated with the third order fit increases greatly, a clear situation of over-fitting.

The same techniques are used when generating multi-variate fits with many more input parameters, only the same visualisation is not possible. It is therefore important to consider the *SSE* and R^2 values.

Applying to the multi-variate fit

A polynomial equation of the form seen in equation B.6 is used but this time with six input parameters. The six input parameters consist of the inbound ball velocity in three directions (v_{ix}, v_{iy}, v_{iz}), the impact position in two dimensions (i_{px}, i_{py}) and the restrictive handle torque (T). The polynomial equation becomes:

$$v_{po} = \left(A + B \cdot v_{ix} + C \cdot v_{iy} + D \cdot v_{iz} + E \cdot i_{px} + F \cdot i_{py} + G \cdot T\right)^n \quad \textbf{[B.8]}$$

Where v_{po} is the predicted outbound velocity and n defines the order of the polynomial fit. An expansion of equation B.8 results in a number of terms (v_{ix}^2, $v_{ix}v_{iy}$ etc..), each with a corresponding weighting(B^2, BC etc..) these weights must be determined in order to achieve a fit to the data.

As the value of n increases, the number of weighted terms in the equation increases greatly as illustrated in table B.9.

Value of n	Number of terms
1	7
2	28
3	84
4	210

Table B.9. A table illustrating how the number of weighted terms contained within the polynomial equation increase greatly as the order of the fit increases

As the number of terms increases the number of data points necessary to ensure the fit is well determined increases also. It seems from Table B.9 that with 878 data points, the lower order polynomial fits would be most appropriate.

Multi-variate validation

As mentioned, an important consideration when choosing an appropriate fit is a minimal *SSE* value and ensuring that the fit is validated against data not used in training.

A cross-validation method was used to reveal potential over-fitting and compare the errors arising from polynomial fits of different orders. The literature review in chapter 2 includes more information regarding cross-validation techniques. Kohavi **1995** compares the n-fold and leave one out cross-validation techniques and shows that in most cases, the n-fold technique is the more appropriate method to use. The n-fold cross-validation technique shuffles the experimental data then splits it into n discrete portions. One of these portions is used to validate the polynomial fit generated by the other n-1 portions. This is explained in more detail below.

To generate the polynomial fits a powerful Matlab function, *polyfitn* was obtained from the Matlab online user community (Mathworks.com **2007**). This function allows the user to specify a polynomial equation (as in equation B.8). The function will then generate a series of accurately weighted terms that best fit a given set of experimental data. It is necessary to calculate two polynomial fits, one fitting the input variables to the post-impact ball velocities in the local *z* direction, the other fitting in the *y* direction.

The function *polyfitn* was used as part of a custom-written Matlab routine to perform a *10*-fold cross-validation assessment of polynomial regressions of different orders. The input data was randomised and split into ten equal portions. Nine of these were used to train a polynomial fit and generate a series of weights *(A, B* etc.) associated with the terms of a polynomial equation. This gives predicted values v_{po}, for sets of input parameters v_{ix}, v_{iy}, v_{iz} etc. The omitted section of the data set was then used to compare the predicted values v_{po} with the experimental values v_o. The *SSE* value was then generated from this information, and the process was repeated, this time omitting a different section of the original data set from the training process. After 10 repeats, an average *SSE* value gives an indication of the suitability of that particular model, and whether over-fitting is occurring. This is described diagrammatically in figure B.10.

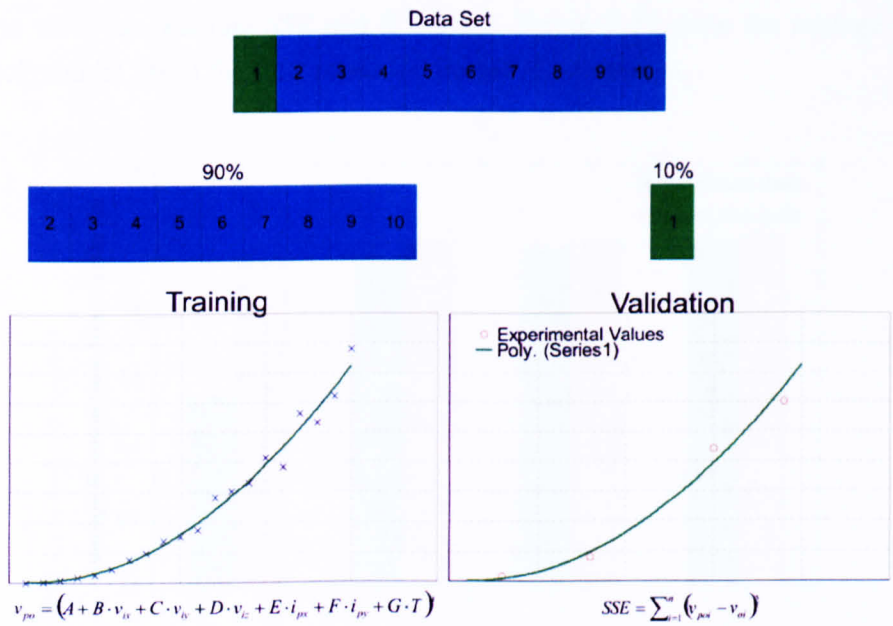

Figure B.10. A diagrammatic explanation of 10-fold cross-validation.

The cross-validation process was executed for polynomial fits of the 1st, 2nd, 3rd and 4th order. As 10 fits were trained for each order, 40 polynomial fits were trained in total. The average *SSE* and R^2 values were calculated for fits of each order. In this way the most suitable polynomial fit to use can be assessed from these values.

When dealing with a regression fit, all of the input values and hence predicted output values are normalised. The values are transformed to have a mean of 0 and standard deviation of 1. Given a data set x, the normalised value $\hat{x}_i$ of an individual data value x_i is given by:

$$\hat{x}_i = \frac{x_i - \bar{x}}{\sigma_x} \qquad \textbf{[B.9]}$$

This not only results in better performance from the fit, but gives a good indication as to whether specific input parameters are within the general input domain (i.e. within 2 standard deviations).

When a suitable function had been chosen, experimental results were generated using the function *polyfitn*. During validation, 10 separate fits were generated for each order. The 10 fits of the chosen order were used to generate 10 experimental values. The average of these predicted values was used as an overall value. With polynomial fits in both the local y and z directions, post-impact ball velocity and trajectories can be predicted when given specific values of the pre-impact ball velocity, impact position and handle torque.

B.4 Results

It is not possible to view the results of the cross-validation process directly. It is possible to view the resulting *SSE* and R^2 values. Figure B.11 show the average R^2 values over 10 polynomial fits of the first, second, third and fourth orders.

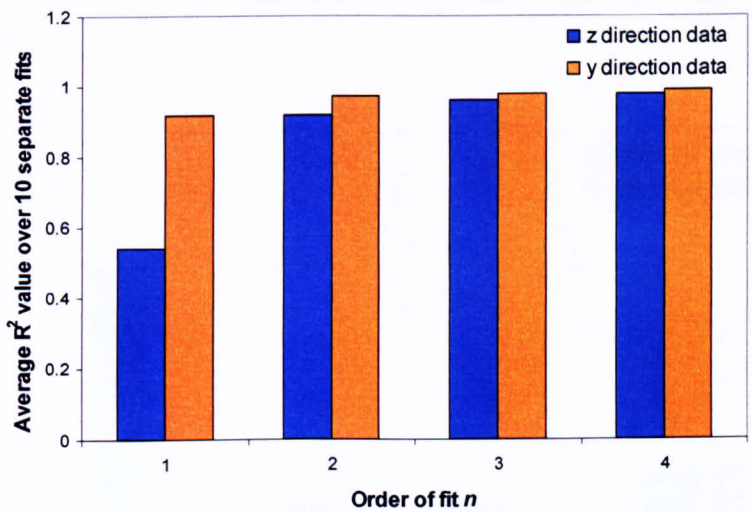

Figure B.11. The average R^2 value of ten fits of the 1st, 2nd, 3rd and 4th orders.

From figure B.11 it seems that the quality of fit improves as the order of fit increases. The ability of the polynomial equation to fit data increases as the order increases. Unfortunately the fit is also more likely to fit the noise and experimental error inherent within the data.

Figure B.12 shows the average *SSE* value of the data as the order of fit increases. In this case it is for the data used to train the experimental fit.

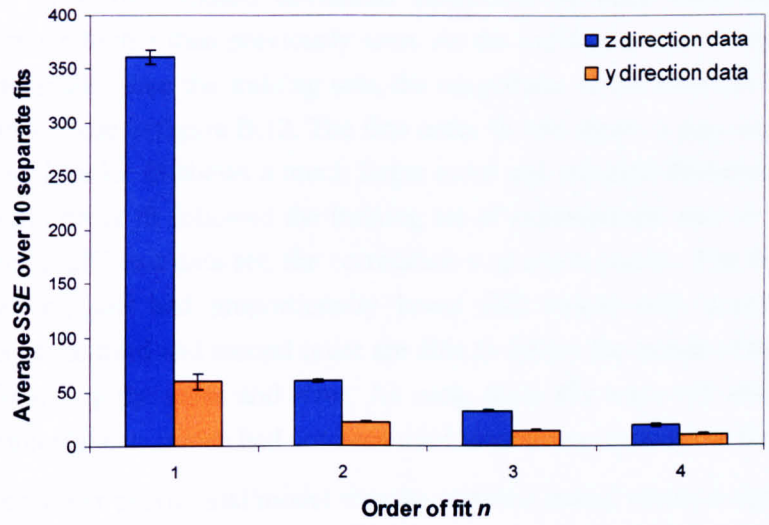

Figure B.12. The average *SSE* value of the polynomial fits for ten fits of the 1st, 2nd, 3rd and 4th order.

Figure B.12 shows that as the order of fit increases, the *SSE* value decreases correspondingly. This further reinforces that fact that as the order of the fit increases its ability to follow the given data increases. For experimental outputs in the *z* direction the low R^2 and high *SSE* value of the first order fit shows that it is unable to accurately model the experimental data. If the same polynomial fits are validated against experimental data not used in the generation of the fits a different result is seen. Figure B.13 shows the results of such an exercise.

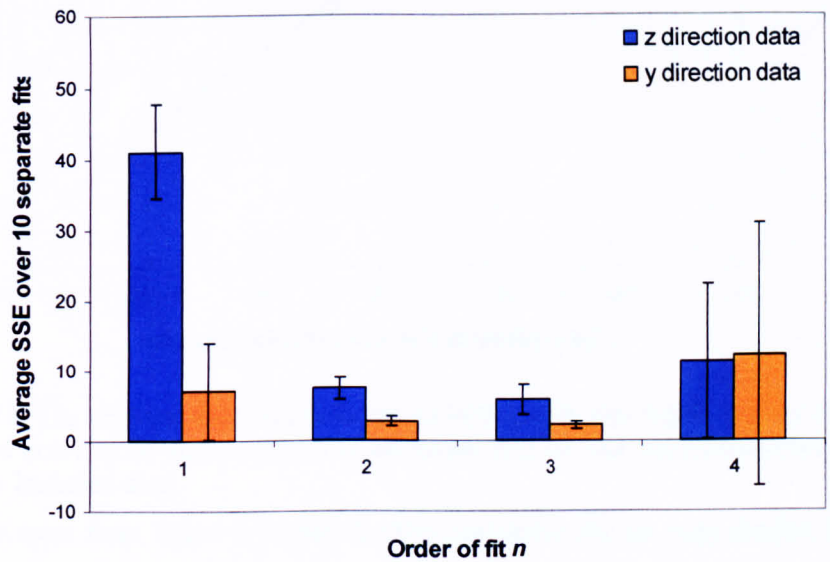

Figure B.13. The average *SSE* value of the polynomial fits for ten fits of the 1st, 2nd, 3rd and 4th order. A validation set of experimental data has been used in this case.

In figure B.13 the standard deviations (indicated by error bars) of the data are proportionally much higher than previously seen. As the validation sets of experimental data sets were much smaller than the training sets, the magnitude of the errors in figure B.13 are much smaller than those in figure B.12. The first order fit still shows a poor correlation and in this case the fourth order fit shows a much larger error and standard deviation than previous results. The fourth order fit followed the training set of experimental data so well that when validated against a different data set, the correlation was much poorer. The third and second order fits however, still had proportionally lower *SSE* values with acceptable standard deviations. Fits of the third and second order are able to follow the trends of the experimental data without following the noise and error. As such, these fits were still able to follow the trends of experimental data which had not been used to generate the original fit.

The second order polynomial model was the simplest model which accurately predicted the experimental values according to the R^2 and *SSE* values. Figure B.14 shows the original restricted data from figure B.2 with two regressive fits. One fit is a standard second order regressive fit based on the data points included in the plot. The second regressive fit was generated by using the multi-variate second order fit described above. The input velocity in the x and y directions, the impact position in the x and y directions and the restrictive torque were all set to zero.

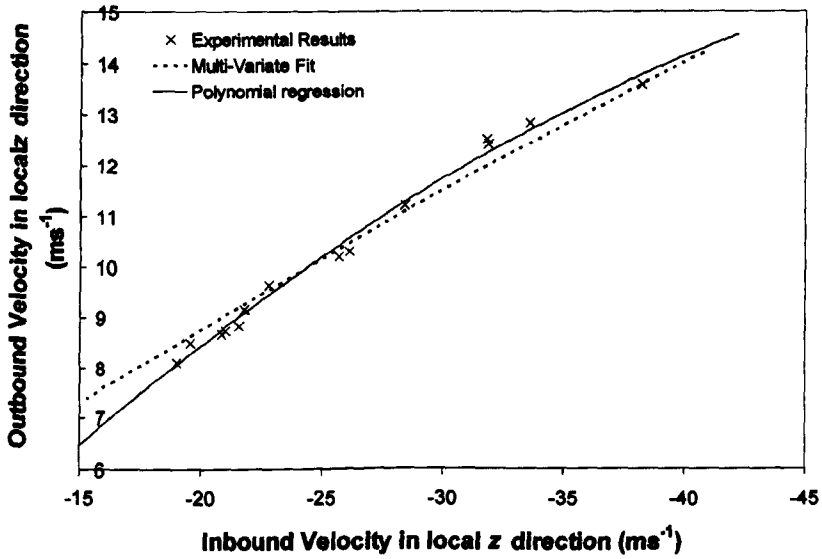

Figure B.14. The original restricted data shown in B.2 with two regressive fits included. One is the second order multi-variate fit described above The second is a standard second order fit based on the included data.

It may seem from figure B.14 that the two regressive fits are very similar, but there are marked differences. The multi-variate fit was generated using the 98% of the data which was not included in the plot. As such it is a much more reliable predictor of the experimental behaviour than the simple regressive fit. The two fits diverge at inbound velocity values lower than 25 ms^{-1}. Below 25 ms^{-1} the data points in figure B.14 become sparse, below 20 ms^{-1} they

stop altogether. The simple regressive fit becomes very inaccurate below 20 ms^{-1}, diverging considerably from the multi-variate fit.

B.5 Discussion

In terms of the most appropriate regression tool to use for modelling experimental outcomes, the R^2 values in figure B.11 illustrate that a polynomial regression is sufficient to map the changing behaviour of a post-impact ball.

As would be expected, as the order of the polynomial equation increases, a better fit to the data is achieved; the *SSE* values drop and the R^2 values increase. Over fitting occurs when the order of the fit is so high that it begins to fit the noise present in the experimental data. When the fit is validated against a different set of data, this over-fitting becomes apparent. Figure B.13 shows a sudden large increase in *SSE* from the third to the fourth order model. In a similar sense, the linear first order model is unsuitable due to its inability to accurately map the behaviour of the ball, with accordingly poor R^2 and *SSE* values. The differences between fits of the second and third order are seemingly very small in terms of *SSE* and R^2 values; no obvious over-fitting occurs, and both fit the data sufficiently well.

The second order model was chosen to model the experimental data. The second order model is the simplest fit which accurately models the experimental data and contains considerably fewer weighted terms than the third order model. The improvement in *SSE* values from the second to the third order model is minimal, both for the average error and standard deviation. A single case of over-fitting could result in a large inherent error which is not immediately apparent from the given predicted values. This is less likely to occur for a lower order model.

Artificially restricting the data points in order to observe trends is a crude method of analysis. The data is considerably more sparse and contains more noise due to an inability to strictly control every experimental parameter. Figure B.14 reveals that the multi-variate fit generally has a greater range and confidence of prediction as every single data point is used to generate the fit. Once fitted to the data, any experimental value can be predicted by using exact input parameters. This is a much more accurate and controlled method of obtaining experimental trends from data with several independent input parameters.

When using experimental methods to create multi-variate fits; the possibility exists to use one to replace a physically based predictive model.

In this case, the experimental parameters have been relatively restricted, but multi-variate regression techniques can be used to map many more parameters. It is theoretically possible to monitor the effects of changes in the dimensions and specification of the racket, stringbed, ball and even atmospheric conditions. Realistically this would require significant and incremental changes in each of these variables, moving the requisite number of data points from the thousands into the millions. To add to this, a predictive tool based on

regression alone gives us no further understanding of the physical processes involved with the impact and no further insight into how particular interactions might be governed or controlled. The experimental aspect of this study has been restricted to a single racket with tightly controlled input parameters. A single racket was used for reasons of time effectiveness and as an exhibitive case in point towards the validation of the outcome of a physically based predictive model.

The strength in using regressive techniques comes from being able to predict experimental outcomes for a set of inputs that weren't implicitly part of the original experiment. Using a multi-variate fit a single experiment can be used to isolate and validate separate aspects of the predictive model.

B.6 Chapter Summary

This chapter showed the calculation of an accurate and methodologically justified way to validate a predictive model; the multi-variate regressive fit.

A single racket, chosen for its high stiffness, was tested using a methodology devised in the previous chapter. The results from this experiment were processed using a set of polynomial regressive fits. A cross-validation technique showed that a fit of the second order would be most suitable in this case. Using this polynomial fit, predicted values can be calculated for any combination of input parameters within the original input domain and will form the basis of a robust model validation.

C. Polyfitn.m

C.1 Introduction

Find below the polyfitn MATLAB file which was used to generate the multi-variate models. Every line of text, including the comments has been included. It should be noted that this function works in conjunction with the series of symbolic polynomial MATLAB files created by the same author D'Errico **2006**.

C.2 Polyfitn

The text is presented in two columns starting on the next page

```
function polymodel =
polyfitn(indepvar,depvar,modelterms)
% polyfitn: fits a general polynomial regression
model in n dimensions
%          usage:          polymodel          =
polyfitn(indepvar,depvar,modelterms)
%
% Polyfitn fits a polynomial regression model of one
or more
% independent variables, of the general form:
%
%  z = f(x,y,...) + error
%
% arguments: (input)
%  indepvar - (n x p) array of independent variables
as columns
%       n is the number of data points
%       p is the dimension of the independent variable
space
%
%       IF n == 1, then I will assume there is only a
%       single independent variable.
%
%  depvar    - (n x 1 or 1 x n) vector - dependent
variable
%       length(depvar) must be n.
%
%       Only 1 dependent variable is allowed, since I
also
%       return statistics on the model.
%
%  modelterms - defines the terms used in the model
itself
%
%           IF modelterms is a scalar integer, then it
designates
%           the overall order of the model. All possible
terms
%           up to that order will be employed. Thus, if
order
%           is 2 and p == 2 (i.e., there are two variables)
then
%           the terms selected will be:
%
%             {constant, x, x^2, y, x*y, y^2}
%
%              Beware the consequences of high order
polynomial
%           models.
%
%       IF modelterms is a (k x p) numeric array, then
each
%           row of this array designates the exponents of one
%           term in the model. Thus to designate a model with
%           the above list of terms, we would define modelterms
as
%
%           modelterms = [0 0;1 0;2 0;0 1;1 1;0 2]
%
%       If modelterms is a character string, then it will be
%           parsed as a list of terms in the regression model.
%              The terms will be assume to be separated by a
comma
%           or by blanks. The variable names used must be legal
%           matlab variable names. Exponents in the model may
%           may be any real number, positive or negative.
%
%           For example, 'constant, x, y, x*y, x^2, x*y*y'
%           will be parsed as a model specification as if you
%           had supplied:
%           modelterms = [0 0;1 0;0 1;1 1;2 0;1 2]
%
%           The word 'constant' is a keyword, and will denote a
%           constant terms in the model. Variable names will be
%           sorted in alphabetical order as defined by sort.
%           This order will assign them to columns of the
%           independent array. Note that 'xy' will be parsed as
%           a single variable name, not as the product of x and y.
%
%       If modelterms is a cell array, then it will be taken
%           to be a list of character terms. Similarly,
%
%           {'constant', 'x', 'y', 'x*y', 'x^2', 'x*y^-1'}
%
%           will be parsed as a model specification as if you
%           had supplied:
%
%           modelterms = [0 0;1 0;0 1;1 1;2 0;1 -1]
%
% Arguments: (output)
% polymodel - A structure containing the regression model
%       polymodel.ModelTerms = list of terms in the model
%       polymodel.Coefficients = regression coefficients
%              polymodel.ParameterVar = variances of model
coefficients
%           polymodel.ParameterStd = standard deviation of
model coefficients
%       polymodel.R2 = R^2 for the regression model
%       polymodel.RMSE = Root mean squared error
%       polymodel.VarNames = Cell array of variable names
%         as parsed from a char based model specification.
%
%       Note 1: Because the terms in a general polynomial
%       model can be arbitrarily chosen by the user, I must
%       package the erms and coefficients together into a
```

```
%       structure. This also forces use of a special evaluation
%    tool: polyvaln.
%
%    Note 2: A polymodel can be evaluated for any set
%          of values with the function polyvaln. However, if
%    you wish to manipulate the result symbolically using
%     my own sympoly tools, this structure can be converted
%               to a sympoly using the function polyn2sympoly.
%
% Find my sympoly toolbox here:
%
http://www.mathworks.com/matlabcentral/fileexchange/loadFile.do?objectId=9577&objectType=FILE
%
% See also: polyvaln, polyfit, polyval, polyn2sympoly, sympoly
%
% Author: John D'Errico
% Release: 2.0
% Release date: 2/19/06

if nargin<1
 help polyfitn
 return
end

% get sizes, test for consistency
[n,p] = size(indepvar);
if n == 1
 indepvar = indepvar';
 [n,p] = size(indepvar);
end
[m,q] = size(depvar);
if m == 1
 depvar = depvar';
 [m,q] = size(depvar);
end
% only 1 dependent variable allowed at a time
if q~=1
 error 'Only 1 dependent variable allowed at a time.'
end

if n~=m
 error 'indepvar and depvar are of inconsistent sizes.'
end

% Automatically scale the independent variables to unit variance
stdind = sqrt(diag(cov(indepvar)));
if any(stdind==0)
 warning 'Constant terms in the model must be entered using modelterms'
 stdind(stdind==0) = 1;
end
% scaled variables
indepvar_s = indepvar*diag(1./stdind);

% do we need to parse a supplied model?
varlist = {};
if iscell(modelterms) || ischar(modelterms)
 [modelterms,varlist] = parsemodel(modelterms,p);
elseif length(modelterms) == 1
 % do we need to generate a set of modelterms?
 modelterms = buildcompletemodel(modelterms,p);
elseif size(modelterms,2)~=p
 error 'Modelterm must be a scalar or have the same # of columns as indepvar'
end
nt = size(modelterms,1);

% check for replicate terms
if nt>1
 mtu = unique(modelterms,'rows');
 if size(mtu,1)<nt
  warning 'Replicate terms identified in the model.'
 end
end

% build the design matrix
M = ones(n,nt);
scalefact = ones(1,nt);
for i = 1:nt
 for j = 1:p
  M(:,i) = M(:,i).*indepvar_s(:,j).^modelterms(i,j);
  scalefact(i) = scalefact(i)/(stdind(j)^modelterms(i,j));
 end
end

% estimate the model using QR. do it this way to provide a
% covariance matrix when all done. Use a pivoted QR for
% maximum stability.
[Q,R,E] = qr(M,0);

polymodel.ModelTerms = modelterms;
polymodel.Coefficients(E) = R\(Q'*depvar);
yhat = M*polymodel.Coefficients(:);

% recover the scaling
polymodel.Coefficients=polymodel.Coefficients.*scalefact;
```

```
% variance of the regression parameters
s = norm(depvar - yhat);
if n > nt
 Rinv = R\eye(nt);
 Var(E) = s^2*sum(Rinv.^2,2)/(n-nt);
 polymodel.ParameterVar = Var.*(scalefact.^2);
 polymodel.ParameterStd =
sqrt(polymodel.ParameterVar);
else
 % we cannot form variance or standard error
estimates
 % unless there are at least as many data points as
 % parameters to estimate.
 polymodel.ParameterVar = inf(1,nt);
 polymodel.ParameterStd = inf(1,nt);
end

% R^2
polymodel.R2 = 1 - (s/norm(depvar-mean(depvar))
)^2;

% RMSE
polymodel.RMSE = sqrt(mean((depvar - yhat).^2));

% if a character 'model' was supplied, return the list
% of variables as parsed out
polymodel.VarNames = varlist;

%
============================================
=========
% ============== begin subfunctions
==============
%
============================================
=========
function [modelterms,varlist] =
buildcompletemodel(order,p)
%
% arguments: (input)
% order - scalar integer, defines the total (maximum)
order
%
% p - scalar integer - defines the dimension of the
%     independent variable space
%
% arguments: (output)
% modelterms - exponent array for the model
%
% varlist - cell array of character variable names

% build the exponent array recursively
if p == 0
 % terminal case
 modelterms = [];
elseif (order == 0)
 % terminal case
 modelterms = zeros(1,p);
elseif (p==1)
 % terminal case
 modelterms = (order:-1:0)';
else
 % general recursive case
 modelterms = zeros(0,p);
 for k = order:-1:0
  t = buildcompletemodel(order-k,p-1);
  nt = size(t,1);
  modelterms = [modelterms;[repmat(k,nt,1),t]];
 end
end

%
============================================
=========
function [modelterms,varlist] = parsemodel(model,p);
%
% arguments: (input)
% model - character string or cell array of strings
%
% p   - number of independent variables in the model
%
% arguments: (output)
% modelterms - exponent array for the model

modelterms = zeros(0,p);
varlist = {};
while ~isempty(model)
 if iscellstr(model)
  term = model{1};
  model(1) = [];
 else
  [term,model] = strtok(model,' ,');
 end

 % We've stripped off a model term. Now parse it.

 % Is it the reserved keyword 'constant'?
 if strcmpi(term,'constant')
  modelterms(end+1,:) = 0;
 else
  % pick this term apart
  expon = zeros(1,p);
  while ~isempty(term)
   vn = strtok(term,'*/^, ');
   k = find(strncmp(vn,varlist,length(vn)));
```

```
    if isempty(k)
     % its a variable name we have not yet seen

     % is it a legal name?
     nv = length(varlist);
     if ismember(vn(1),'1234567890_')
      error(['Variable is not a valid name: "',vn,""])
     elseif nv>=p
      error 'More variables in the model than
columns of indepvar'
     end

     varlist{nv+1} = vn;

     k = nv+1;
    end
    % variable must now be in the list of vars.

    % drop that variable from term
    i = strfind(term,vn);
    term = term((i+length(vn)):end);

    % is there an exponent?
    eflag = false;
    if strncmp('^',term,1)
     term(1) = [];
     eflag = true;
    elseif strncmp('.^',term,2)
     term(1:2) = [];
     eflag = true;
    end

    % If there was one, get it
    ev = 1;
    if eflag
     ev = sscanf(term,'%f');
     if isempty(ev)
       error 'Problem with an exponent in parsing the model'
     end
    end
    expon(k) = expon(k) + ev;

    % next monomial subterm?
    k1 = strfind(term,'*');
    if isempty(k1)
     term = '';
    else
     term(k1(1)) = ' ';
    end

   end

   modelterms(end+1,:) = expon;

  end

end

% Once we have compiled the list of variables and
% exponents, we need to sort them in alphabetical order
[varlist,tags] = sort(varlist);
modelterms = modelterms(:,tags);
```